Electronic Supplementary Information

Sequential self-assembly of calix[4]resorcinarene-based heterobimetallic Cd_8Pt_8 nano-Saturn complexes

Lipeng He,[†ab] Lijie Li,[†ac] Shi-Cheng Wang,[a] and Yi-Tsu Chan*[a]

[a] Department of Chemistry, National Taiwan University, Taipei 10617, Taiwan
[b] Key Laboratory of Nonferrous Metals Chemistry and Resources Utilization of Gansu Province, College of Chemistry and Chemical Engineering, Lanzhou University, Lanzhou 730000, P. R. China
[c] School of Physical Science and Technology, Lanzhou University, Lanzhou 730000, P. R. China
[†] Equal contribution.

*Correspondence: ytchan@ntu.edu.tw

Table of Contents

General Information

Materials

Unless otherwise noted, reagents and solvents were purchased from Fisher Scientific, AK Scientific, and Sigma-Aldrich without further purification. Column chromatography was conducted using silica gel (75-200 μm) from Fuji Silysia GS series or basic Al_2O_3 (50-200 μm) from Acros Organics. The mixed solvent of toluene/H_2O/*t*-BuOH (3/3/1, v/v/v) and 1,4-dioxane were degassed with N_2 for 30 min before used. All reaction conditions dealing with air- and/or moisture-sensitive compounds were conducted in a N_2 atmosphere.

NMR Spectroscopy

^{1}H and ^{13}C NMR spectra were recorded at 25 °C on Bruker DPX-400, Bruker AVIII-400, and Bruker AVIII-500 NMR spectrometers. COSY, ROESY, DOSY, ^{31}P NMR, and ^{113}Cd NMR spectra were recorded at 25 °C on a Bruker AVIII-500 NMR spectrometer. ^{113}Cd NMR spectra were referenced to an external standard of $Cd(ClO_4)_2$ (δ = 0 ppm).

Mass Spectrometry and Traveling Wave Ion Mobility (TWIM) Experiments

ESI mass spectrometry and TWIM experiments were conducted on a Waters Synapt HDMS G2 instrument with a LockSpray ESI source using the literature parameters.[1] MALDI-TOF spectrometry was conducted on a Bruker autoflex™ speed MALDI TOF/TOF mass spectrometer with a 355 nm frequency tripled Nd:YAG SmartBeam® laser.

Molecular Modeling and Collision Cross Sections (CCSs)

Energy-minimized structures were obtained following the settings in the literature.[1] Calculations were proceeded with Geometry Optimization and followed by Anneal in the Forcite module of Materials Studio version 7.0 program (Accelrys Software, Inc.). For each structure, 200 conformations were generated after annealing and converted into the theoretical CCSs using projection approximation (PA) and trajectory method (TM) in MOBCAL.[2] The experimental calibration of CCS curve was established according to the reported protocol,[3] and the CCS values in He drift gas were used for calibration. A plot of corrected drift times versus corrected cross sections of calibrants fitted with power functions was used as a calibration curve for cross section measurements. **Note**: In the calculation of theoretical CCSs of nano-Saturn complexes, the coordination geometry of *trans*-Pt^{II} might be transformed to undesired structures during the annealing process. Hence, the *trans*-Pt^{II} coordination geometry was preferentially fixed.

Synthesis of Ligands

S1,[4] **S2**,[5] **S3**,[6] **S4**,[7] **S5a**,[8] **S5b**,[9] **S10**,[10] **L**[1],[11] and **L**[4][12] were synthesized according to the literature and showed identical ^{1}H NMR spectra to those reported.

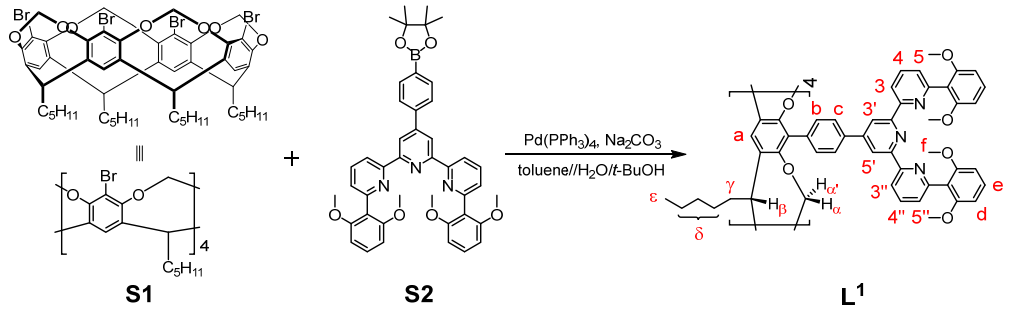

Scheme S1. Synthesis of ligand **L**[1].

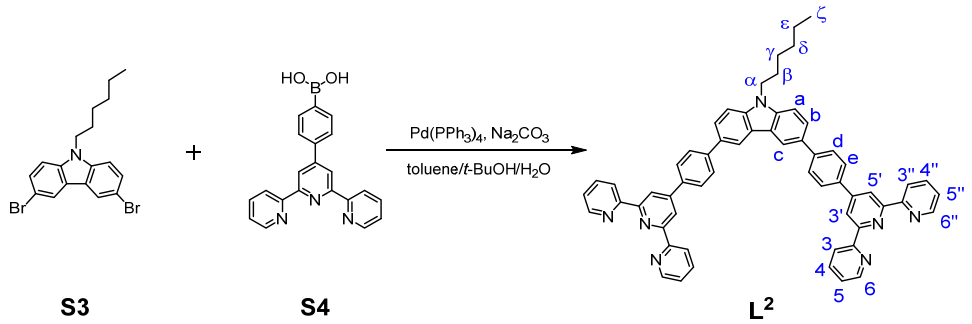

Scheme S2. Synthesis of ligand **L**[2].

Ligand L[2]: To a degassed Schlenk tube containing **S3** (1.0 mmol, 410.0 mg), **S4** (2.2 mmol, 776.0 mg), $Pd(PPh_3)_4$ (0.1 mmol, 116.0 mg), and Na_2CO_3 (12.3 mmol, 1.3 g), a mixed solvent (70 mL) of toluene/H_2O/*t*-BuOH (3/3/1, v/v/v) was added. The mixture was stirred at 80 ºC for 24 h. After cooling to 25 °C, the mixture was poured into water and then extracted with CH_2Cl_2 for three times. The organic phase was evaporated to dryness under reduced pressure. The crude product was purified by flash column chromatography (Al_2O_3) using CH_2Cl_2/MeOH (25:1, v/v) as eluent. The further purification was achieved through recrystallization from CH_2Cl_2/MeOH (1:3, v/v) to give **L**[2] as a white solid in 75% yield (0.8 mmol, 650.0 mg). ^{1}H NMR (500 MHz, $CDCl_3$): δ (ppm) 8.85 (s, 4H), 8.77 (d, J = 4.0 Hz, 4H), 8.71 (d, J = 7.9 Hz, 4H), 8.49 (d, J = 1.6 Hz, 2H), 8.07 (d, J = 8.3 Hz, 4H), 7.93-7.89 (m, 8H), 7.83 (dd, J = 8.5, 1.8 Hz, 2H), 7.52 (d, J = 8.5 Hz, 2H), 7.38 (ddd, J = 7.4, 4.8, 1.2 Hz, 4H), 4.38 (t, J = 7.2 Hz, 2H), 1.95 (t, J = 7.5 Hz, 2H), 1.46 (dd, J = 14.6, 7.4 Hz, 2H), 1.39-1.31 (m, 4H), and 0.90 (t, J = 7.1 Hz, 3H). ^{13}C NMR (100 MHz, $CDCl_3$): δ (ppm) 156.52, 156.10, 150.08, 149.29, 142.87, 140.80, 136.98, 136.48, 131.76, 127.87, 127.78, 125.50, 123.92, 123.74, 121.52, 119.15, 118.79, 109.37, 43.55, 31.76, 29.19, 27.16, 22.72, and 14.19. MALDI-TOF-MS (*m/z*): calcd for $[C_{60}H_{47}N_7 + H]^+$: 866.3966,

found: 866.3975; calcd for $[C_{60}H_{47}N_7 + Na]^+$: 888.3785, found: 888.3794; calcd for $[C_{60}H_{47}N_7 + K]^+$: 904.3525, found: 904.3534.

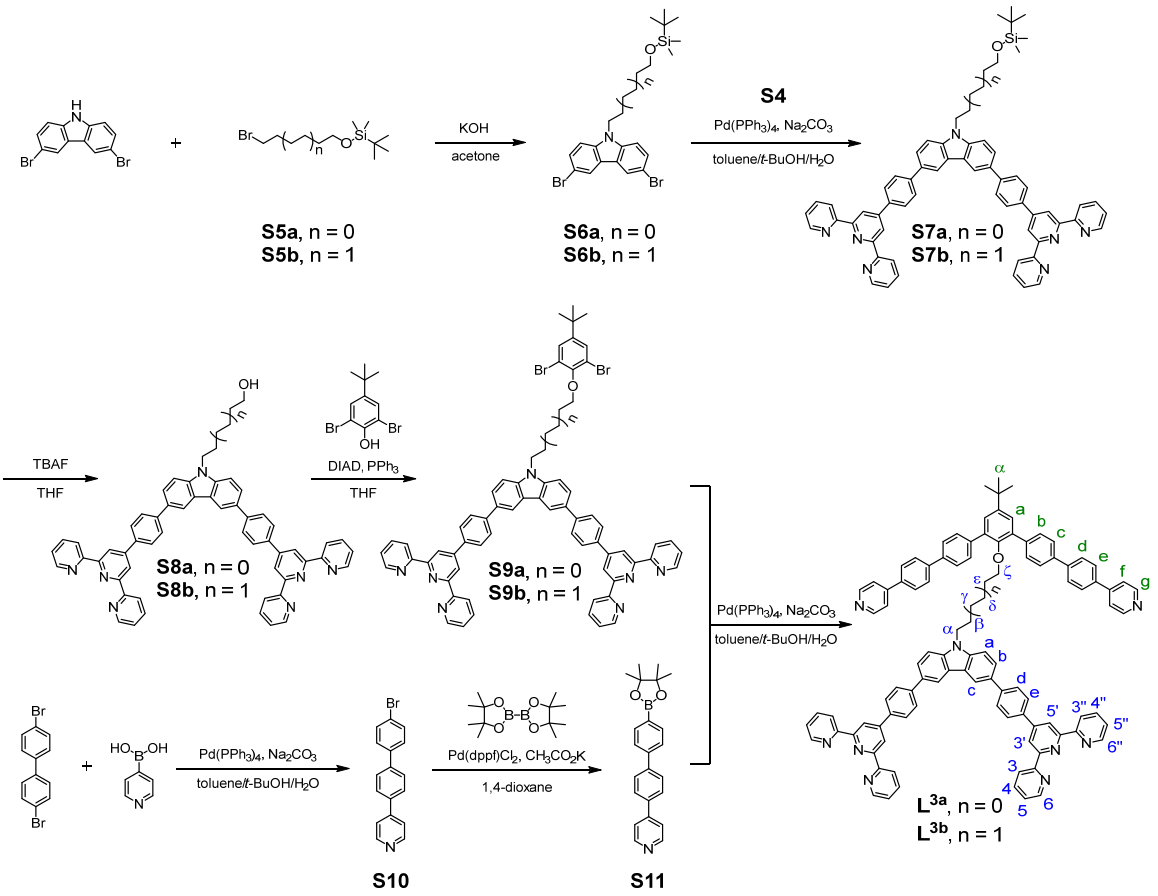

Scheme S3. Synthesis of ligands $\mathbf{L^{3a}}$ and $\mathbf{L^{3b}}$.

Compound S6: To an acetone solution (20 mL) containing 3,6-dibromocarbazole (2.0 mmol, 650.0 mg) and **S5** (2.4 mmol), KOH (6.0 mmol, 828.0 mg) was added. The mixture was refluxed for 12 h. After cooling to 25 °C, the mixture was extracted with CH_2Cl_2 and washed successively with H_2O and brine. The combined organic layer was dried over $MgSO_4$, and then evaporated to dryness under reduced pressure. The residue was subjected to column chromatography (SiO_2, EA/Hexane = 30:1, v/v) to give **S6**.

S6a was obtained as a liquid in 70% yield (1.4 mmol, 714.0 mg). ^{1}H NMR (400 MHz, $CDCl_3$): δ (ppm) 8.10 (d, J = 1.9 Hz, 2H), 7.55 (dd, J = 8.7, 1.9 Hz, 2H), 7.27 (d, J = 8.7 Hz, 2H), 4.25 (t, J = 7.3 Hz, 2H), 3.61 (t, J = 6.0 Hz, 2H), 1.95-1.87 (m, 2H), 1.56-1.50 (m, 2H), 0.88 (s, 9H), and 0.03 (s, 6H). ^{13}C NMR (100 MHz, $CDCl_3$): δ (ppm) 139.36, 129.09, 123.53, 123.33, 112.05, 110.52, 62.63, 43.29, 30.25, 26.06, 25.65, 18.42, and -5.19. MALDI-TOF-MS (*m/z*): calcd for $[C_{22}H_{29}Br_2NOSi + H]^+$: 512.0437; found: 512.0405.

S6b was obtained as a liquid in 68% yield (1.4 mmol, 732.0 mg). ^{1}H NMR (400 MHz, $CDCl_3$): δ (ppm) 8.14 (d, J = 1.6 Hz, 2H), 7.56 (dd, J = 8.7, 1.9 Hz, 2H), 7.28 (d, J = 8.7, 3H), 4.24 (t, J = 7.2 Hz, 2H), 3.55 (t, J = 6.3 Hz, 2H), 1.87-1.80 (m, 2H), 1.55-1.43 (m, 2H), 1.38-1.32 (m, 4H), 0.87 (s, 9H), and 0.02 (s, 6H). ^{13}C NMR (100 MHz, $CDCl_3$): δ (ppm) 139.39, 129.11, 123.54, 123.36, 112.06, 110.48, 63.09, 43.36, 32.73, 28.98, 27.12, 26.11, 25.73, 18.50, and -5.15. MALDI-TOF-MS (*m/z*): calcd for $[C_{24}H_{33}Br_2NOSi + H]^+$: 540.0750; found: 540.0719.

Compound S7: To a degassed Schlenk tube containing **S6** (1.0 mmol, 292.5 mg), **S4** (2.2 mmol, 776.0 g), $Pd(PPh_3)_4$ (0.1 mmol, 116.0 mg), and Na_2CO_3 (12.3 mmol, 1.3 g), a mixed solvent (70.0 mL) of toluene/H_2O/*t*-BuOH (3/3/1, v/v/v) was added. The reaction mixture was stirred at 80 ºC for 24 h. After cooling to room temperature, the mixture was poured into water and then extracted with CH_2Cl_2 for three times. The combined organic layer was washed with H_2O and brine, dried over $MgSO_4$, and evaporated to dryness under reduced pressure. The residue was purified by recrystallization from CH_2Cl_2/MeOH to afford **S7**.

S7a was obtained as a brown solid in 72% yield (0.7 mmol, 697.0 mg). ^{1}H NMR (400 MHz, $CDCl_3$): δ (ppm) 8.84 (s, 4H), 8.76 (d, J = 3.9 Hz, 4H), 8.70 (d, J = 8.0 Hz, 4H), 8.48 (d, J = 1.6 Hz, 2H), 8.06 (d, J = 8.4 Hz, 4H), 7.91-7.87 (m, 8H), 7.82 (dd, J = 8.5, 1.8 Hz, 2H), 7.53 (d, J = 8.5 Hz, 2H), 7.36 (ddd, J = 7.4, 4.8, 1.1 Hz, 4H), 4.42 (t, J = 7.1 Hz, 2H), 3.67 (t, J = 6.1 Hz, 2H), 2.08-2.01 (m, 2H), 1.68-1.62 (m, 2H), 0.91 (s, 9H), and 0.06 (s, 6H). ^{13}C NMR (100 MHz, $CDCl_3$): δ (ppm) 156.46, 156.05, 150.09, 149.26, 142.88, 140.77, 137.03, 136.45, 131.78, 127.87, 127.79, 125.52, 123.94, 123.74, 121.55, 119.16, 118.81, 109.41, 62.81, 43.39, 30.48, 26.12, 25.88, 18.49, and -5.14. MALDI-TOF-MS (*m/z*): calcd for $[C_{64}H_{57}N_7OSi + H]^+$: 968.4467; found: 968.4412.

S7b was obtained as a yellowish solid in 70% yield (0.7 mmol, 698.0 mg). ^{1}H NMR (400 MHz, $CDCl_3$): δ (ppm) 8.84 (s, 4H), 8.77 (d, J = 4.2 Hz, 4H), 8.70 (d, J = 8.1 Hz, 4H), 8.49 (s, 2H), 8.06 (d, J = 8.3 Hz, 4H), 7.91-7.87 (m, 8H), 7.83 (d, J = 8.6 Hz, 2H), 7.52 (d, J = 8.4 Hz, 2H), 7.37 (t, J = 5.6 Hz, 4H), 4.38 (t, J = 6.7 Hz, 2H), 3.60 (t, J = 6.3 Hz, 2H), 2.00-1.93 (m, 2H), 1.56-1.50 (m, 2H), 1.47-1.42 (m, 4H), 0.90 (s, 9H), and 0.04 (s, 6H). ^{13}C NMR (100 MHz, $CDCl_3$): δ (ppm) 156.49, 156.06, 150.03, 149.27, 142.84, 140.76, 136.95, 136.45, 131.75, 127.84, 127.75, 125.49, 123.90, 123.72, 121.50, 119.13, 118.76, 109.33, 63.19, 43.42, 32.81, 29.22, 27.25, 26.13, 25.82, 18.51, and -5.12. MALDI-TOF-MS (*m/z*): calcd for $[C_{66}H_{61}N_7OSi + H]^+$: 996.4780; found: 996.4793.

Compound S8: To a THF solution (20 mL) of **S7** (0.6 mmol), tetrabutylammonium fluoride (2 mL, 1.0 M in THF) was added at 0 °C. After the mixture was stirred at 25 °C for 12 h, the solvent was evaporated under reduced pressure. The residue was purified by recrystallization from CH_2Cl_2/MeOH to give **S8**.

S8a was obtained as a yellowish solid in 90% yield (0.5 mmol, 461.2 mg). ^{1}H NMR (400 MHz, $CDCl_3$): δ (ppm) 8.83 (s, 4H), 8.76 (d, J = 4.8 Hz, 4H), 8.70 (d, J = 7.9 Hz, 4H), 8.48 (s, 2H), 8.05 (d, J = 8.2

Hz, 4H), 7.92-7.87 (m, 8H), 7.82 (d, J = 8.4 Hz, 2H), 7.53 (d, J = 8.5 Hz, 2H), 7.37 (t, J = 6.4 Hz, 4H), 4.45 (t, J = 7.1 Hz, 2H), 3.70 (q, J = 6.1 Hz, 2H), 2.11-2.03 (m, 2H), and 1.73-1.57 (m, 2H). ^{13}C NMR (100 MHz, $CDCl_3$): δ (ppm) 156.48, 156.05, 150.05, 149.27, 142.79, 140.71, 137.03, 136.44, 131.82, 127.85, 127.77, 125.55, 123.95, 123.74, 121.57, 119.16, 118.79, 109.37, 62.57, 43.24, 30.44, and 25.78. MALDI-TOF-MS (*m/z*): calcd for $[C_{58}H_{43}N_7O + H]^+$: 854.3602; found: 854.3624.

S8b was obtained as a yellowish solid in 92% yield (0.6 mmol, 488.8 mg). ^{1}H NMR (400 MHz, $CDCl_3$): δ (ppm) 8.84 (s, 4H), 8.76 (d, J = 4.0 Hz, 4H), 8.70 (d, J = 7.9 Hz, 4H), 8.49 (d, J = 1.6 Hz, 2H), 8.06 (d, J = 8.3 Hz, 4H), 7.94-7.87 (m, 8H), 7.83 (dd, J = 8.5, 1.7 Hz, 2H), 7.52 (d, J = 8.6 Hz, 2H), 7.37 (ddd, J = 7.3, 4.8, 1.0 Hz, 4H), 4.39 (t, J = 7.1 Hz, 2H), 3.64 (q, J = 6.2 Hz, 2H), 2.02-1.93 (m, 2H), 1.61-1.55 (s, 2H), and 1.50-1.42 (m, 4H). ^{13}C NMR (100 MHz, $CDCl_3$): δ (ppm) 156.45, 156.01, 149.99, 149.23, 142.77, 140.70, 136.98, 136.37, 131.67, 127.81, 127.71, 125.44, 123.91, 123.68, 121.53, 119.06, 118.74, 109.30, 62.78, 43.33, 32.71, 29.14, 27.21, and 25.71. MALDI-TOF-MS (*m/z*): calcd for $[C_{60}H_{47}N_7O + H]^+$: 882.3915; found: 882.3933.

Compound S9: To a THF solution (10 mL) of **S8** (0.5 mmol), 2,6-dibromo-4-*tert*-butylphenol (1.0 mmol, 306.0 mg), and triphenylphosphine (1.0 mmol, 263.0 mg), diisopropyl azodicarboxylate (1.0 mmol, 202.0 mg) was added at 0 °C. After the resulting solution was stirred at 25 °C for 12 h, the reaction mixture was evaporated to dryness under reduced pressure. The residue was purified by recrystallization from CH_2Cl_2/MeOH to give **S9**.

S9a was obtained as a yellowish solid in 85% yield (0.4 mmol, 485.0 mg). ^{1}H NMR (400 MHz, $CDCl_3$): δ (ppm) 8.84 (s, 4H), 8.76 (d, J = 3.9 Hz, 4H), 8.70 (d, J = 7.9 Hz, 4H), 8.50 (d, J = 1.7 Hz, 2H), 8.06 (d, J = 8.3 Hz, 4H), 7.93-7.87 (m, 8H), 7.84 (dd, J = 8.4, 1.7 Hz, 2H), 7.61 (d, J = 8.6 Hz, 2H), 7.49 (s, 2H), 7.37 (ddd, J = 7.6, 4.9, 1.2 Hz, 4H), 4.55 (t, J = 7.0 Hz, 2H), 4.05 (t, J = 5.9 Hz, 2H), 2.35-2.28 (m, 2H), 2.02-1.95 (m, 2H), and 1.29 (s, 9H). ^{13}C NMR (100 MHz, $CDCl_3$): δ (ppm) 156.45, 156.02, 150.79, 150.07, 150.00, 149.25, 142.79, 140.76, 136.95, 136.40, 131.78, 130.02, 127.82, 127.75, 125.54, 123.90, 123.75, 121.50, 119.11, 118.74, 117.95, 109.51, 72.85, 43.34, 34.73, 31.27, 27.89, and 26.12. MALDI-TOF-MS (*m/z*): calcd for $[C_{68}H_{53}Br_2N_7O + H]^+$: 1144.2731; found: 1144.2764.

S9b was obtained as a yellowish solid in 80% yield (0.4 mmol, 468.0 mg). ^{1}H NMR (400 MHz, $CDCl_3$): δ (ppm) 8.84 (s, 4H), 8.76 (ddd, J = 4.9, 1.8, 0.9 Hz, 4H), 8.70 (dt, J = 8.0, 1.0 Hz, 4H), 8.49 (d, J = 1.5 Hz, 2H), 8.06 (d, J = 8.5 Hz,, 4H), 7.92-7.87 (m, 8H), 7.83 (dd, J = 8.5, 1.8 Hz, 2H), 7.53 (d, J = 8.5 Hz, 2H), 7.47 (s, 2H), 7.36 (ddd, J = 7.4, 4.8, 1.2 Hz, 4H), 4.41 (t, J = 7.1 Hz, 2H), 3.96 (t, J = 6.3 Hz, 2H), 2.01 (q, J = 7.3 Hz, 2H), 1.87 (p, J = 6.5 Hz, 2H), 1.70-1.62 (m, 2H), 1.59-1.51 (m, 2H), and 1.27 (s, 9H). ^{13}C NMR (100 MHz, $CDCl_3$): δ (ppm) 156.47, 156.04, 151.00, 150.00, 149.84, 149.25, 142.83, 140.75, 136.93, 136.40, 131.72, 129.96, 127.81, 127.74, 125.49, 123.88, 123.72, 121.49, 119.11, 118.74, 117.96, 109.36, 73.14, 43.38, 34.68, 31.27, 29.91, 29.10, 27.15, and 25.83. MALDI-TOF-MS (*m/z*): calcd for $[C_{70}H_{57}Br_2N_7O + H]^+$: 1172.3044; found: 1172.3065.

Compound S11: To a degassed Schlenk tube containing **S10** (3.0 mmol, 930.0 mg), bis(pinacolato)diboron (3.6 mmol, 915.0 mg), Pd(dppf)Cl_2 (150.3 μmol, 110.0 mg), and CH_3COOK (9.0 mmol, 880.0 mg), 20 mL of 1,4-dioxane was added. Under N_2, the reaction mixture was stirred at 80 ºC for 12 h. After cooling to room temperature, the mixture was poured into water and then extracted with DCM for three times. The combined organic phase was washed with H_2O and brine, dried over $MgSO_4$, and evaporated to dryness under reduced pressure. The residue was purified by recrystallization from CH_2Cl_2/hexane to afford **S11** as a white solid in 75% yield (2.3 mmol, 800.0 mg). ^{1}H NMR (400 MHz, $CDCl_3$): δ (ppm) 8.68 (d, J = 5.6 Hz, 2H), 7.92 (d, J = 8.3 Hz, 2H), 7.74 (d, J = 2.3 Hz, 4H), 7.66 (d, J = 8.2 Hz, 2H), 7.56 (d, J = 5.6 Hz, 2H), and 1.37 (s, 12H). ^{13}C NMR (100 MHz, $CDCl_3$): δ (ppm) 150.32, 148.02, 142.92, 141.93, 137.30, 135.51, 128.04, 127.53, 126.49, 121.64, 84.04, and 25.03. MALDI-TOF-MS (*m/z*): calcd for $[C_{23}H_{24}BNO_2 + H]^+$: 358.1973; found: 358.1914.

Ligand L^3: To a degassed Schlenk tube containing **S9** (0.3 mmol), **S11** (0.7 mmol, 250.0 mg), Pd(PPh_3)$_4$ (30.3 μmol, 35.0 mg), and Na_2CO_3 (5.0 mmol, 530.0 mg), a mixed solvent (35 mL) of toluene/H_2O/*t*-BuOH (3/3/1, v/v/v) was added. The reaction mixture was stirred at 80 ºC for 24 h. After cooling to room temperature, the mixture was poured into water and then extracted with CH_2Cl_2 for three times. The combined organic layer was washed with H_2O and brine, dried over $MgSO_4$, and evaporated to dryness under reduced pressure. The residue was purified by flash column chromatography (Al_2O_3) using CH_2Cl_2/MeOH (30:1, v/v) as eluent. The crude product was purified by recrystallization from CH_2Cl_2/MeOH to afford **L^3**.

L^{3a} was obtained as a yellowish solid in 80% yield (0.2 mmol, 347.0 mg). ^{1}H NMR (500 MHz, $CDCl_3$): δ (ppm) 8.83 (s, 4H), 8.77 (ddd, J = 4.8, 1.9, 0.9 Hz, 4H), 8.71 (dt, J = 8.0, 1.1 Hz, 4H), 8.64 (d, J = 6.2 Hz, 4H), 8.37 (d, J = 1.7 Hz, 2H), 8.03 (d, J = 8.3 Hz, 4H), 7.91 (td, J = 7.7, 1.8 Hz, 4H), 7.83 (d, J = 8.3 Hz, 4H), 7.73 (d, J = 8.3 Hz, 4H), 7.69 (s, 10H), 7.65 (d, J = 8.4 Hz, 4H), 7.57-7.54 (m, 4H), 7.42 (s, 2H), 7.38 (ddd, J = 7.5, 4.7, 1.2 Hz, 4H), 7.33 (d, J = 8.5 Hz, 2H), 4.13 (t, J = 7.0 Hz, 2H), 3.35 (t, J = 5.7 Hz, 2H), 1.76-1.68 (m, 2H), 1.41 (s, 9H), and 1.36-1.30 (m, 2H). ^{13}C NMR (100 MHz, $CDCl_3$): δ (ppm) 156.45, 156.12, 151.83, 150.42, 149.92, 149.29, 147.79, 147.28, 142.73, 141.58, 140.63, 138.98, 138.89, 137.02, 136.99, 136.52, 134.91, 131.67, 130.28, 127.87, 127.78, 127.72, 127.61, 127.53, 126.82, 125.38, 123.98, 123.64, 121.56, 121.49, 119.09, 118.71, 109.33, 72.76, 43.01, 34.74, 31.68, 27.59, and 25.87. MALDI-TOF-MS (*m/z*): calcd for $[C_{102}H_{77}N_9O + H]^+$: 1445.6357; found: 1445.6310.

L^{3b} was obtained as a white solid in 78% yield (0.2 mmol, 345.0 mg). ^{1}H NMR (500 MHz, $CDCl_3$): δ (ppm) 8.84 (s, 4H), 8.77 (ddd, J = 4.8, 1.8, 0.9 Hz, 4H), 8.71 (dt, J = 8.0, 1.0 Hz, 4H), 8.63 (d, J = 6.2 Hz, 4H), 8.41 (d, J = 1.6 Hz, 2H), 8.04 (d, J = 8.4 Hz, 4H), 7.90 (td, J = 7.8, 1.8 Hz, 4H), 7.85 (d, J = 8.4 Hz, 4H), 7.80-7.67 (m, 14H), 7.65 (d, J = 8.5 Hz, 4H), 7.53 (d, J = 6.3 Hz, 4H), 7.42 (s, 2H), 7.39-7.34 (m, 6H), 4.16 (t, J = 7.2 Hz, 2H), 3.32 (t, J = 5.9 Hz, 2H), 1.70 (q, J = 7.3 Hz, 2H), 1.41 (s, 9H), 1.29-1.22 (m, 2H), and 1.16-1.06 (m, 4H). ^{13}C NMR (125 MHz, $CDCl_3$): δ (ppm) 156.44, 156.10, 152.00,

150.00, 149.63, 149.28, 148.55, 147.14, 142.70, 141.83, 140.65, 139.18, 138.75, 137.09, 136.63, 136.56, 134.92, 131.70, 130.32, 127.92, 127.77, 127.71, 127.64, 127.57, 126.80, 125.43, 124.00, 123.66, 121.68, 121.59, 119.11, 118.80, 109.25, 73.26, 43.27, 34.73, 31.69, 29.86, 28.99, 26.93, and 25.77. MALDI-TOF-MS (*m/z*): calcd for $[C_{104}H_{81}N_9O + H]^+$: 1473.6670; found: 1473.6687.

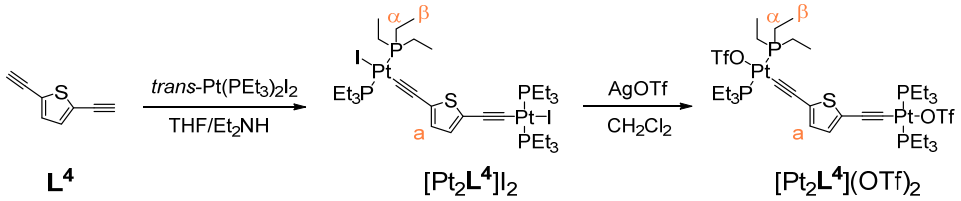

Scheme S4. Synthesis of $[Pt_2\mathbf{L^4}](OTf)_2$.

$[Pt_2\mathbf{L^4}]I_2$: To a 100 mL Schlenk flask containing 2,5-diethynylthiophene (0.7 mmol, 92.4 mg) and *trans*-diiodobis(triethylphosphine)platinum(II) (2.2 mmol, 1.5 g), 40 mL of anhydrous THF and 10 mL of anhydrous Et_2NH were added under N_2. The solution was stirred at room temperature for 10 min, and then CuI (69.8 μmol, 13.3 mg) was added. After being stirred for an additional 3 h at room temperature, the solvent was removed under reduced pressure. The residue was purified by column chromatography (SiO_2) using EA/hexane (3/100-3/50, v/v) as eluent to give $[Pt_2\mathbf{L^4}]I_2$ as a yellow solid in 75% yield (0.5 mmol, 660.0 mg).^{1}H NMR (500 MHz, $CDCl_3$): δ (ppm) 6.67 (s, 2H), 2.23-2.17 (m, 24H), and 1.19-1.12 (m, 36H). ^{13}C NMR (125 MHz, $CDCl_3$): δ (ppm) 127.43, 126.89, 95.13, 93.26, 16.81, and 8.44. ^{31}P NMR (202 MHz, $CDCl_3$): δ (ppm) 8.60 (s, $J_{Pt\text{-}P}$ = 2306.8 Hz). MALDI-TOF-MS (*m/z*): calcd for $[C_{32}H_{62}I_2P_4Pt_2S + H]^+$: 1246.0959; found: 1246.0935.

$[Pt_2\mathbf{L^4}](OTf)_2$: To a CH_2Cl_2 solution (20 mL) of $[Pt_2\mathbf{L^4}]I_2$ (0.1 mmol, 125.0 mg) in a Schlenk tube, AgOTf (0.2 mmol, 57.0 mg) was added. After being stirred at room temperature for 2 h, the suspension was filtered through a glass fiber filter and the volume of the solution was reduced to ~5 mL. Subsequent addition of diethyl ether resulted in the precipitation of $[Pt_2\mathbf{L^4}](OTf)_2$ as a tawny solid. $[Pt_2\mathbf{L^4}](OTf)_2$ was prepared just before self-assembly of the heterobimetallic complex Cd_8Pt_8 and used without further purification.

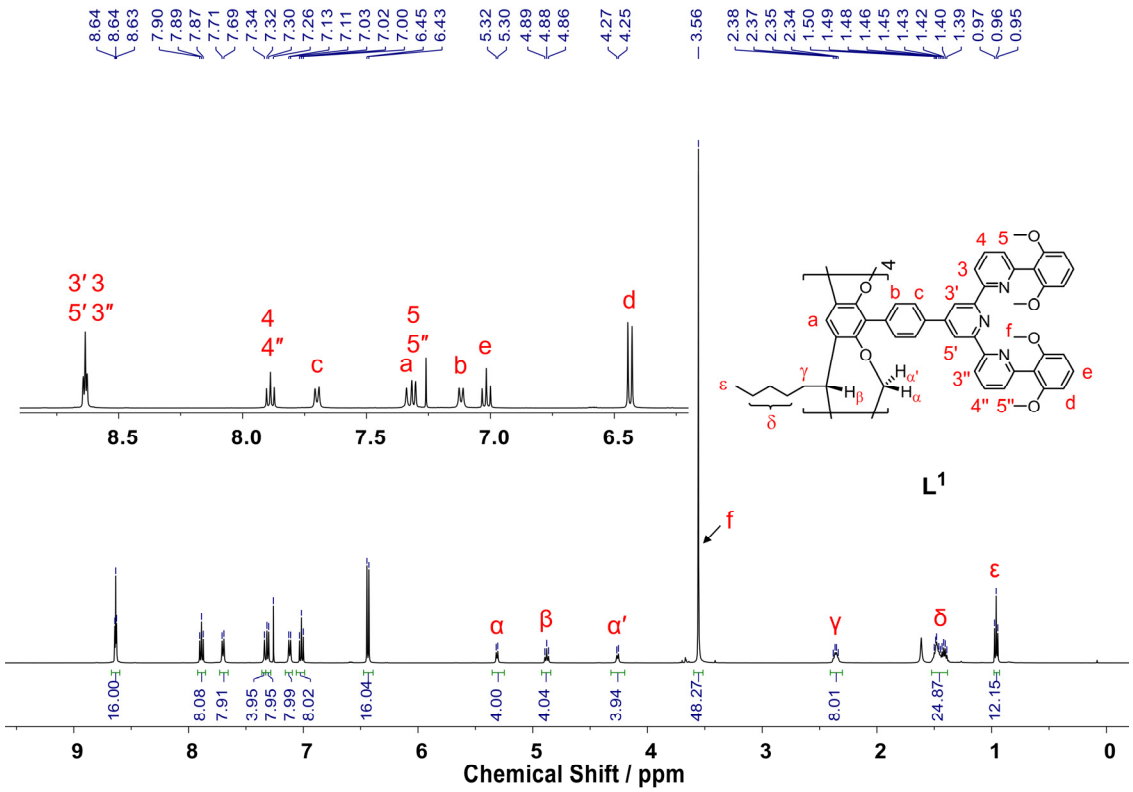

Figure S1. ^{1}H NMR spectrum (500 MHz, $CDCl_3$) of ligand **L^{1}**.

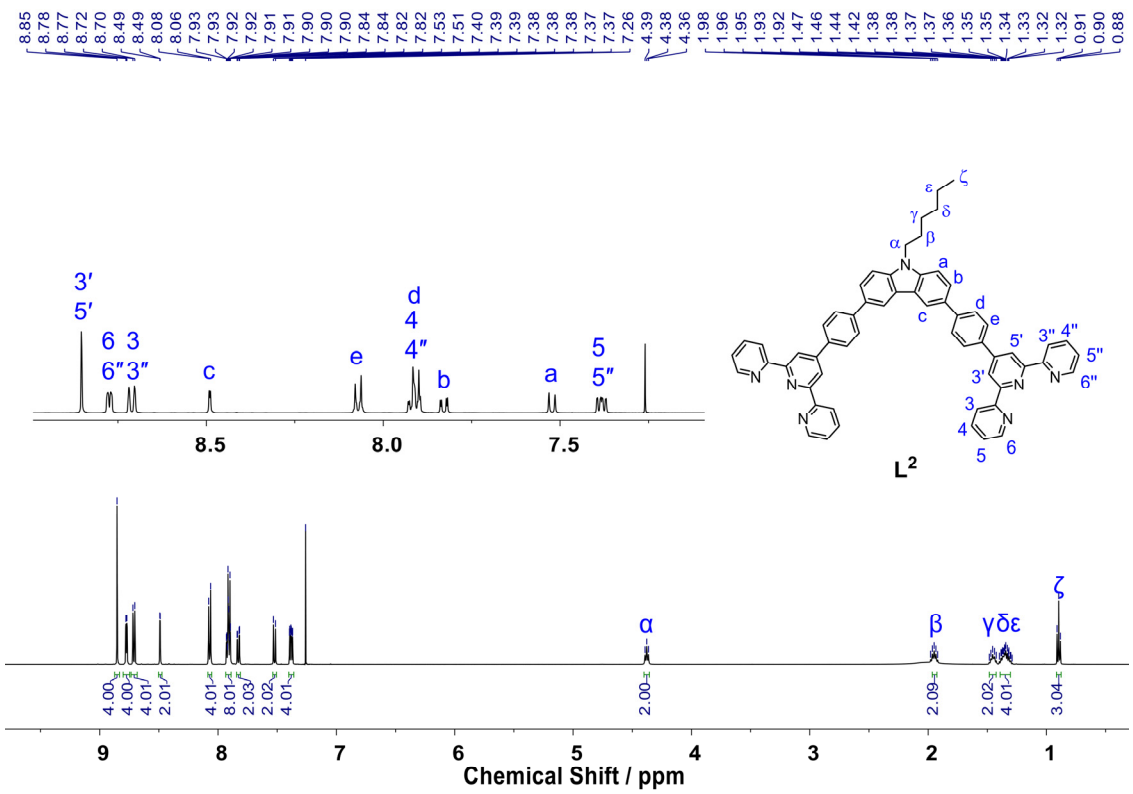

Figure S2. ^{1}H NMR spectrum (500 MHz, $CDCl_3$) of ligand **L^{2}**.

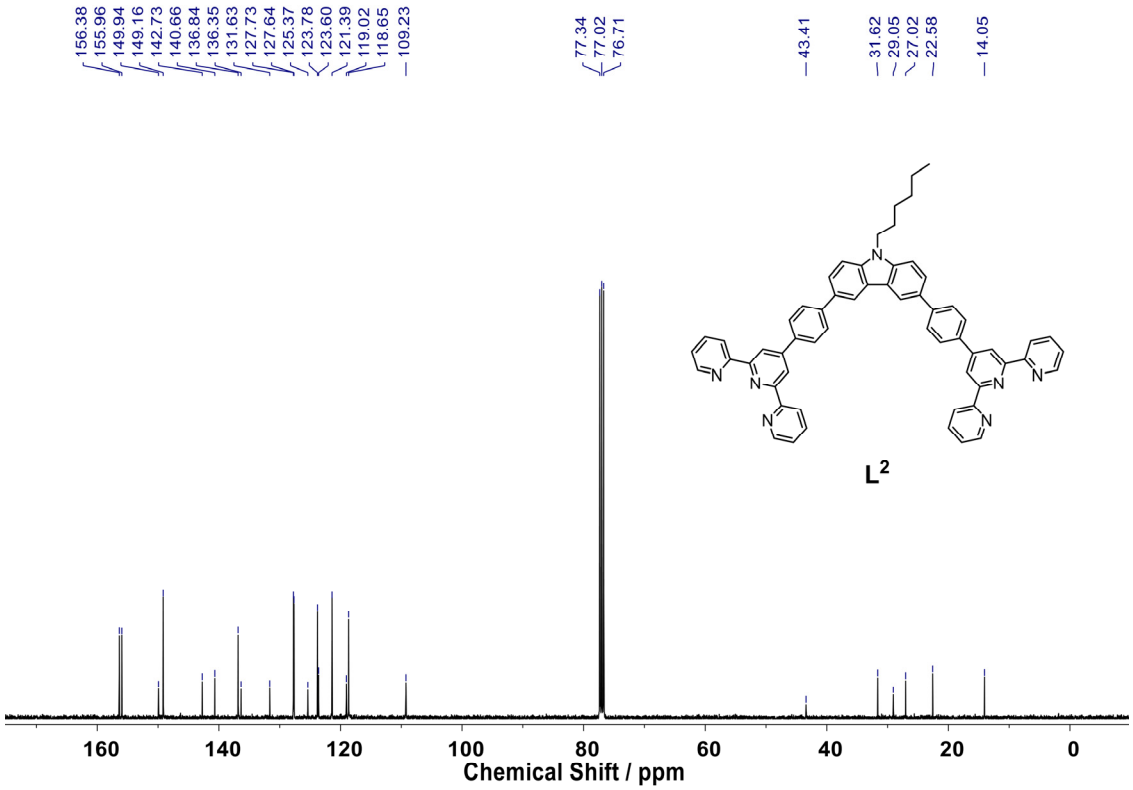

Figure S3. ^{13}C NMR spectrum (100 MHz, $CDCl_3$) of ligand **L²**.

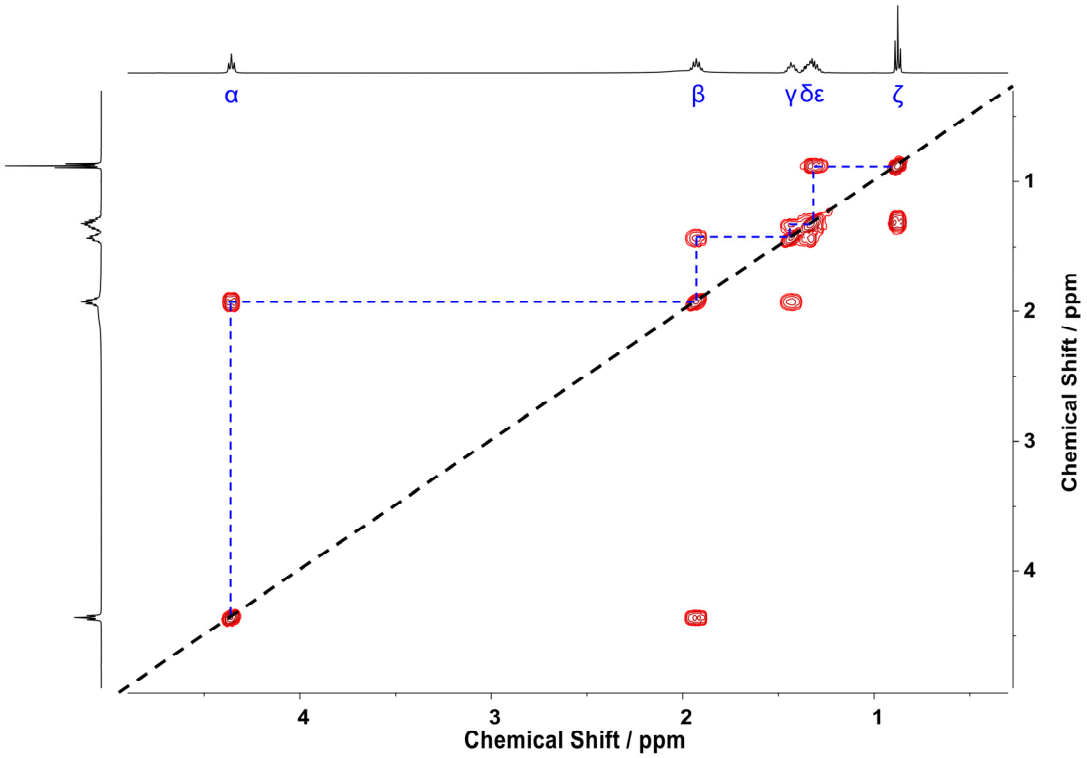

Figure S4. Partial COSY spectrum (500 MHz, $CDCl_3$) of ligand **L²**.

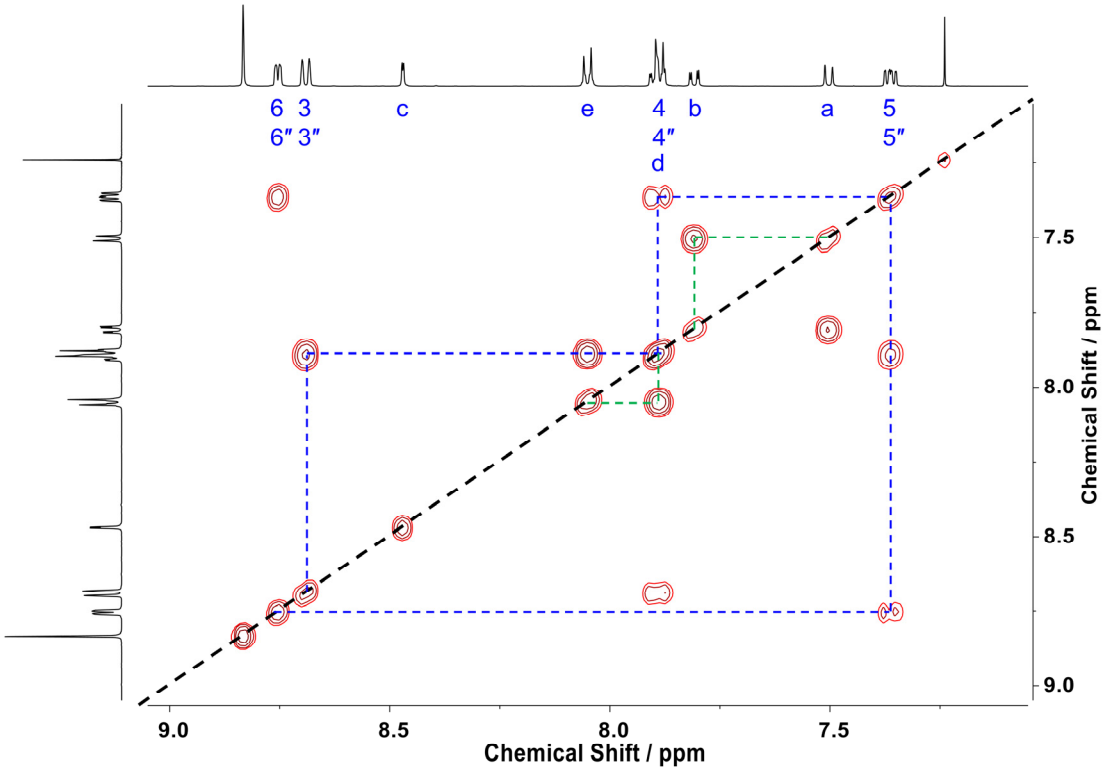

Figure S5. Partial COSY spectrum (500 MHz, $CDCl_3$) of ligand **L²**.

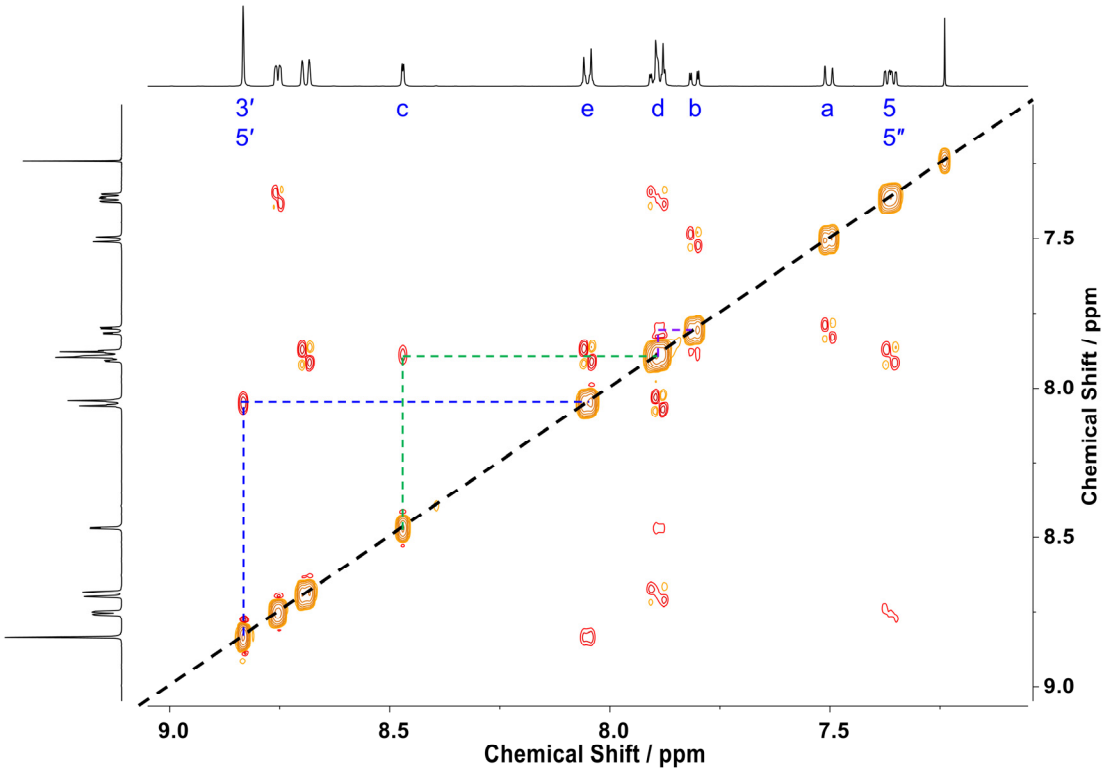

Figure S6. Partial ROESY spectrum (500 MHz, $CDCl_3$) of ligand **L²**.

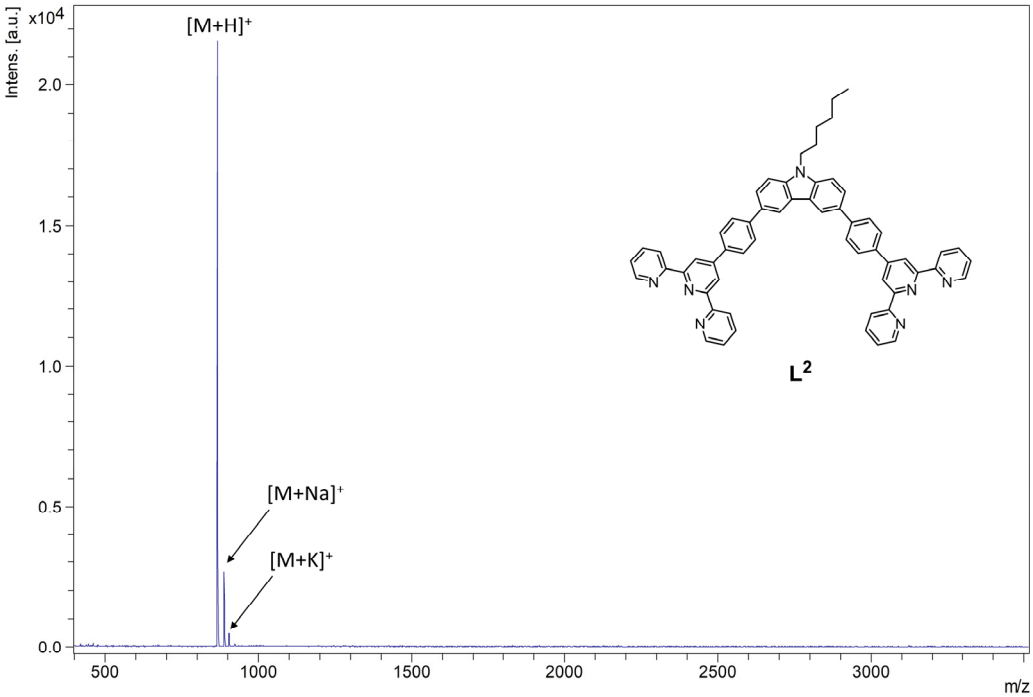

Figure S7. High-resolution MALDI-TOF-MS spectrum of ligand $\mathbf{L^2}$.

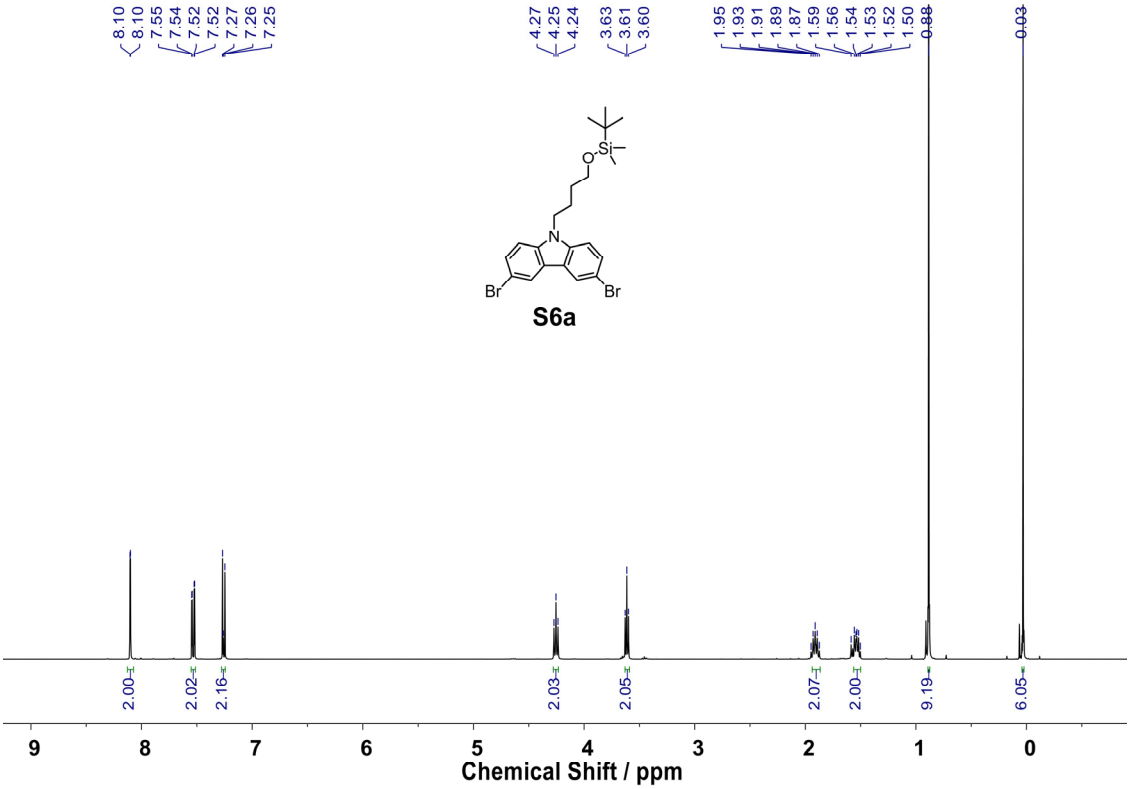

Figure S8. ^{1}H NMR spectrum (400 MHz, $CDCl_3$) of **S6a**.

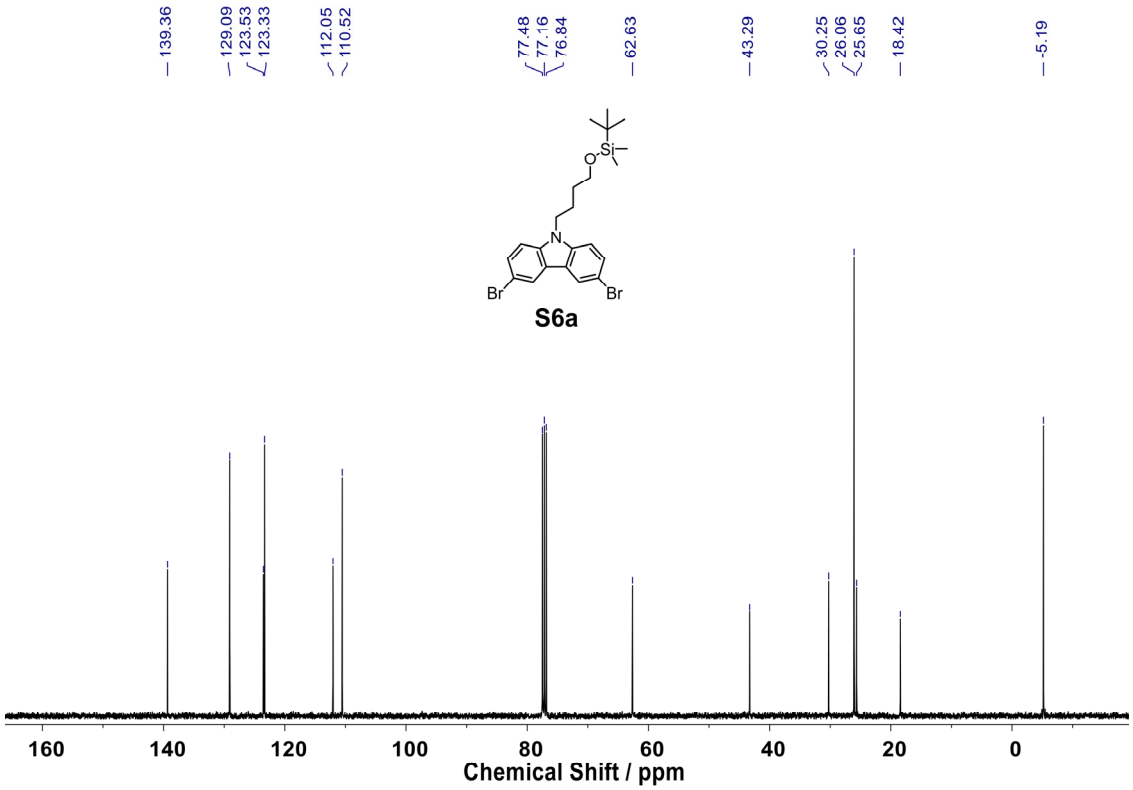

Figure S9. ^{13}C NMR spectrum (100 MHz, $CDCl_3$) of **S6a**.

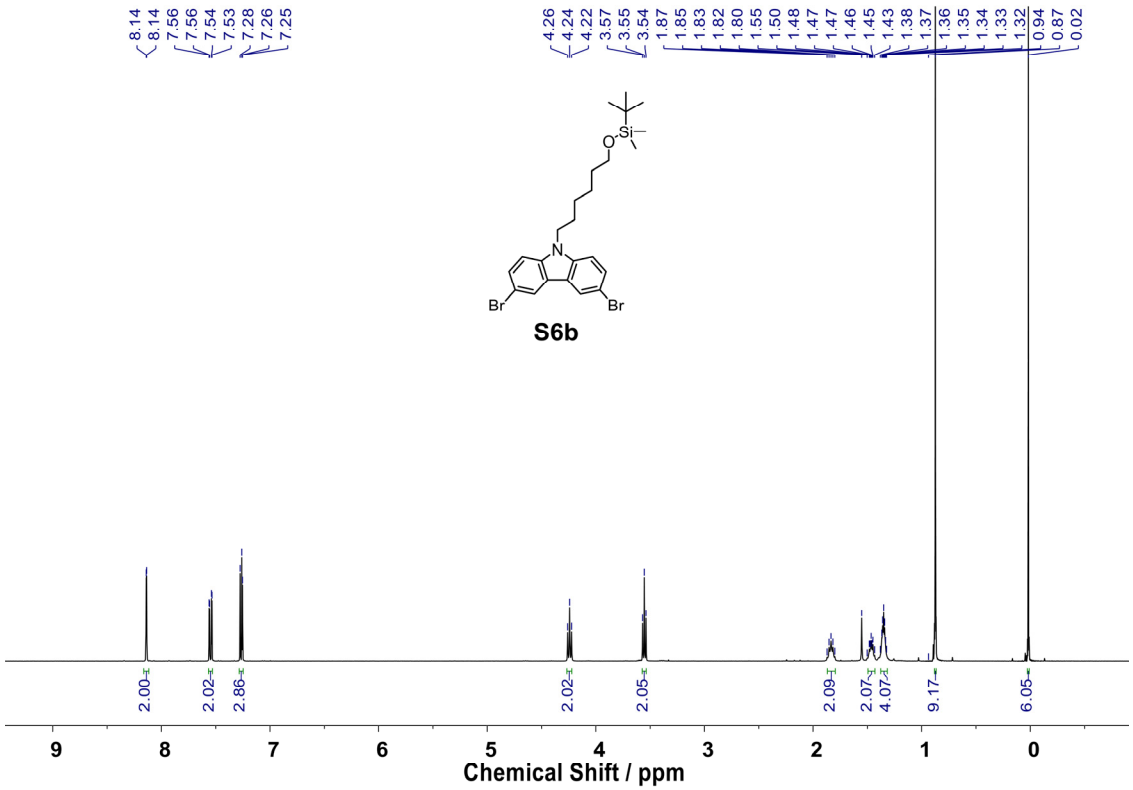

Figure S10. ^{1}H NMR spectrum (400 MHz, $CDCl_3$) of **S6b**.

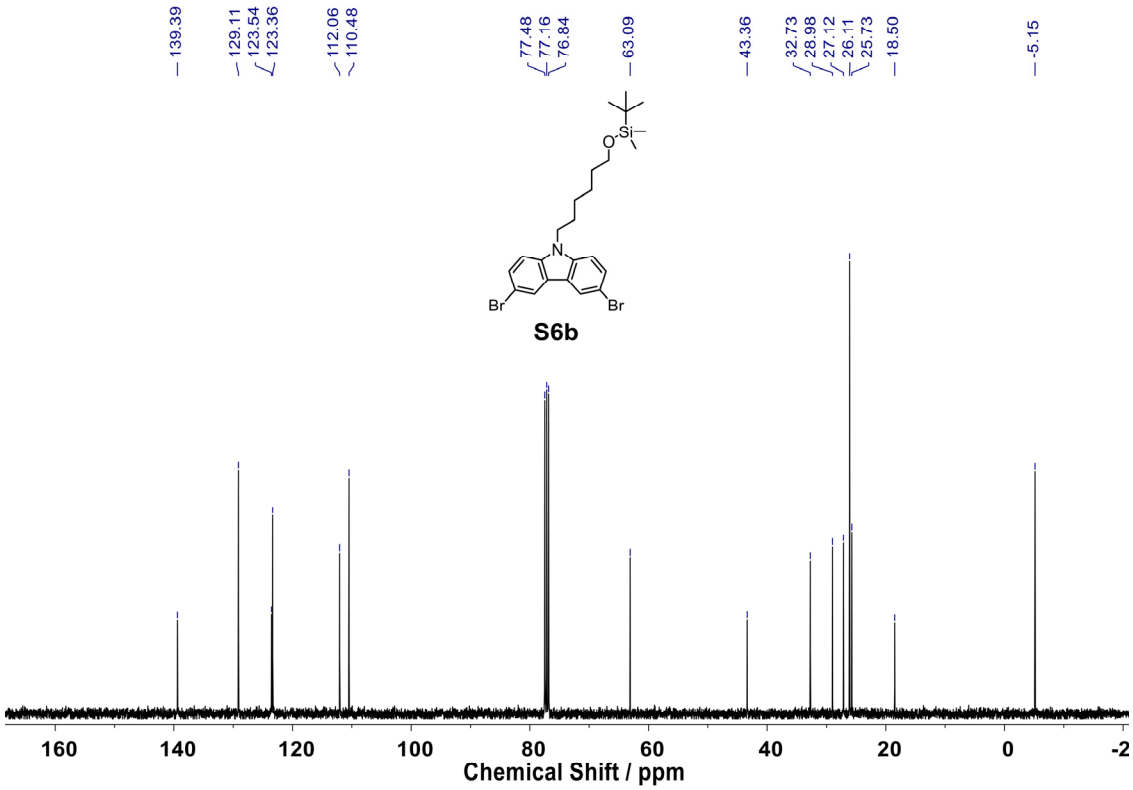

Figure S11. ^{13}C NMR spectrum (100 MHz, $CDCl_3$) of **S6b**.

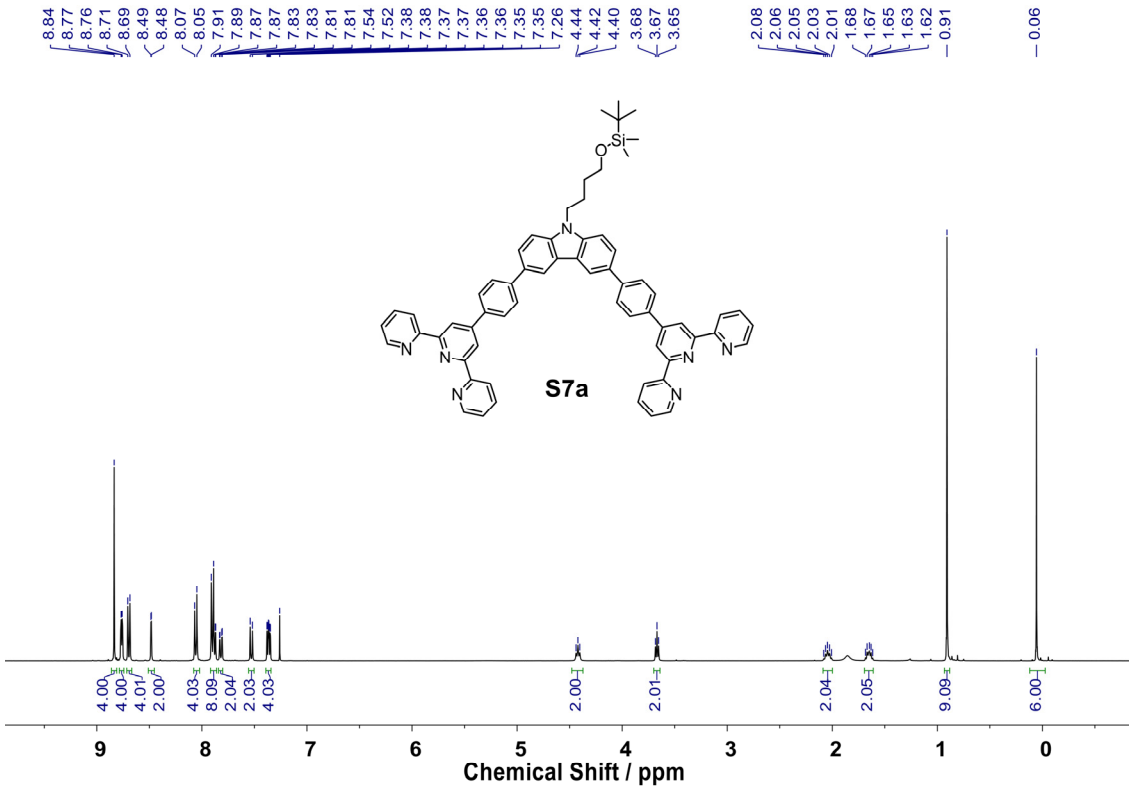

Figure S12. ^{1}H NMR spectrum (400 MHz, $CDCl_3$) of **S7a**.

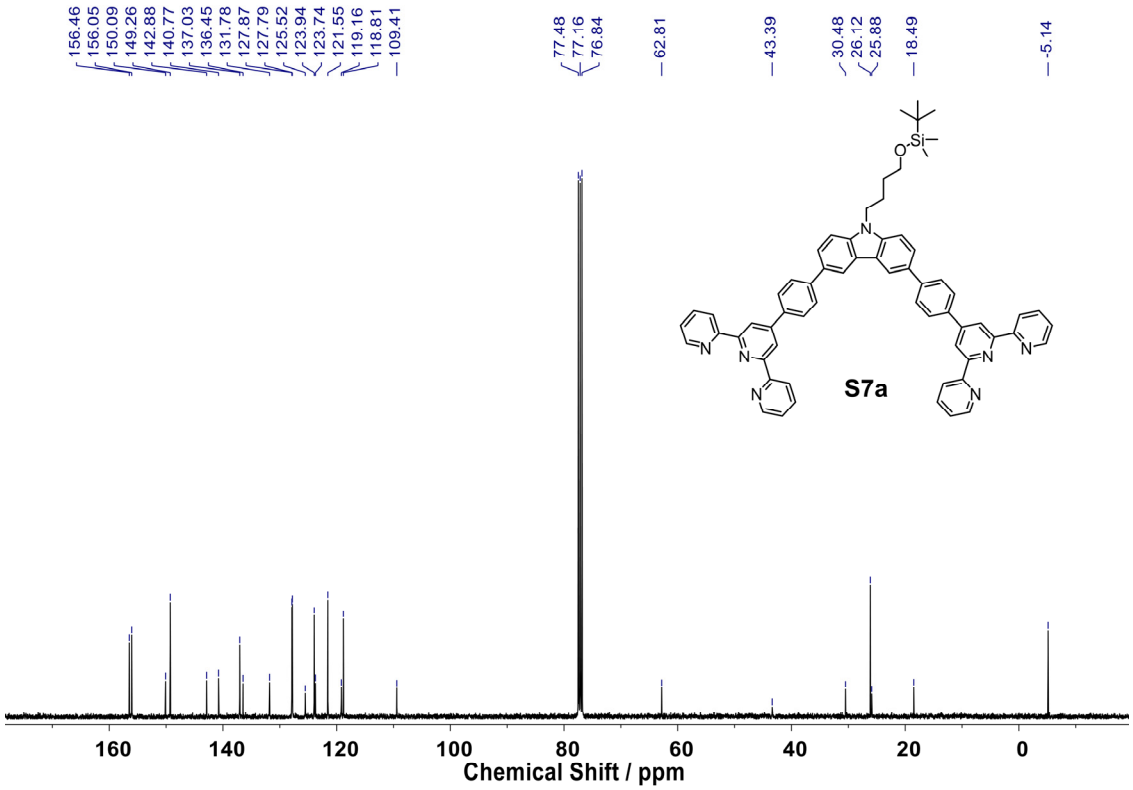

Figure S13. ^{13}C NMR spectrum (100 MHz, $CDCl_3$) of **S7a**.

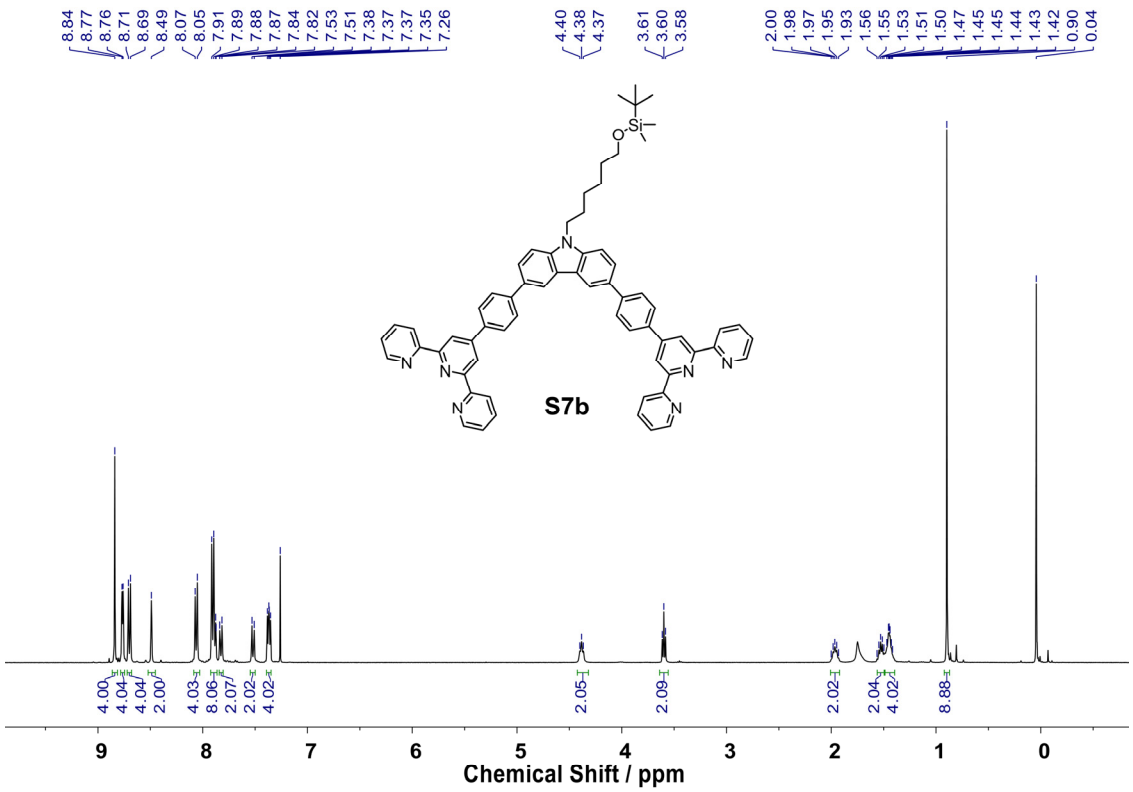

Figure S14. ^{1}H NMR spectrum (400 MHz, $CDCl_3$) of **S7b**.

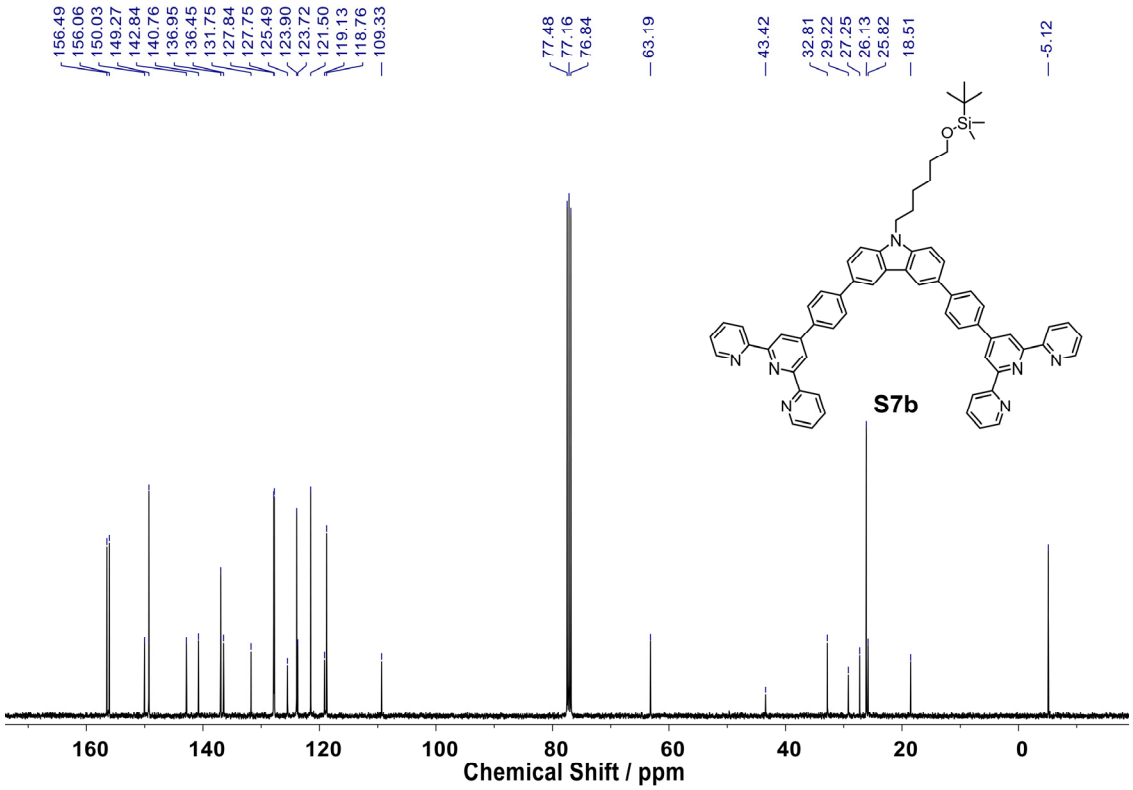

Figure S15. ^{13}C NMR Spectrum (100 MHz, $CDCl_3$) of **S7b**.

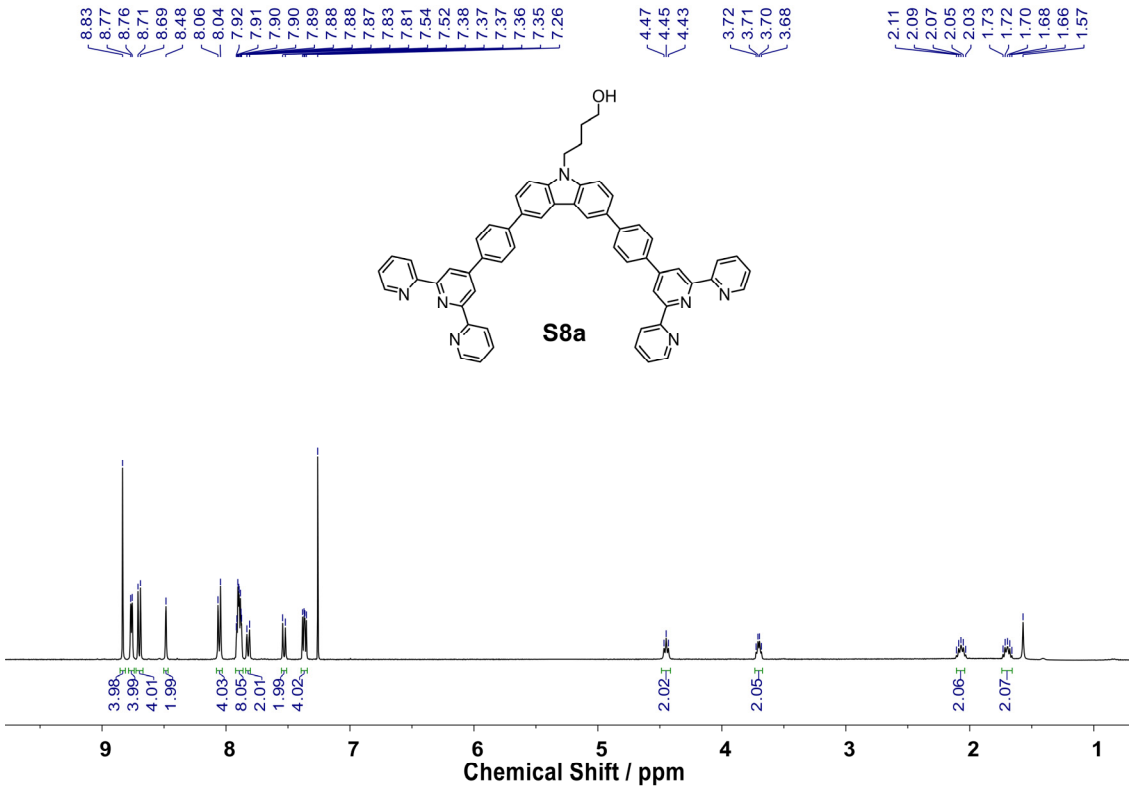

Figure S16. ^{1}H NMR spectrum (400 MHz, $CDCl_3$) of **S8a**.

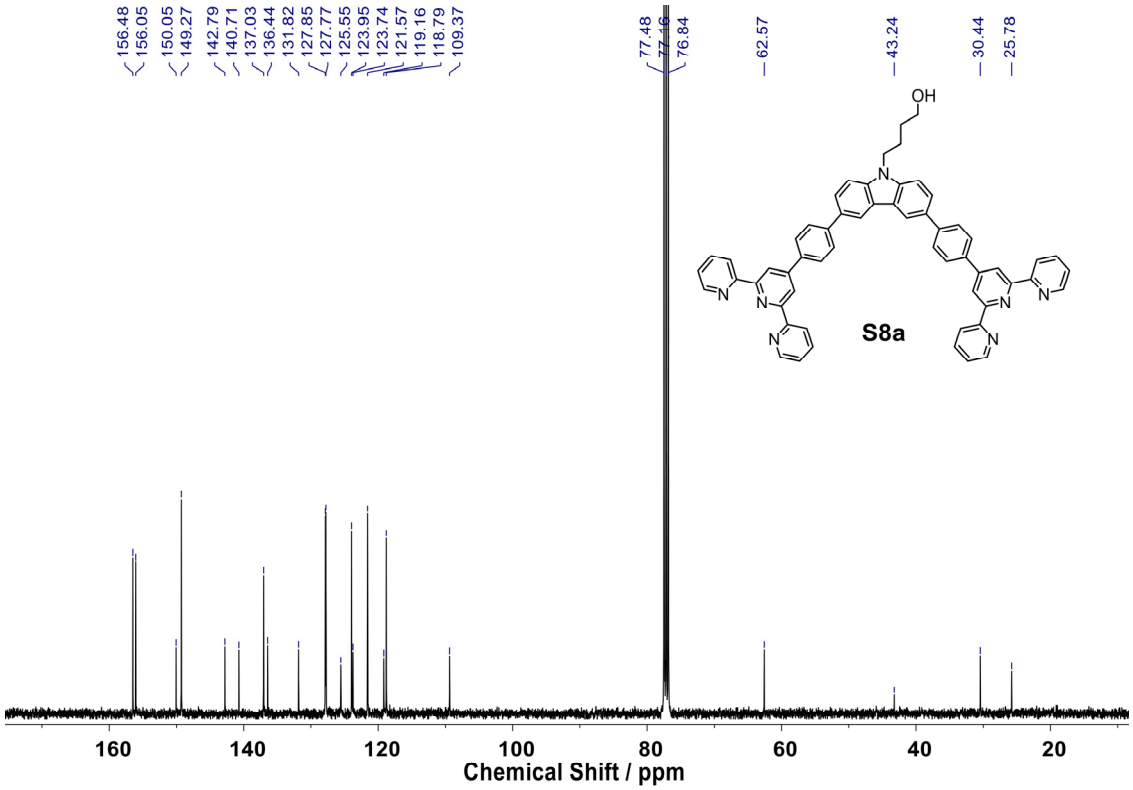

Figure S17. ^{13}C NMR spectrum (100 MHz, $CDCl_3$) of **S8a**.

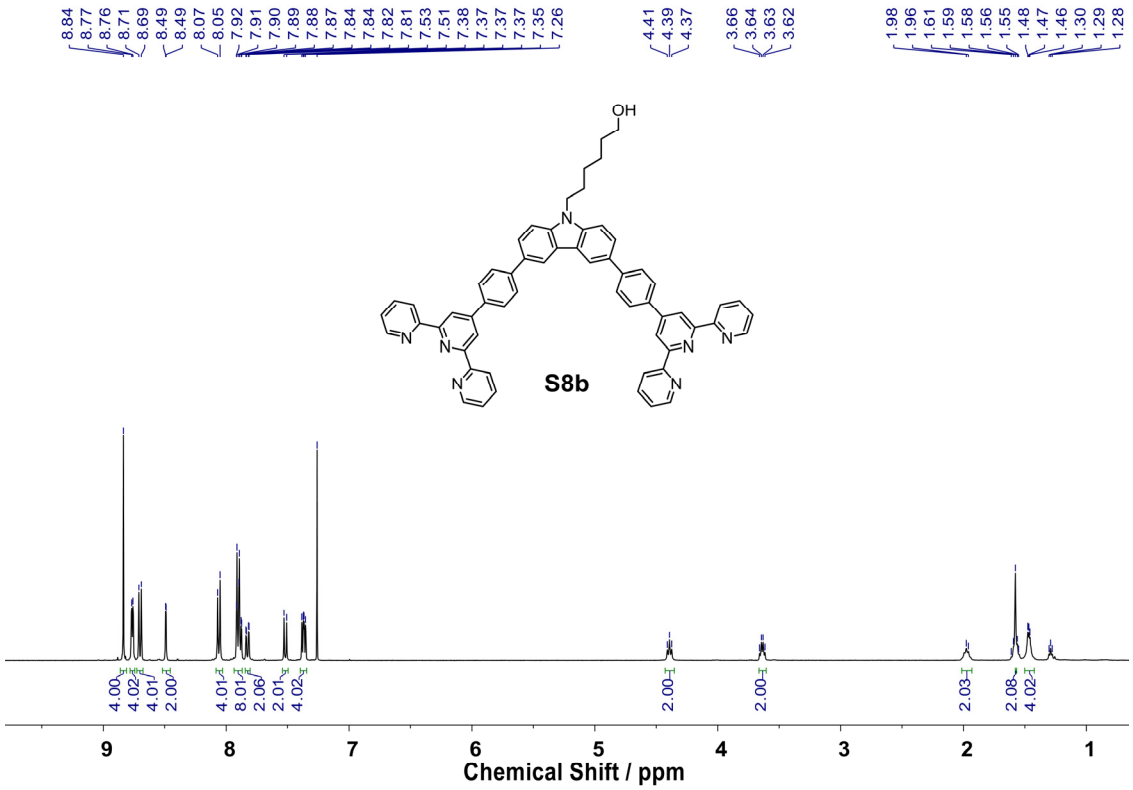

Figure S18. ^{1}H NMR spectrum (400 MHz, $CDCl_3$) of **S8b**.

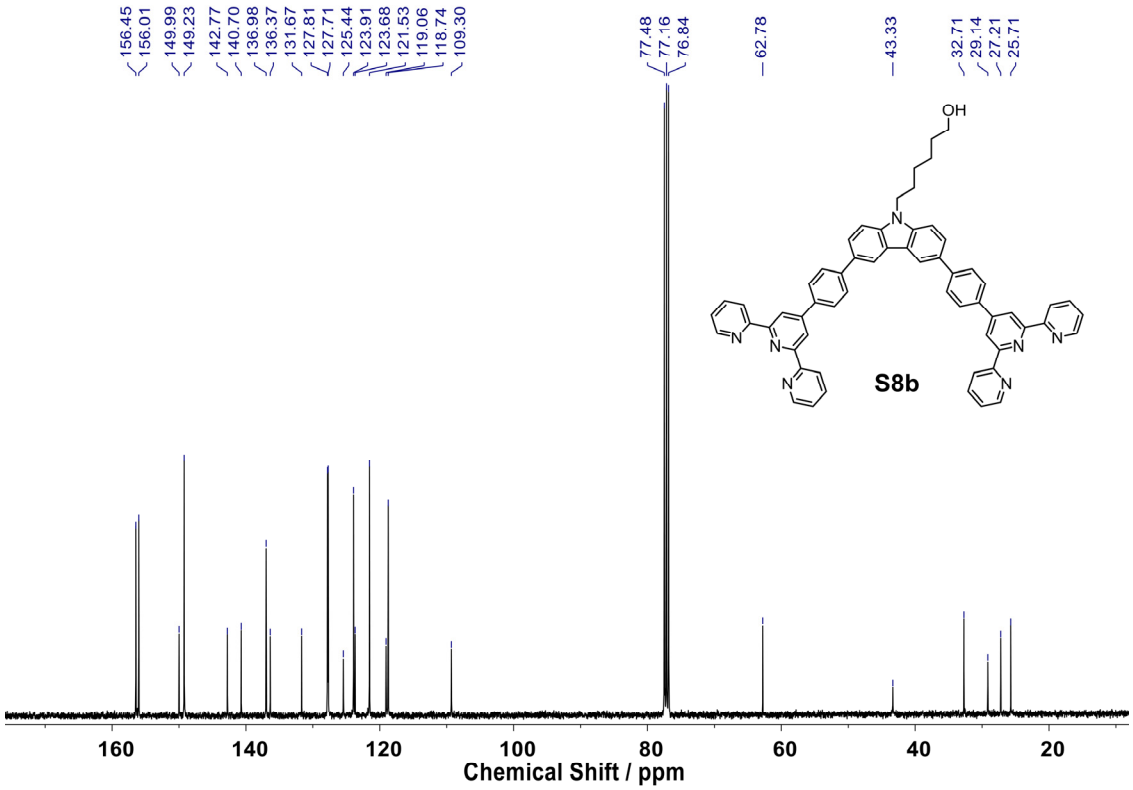

Figure S19. ^{13}C NMR spectrum (100 MHz, $CDCl_3$) of **S8b**.

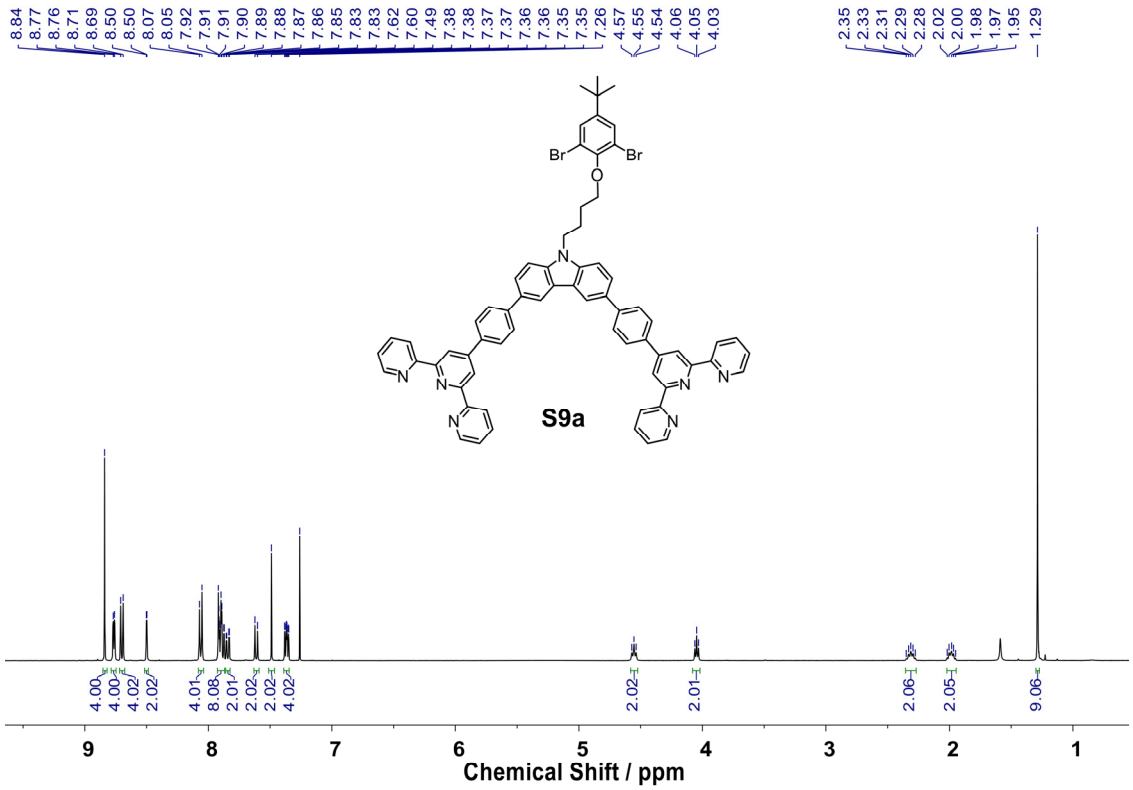

Figure S20. ^{1}H NMR spectrum (400 MHz, $CDCl_3$) of **S9a**.

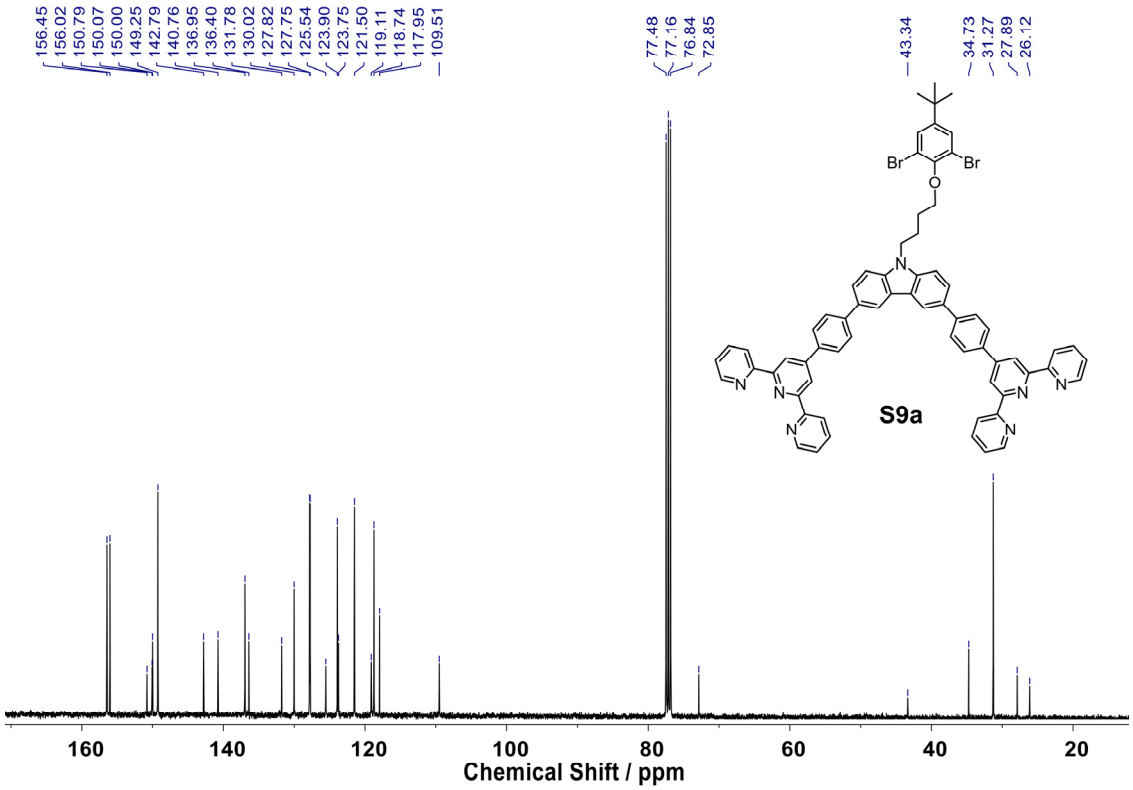

Figure S21. ^{13}C NMR spectrum (100 MHz, $CDCl_3$) of **S9a**.

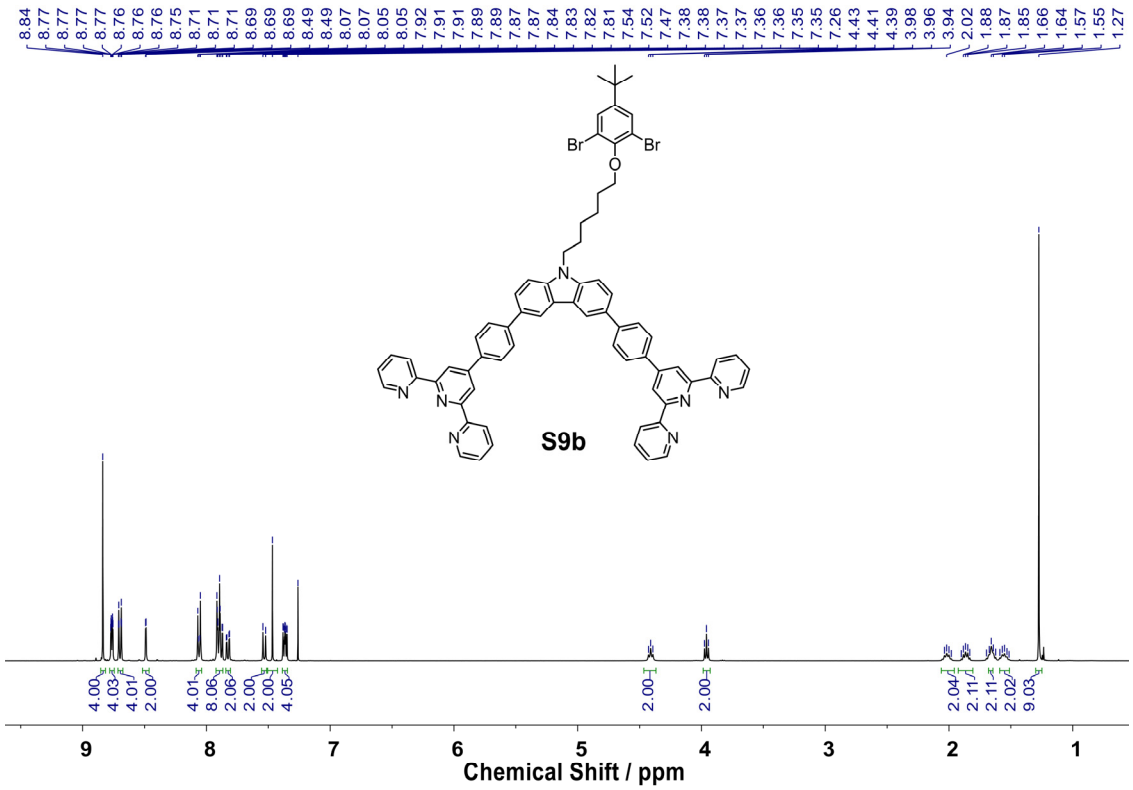

Figure S22. ^{1}H NMR spectrum (400 MHz, $CDCl_3$) of **S9b**.

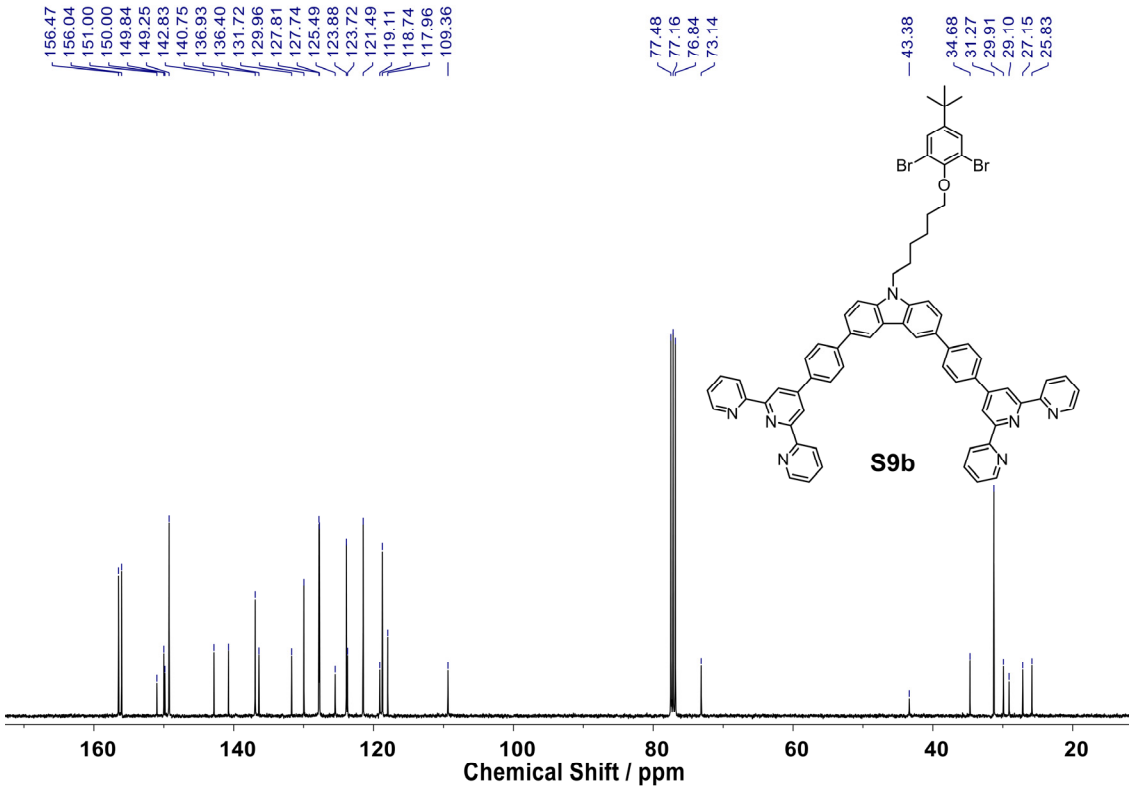

Figure S23. ^{13}C NMR spectrum (100 MHz, $CDCl_3$) of **S9b**.

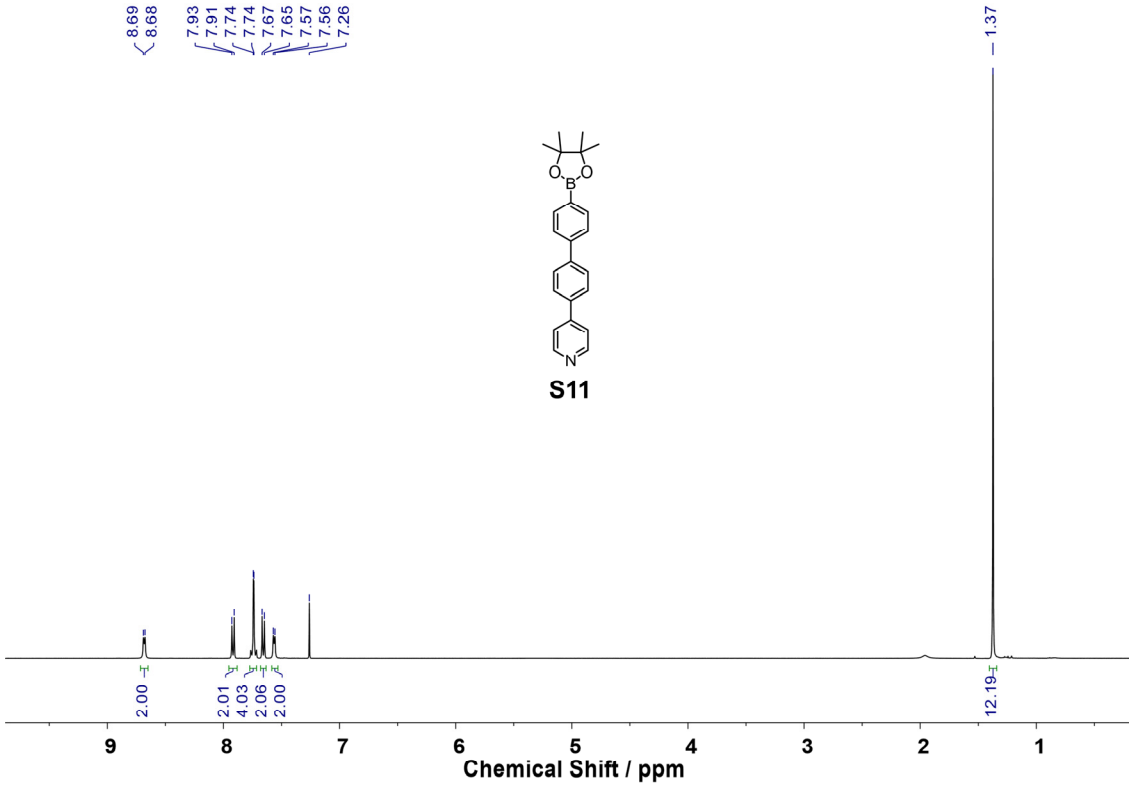

Figure S24. ^{1}H NMR spectrum (400 MHz, $CDCl_3$) of **S11**.

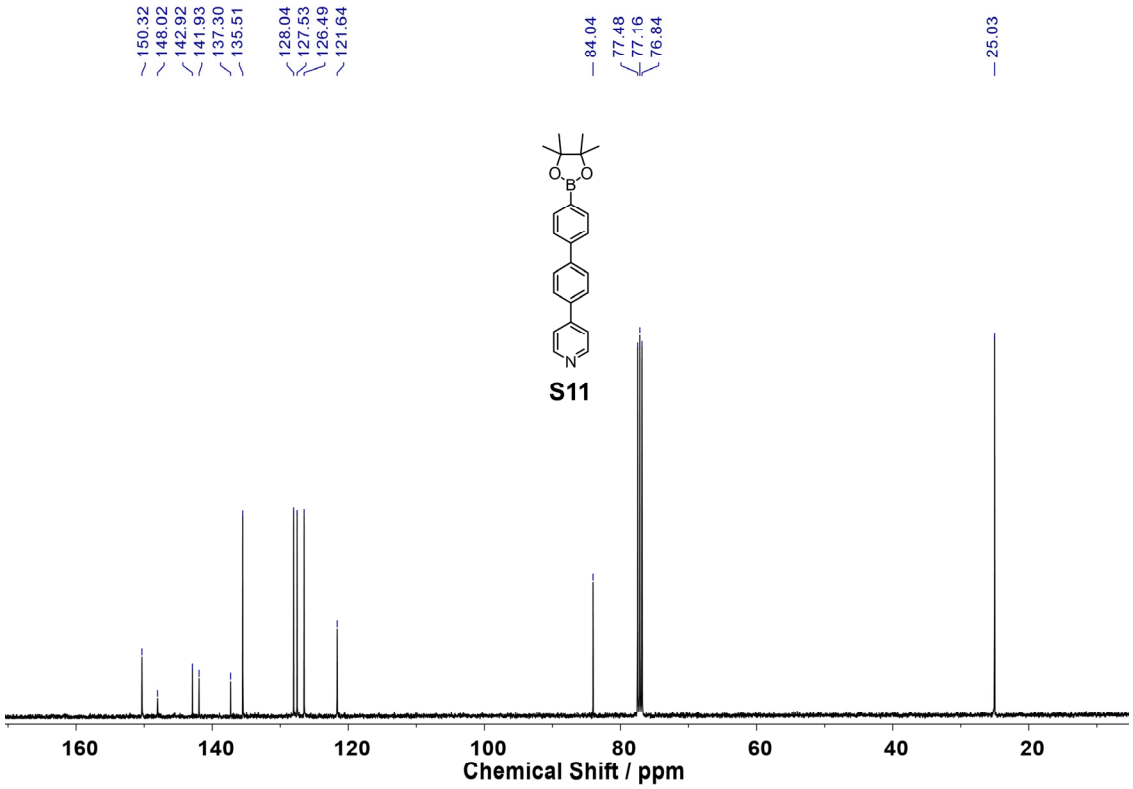

Figure S25. ^{13}C NMR spectrum (100 MHz, $CDCl_3$) of **S11**.

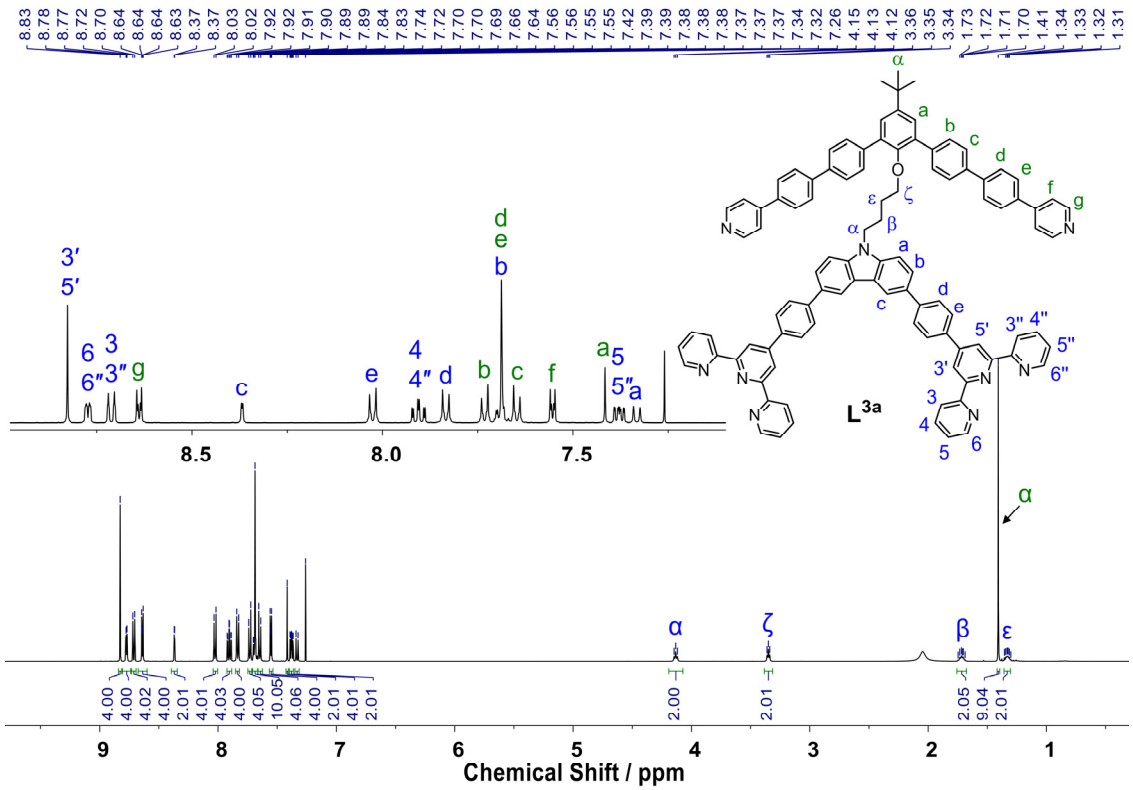

Figure S26. ^{1}H NMR spectrum (500 MHz, $CDCl_3$) of ligand $\mathbf{L^{3a}}$.

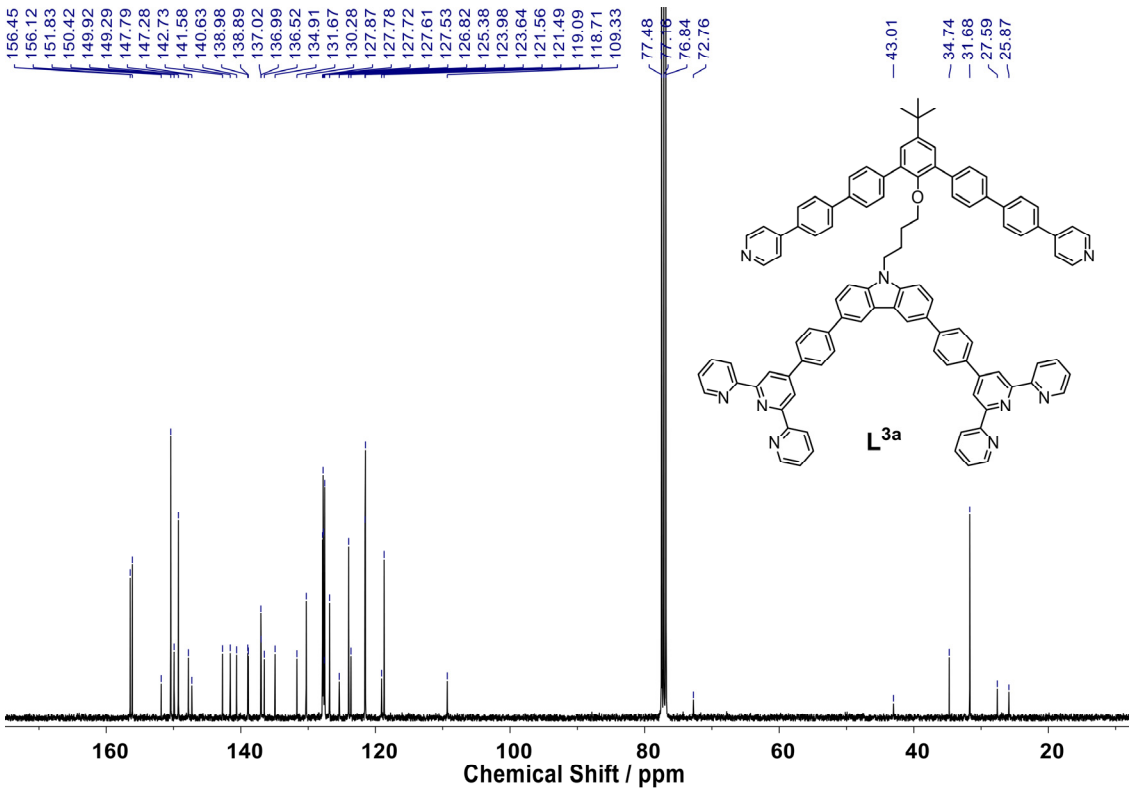

Figure S27. ^{13}C NMR spectrum (100 MHz, $CDCl_3$) of **L^{3a}**.

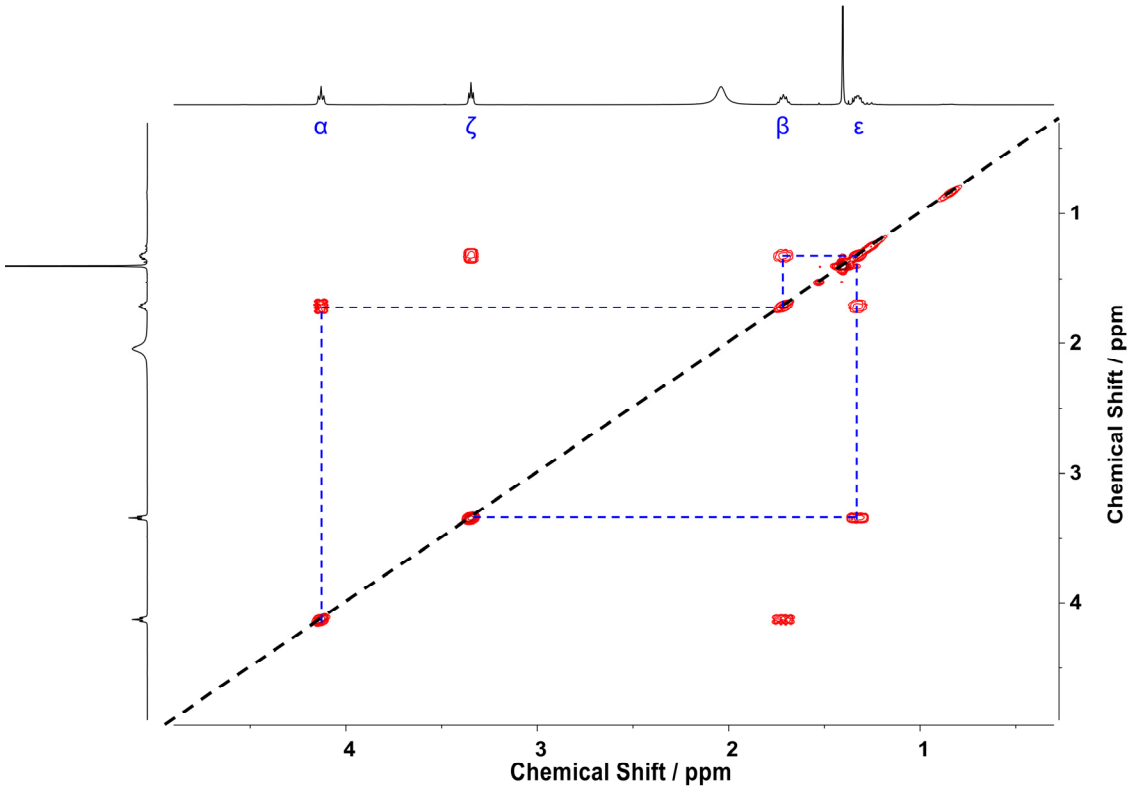

Figure S28. Partial COSY spectrum (500 MHz, $CDCl_3$) of ligand **L^{3a}**.

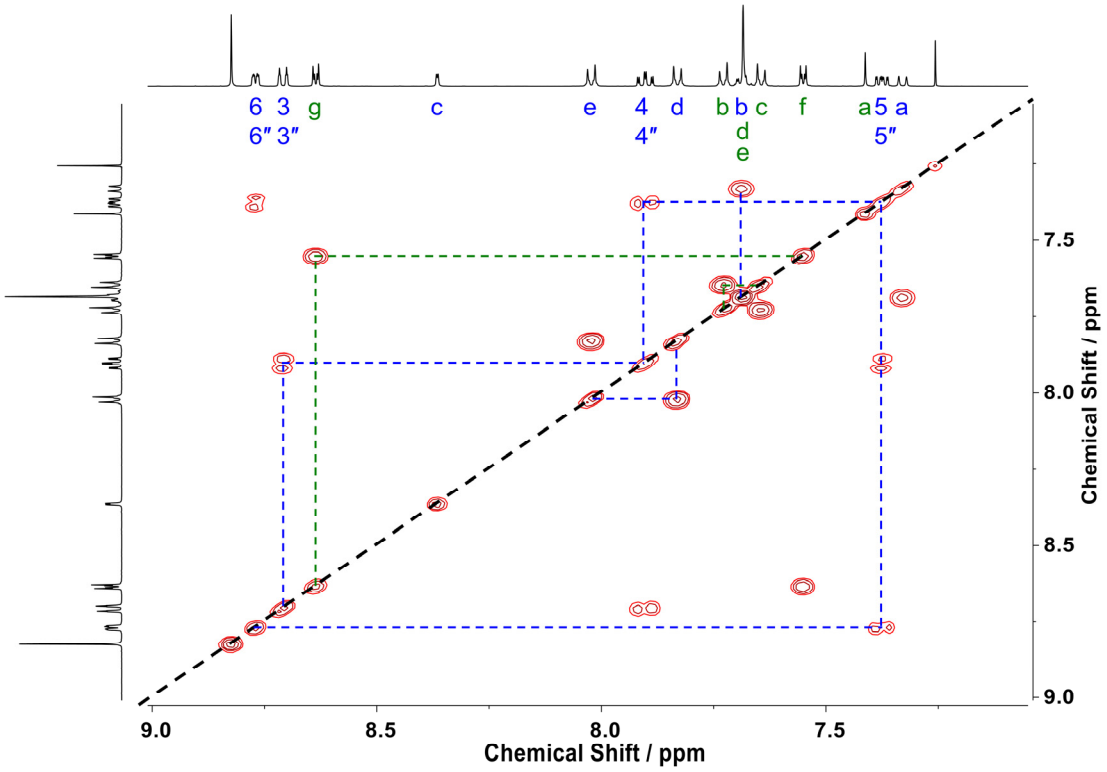

Figure S29. Partial COSY spectrum (500 MHz, $CDCl_3$) of igand $\mathbf{L^{3a}}$.

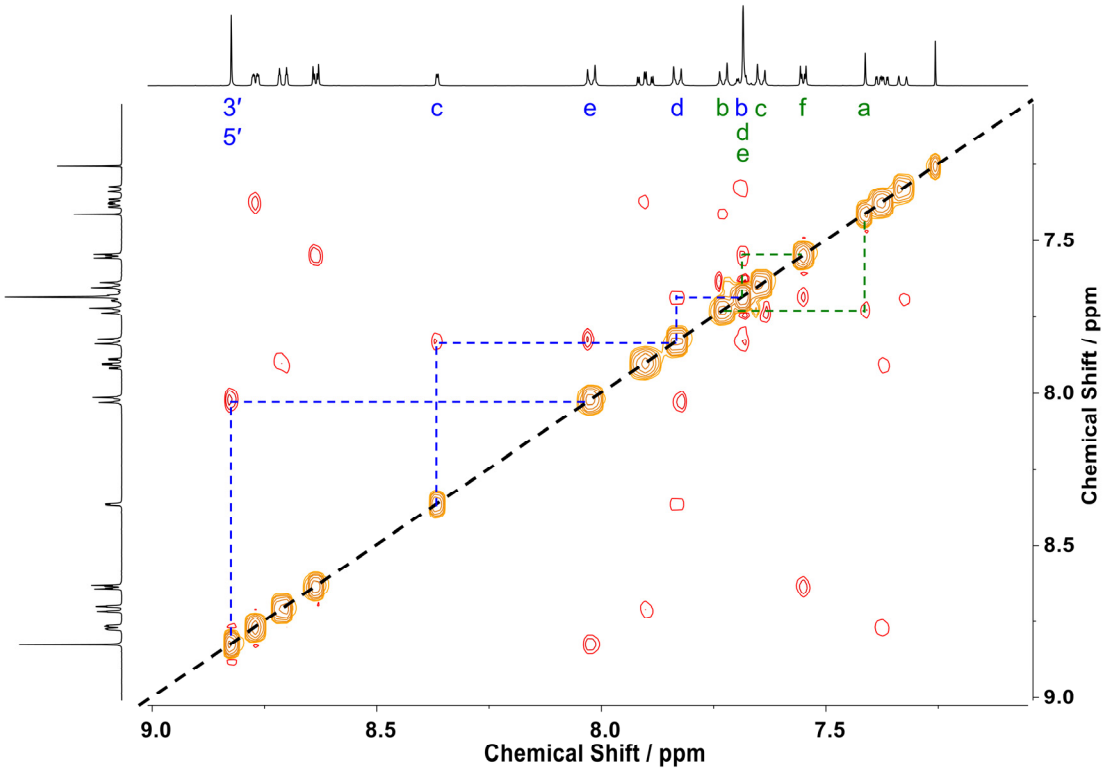

Figure S30. Partial ROESY spectrum (500 MHz, $CDCl_3$) of ligand $\mathbf{L^{3a}}$.

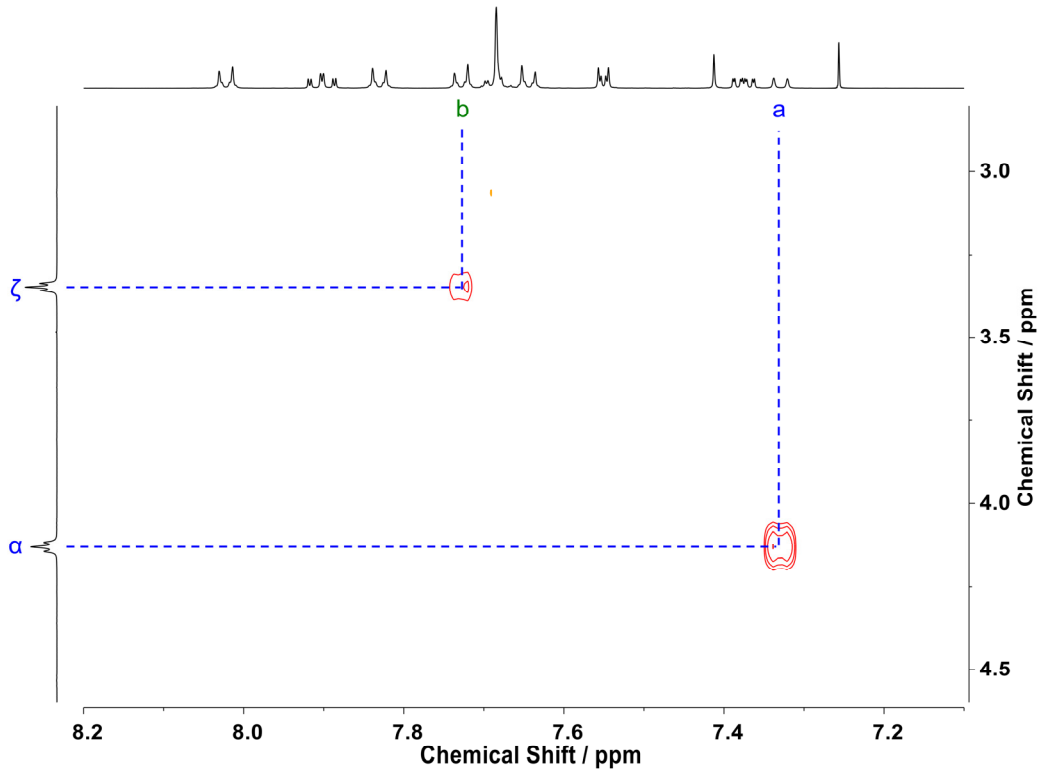

Figure S31. Partial ROESY spectrum (500 MHz, $CDCl_3$) of $\mathbf{L^{3a}}$.

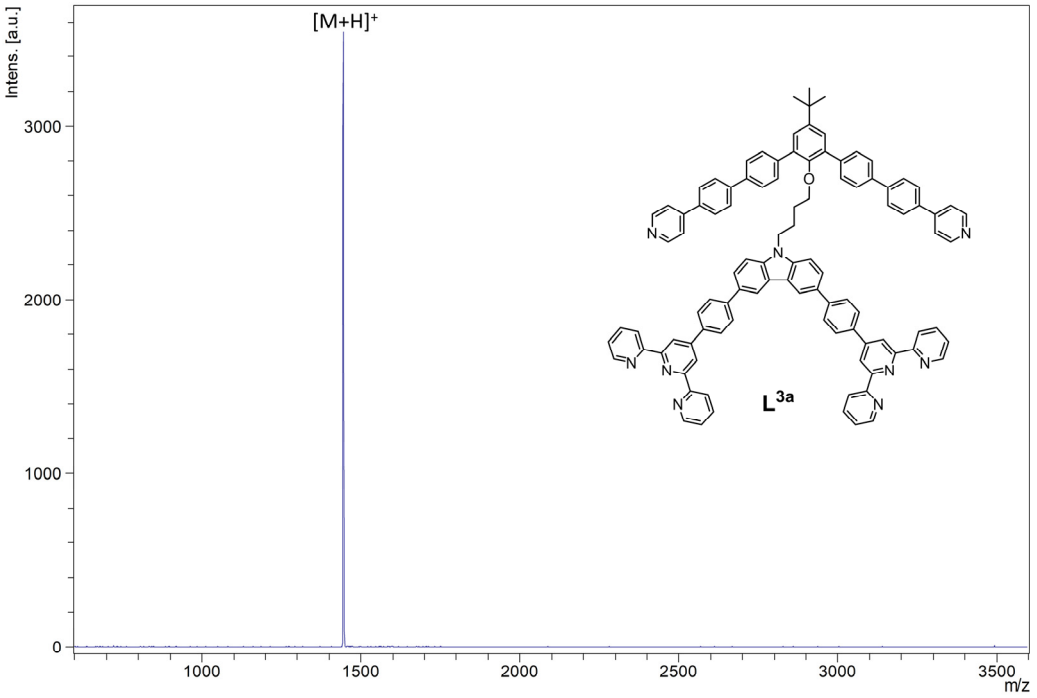

Figure S32. High-resolution MALDI-TOF-MS spectrum of $\mathbf{L^{3a}}$.

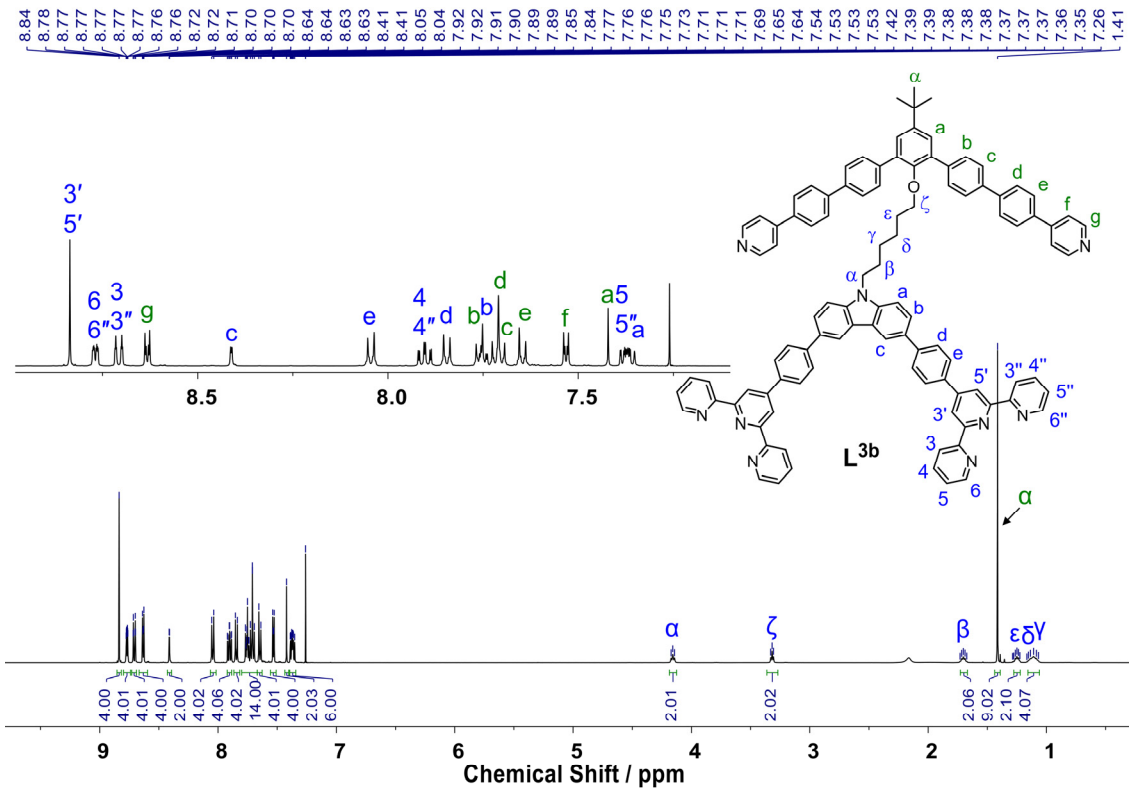

Figure S33. ^{1}H NMR Spectrum (500 MHz, $CDCl_3$) of ligand $\mathbf{L^{3b}}$.

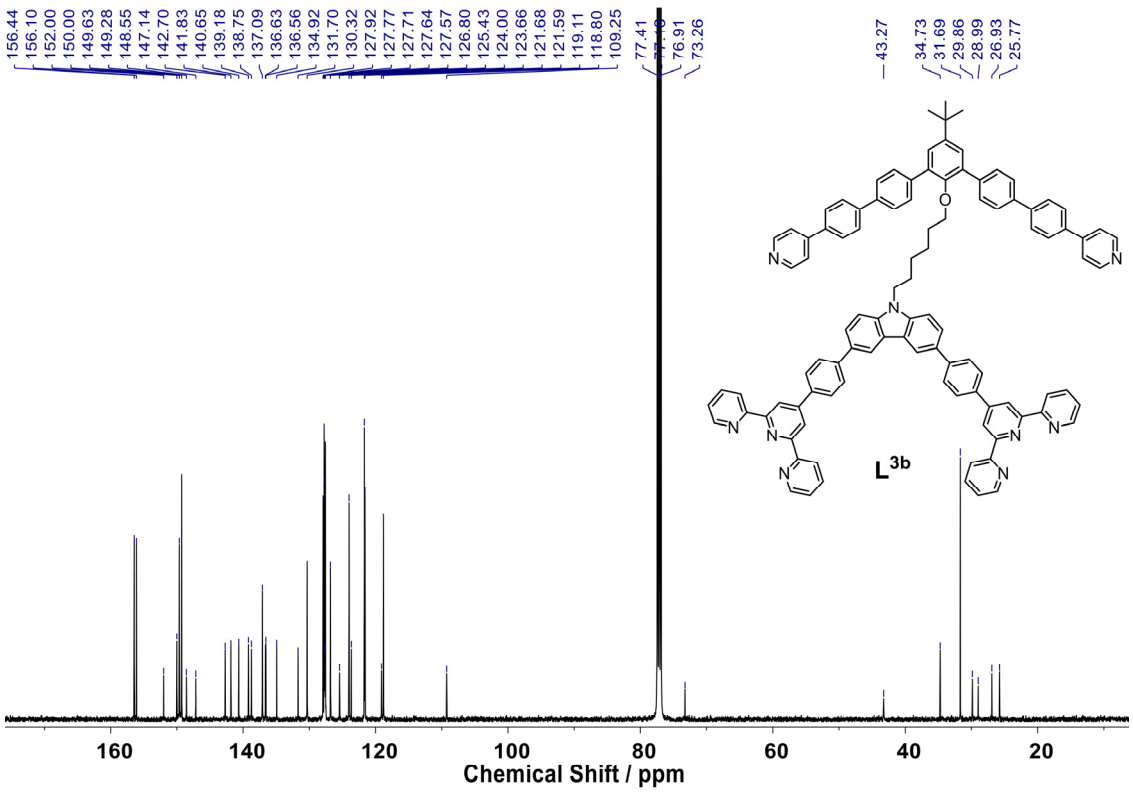

Figure S34. ^{13}C NMR spectrum (125 MHz, $CDCl_3$) of ligand $\mathbf{L^{3b}}$.

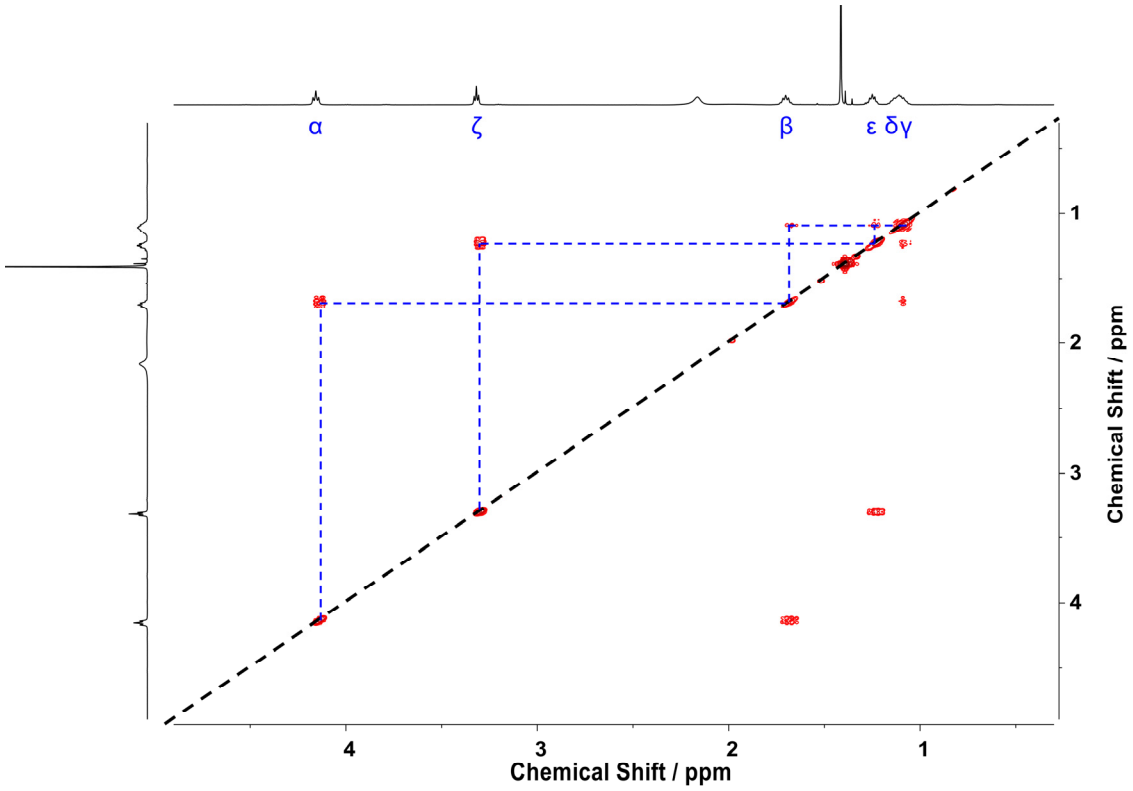

Figure S35. Partial COSY spectrum (500 MHz, $CDCl_3$) of ligand $\mathbf{L^{3b}}$.

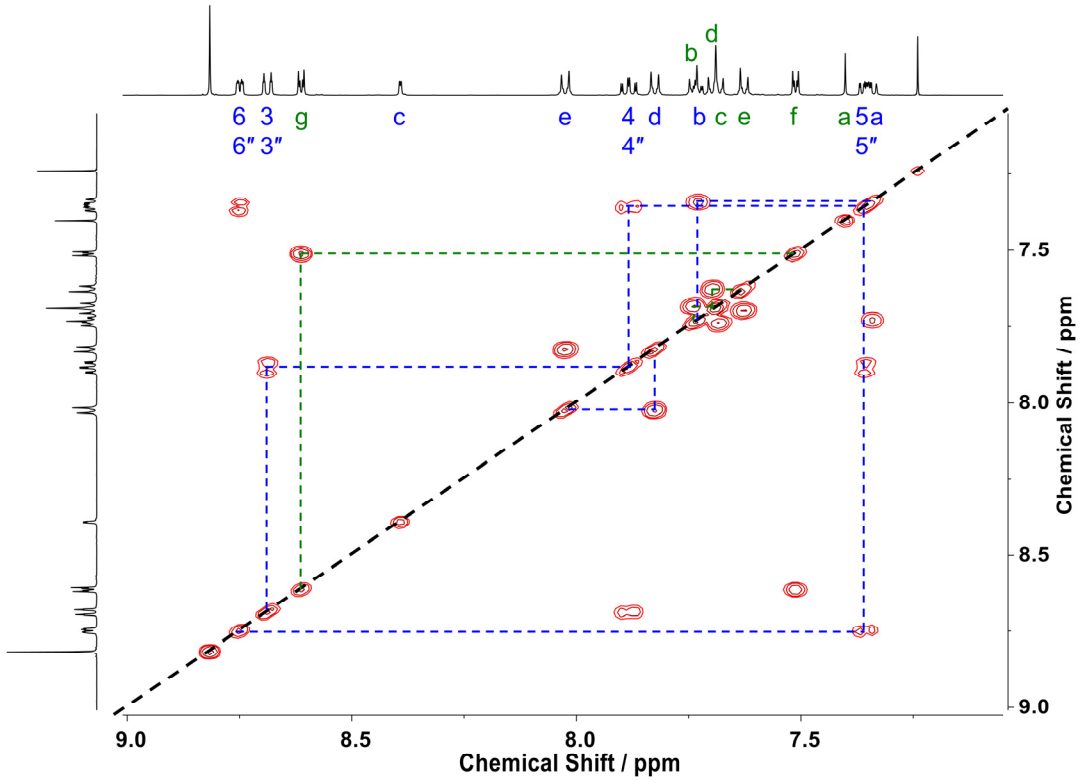

Figure S36. Partial COSY spectrum (500 MHz, $CDCl_3$) of ligand $\mathbf{L^{3b}}$.

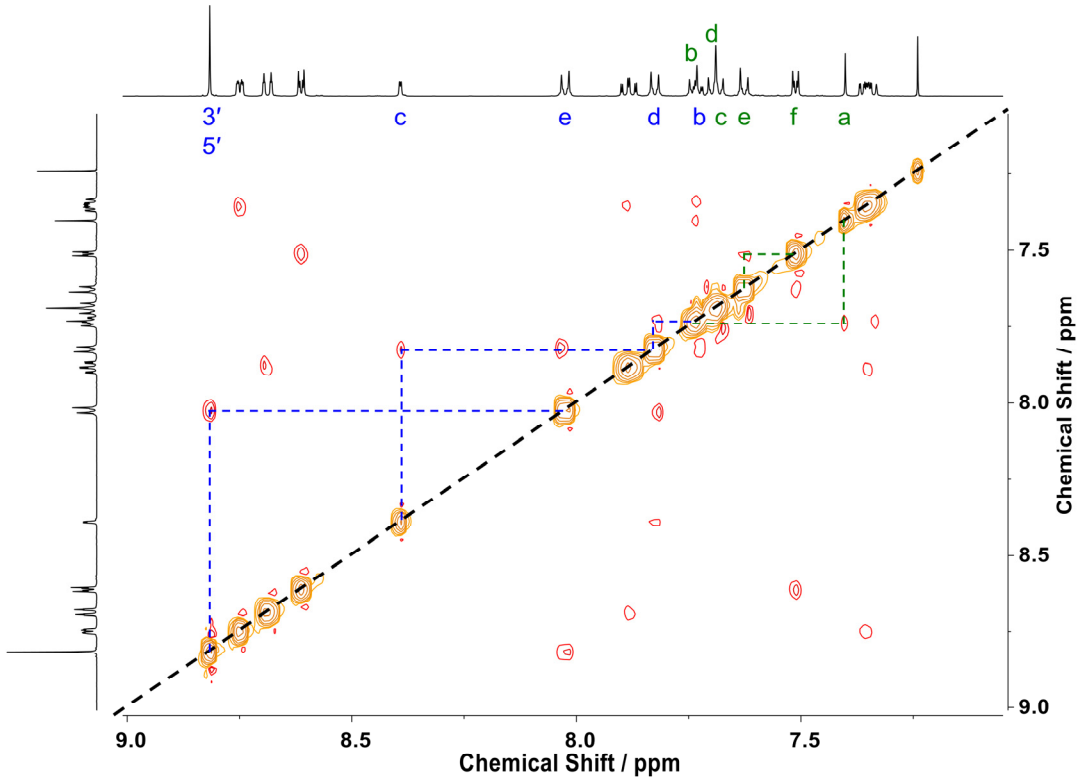

Figure S37. Partial ROESY spectrum (500 MHz, $CDCl_3$) of ligand $\mathbf{L^{3b}}$.

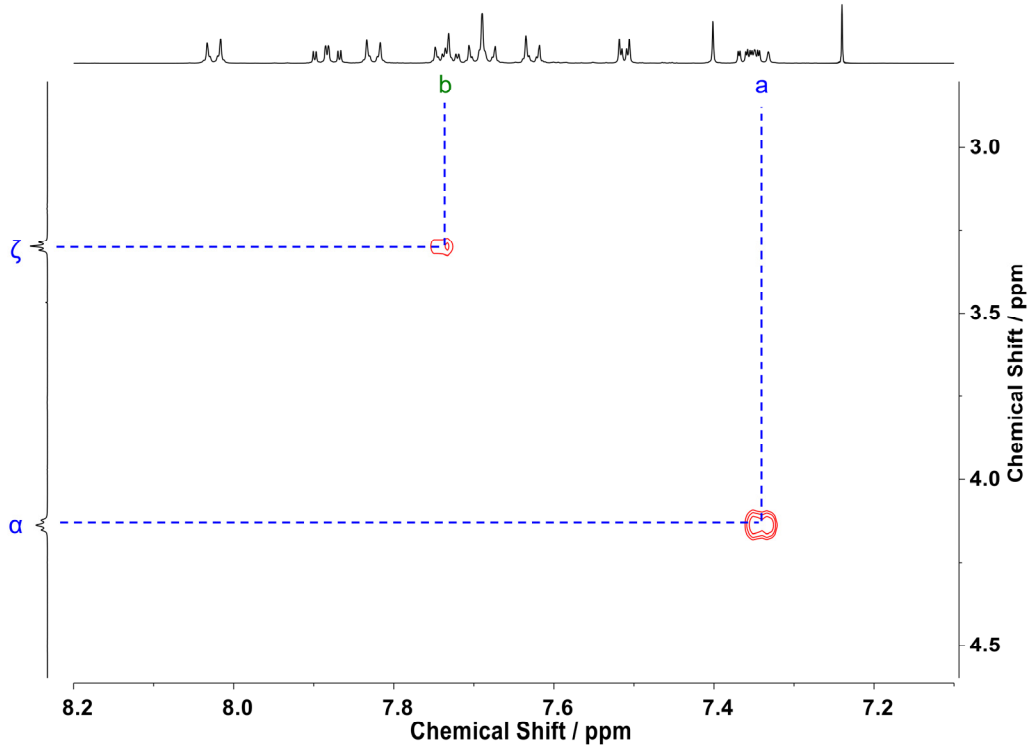

Figure S38. Partial ROESY spectrum (500 MHz, $CDCl_3$) of ligand $\mathbf{L^{3b}}$.

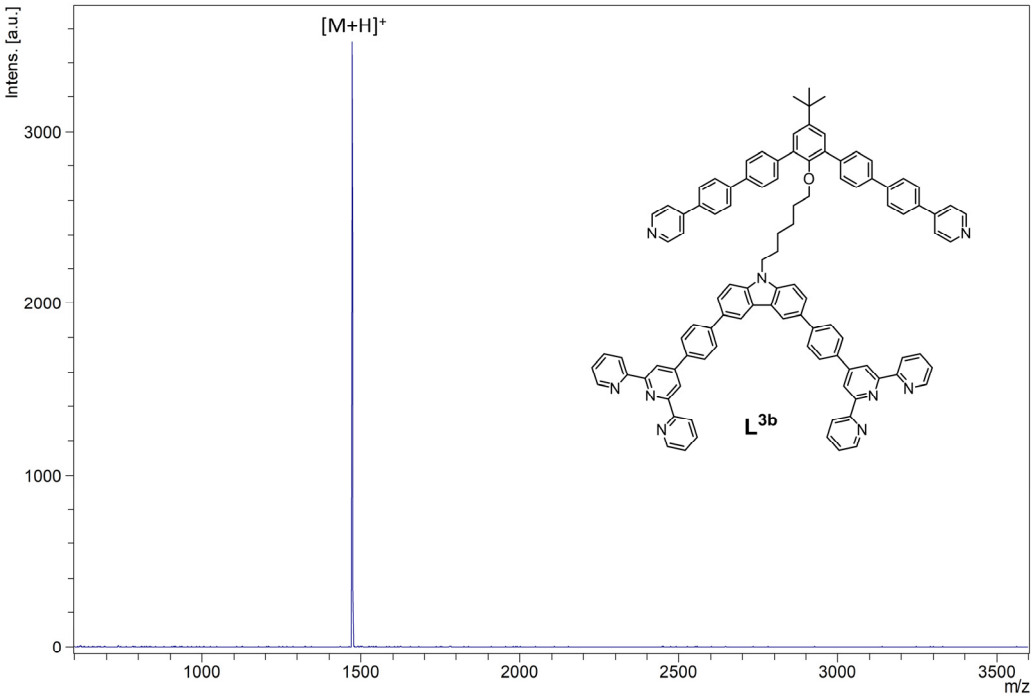

Figure S39. High-resolution MALDI-TOF-MS spectrum of ligand $\mathbf{L^{3b}}$.

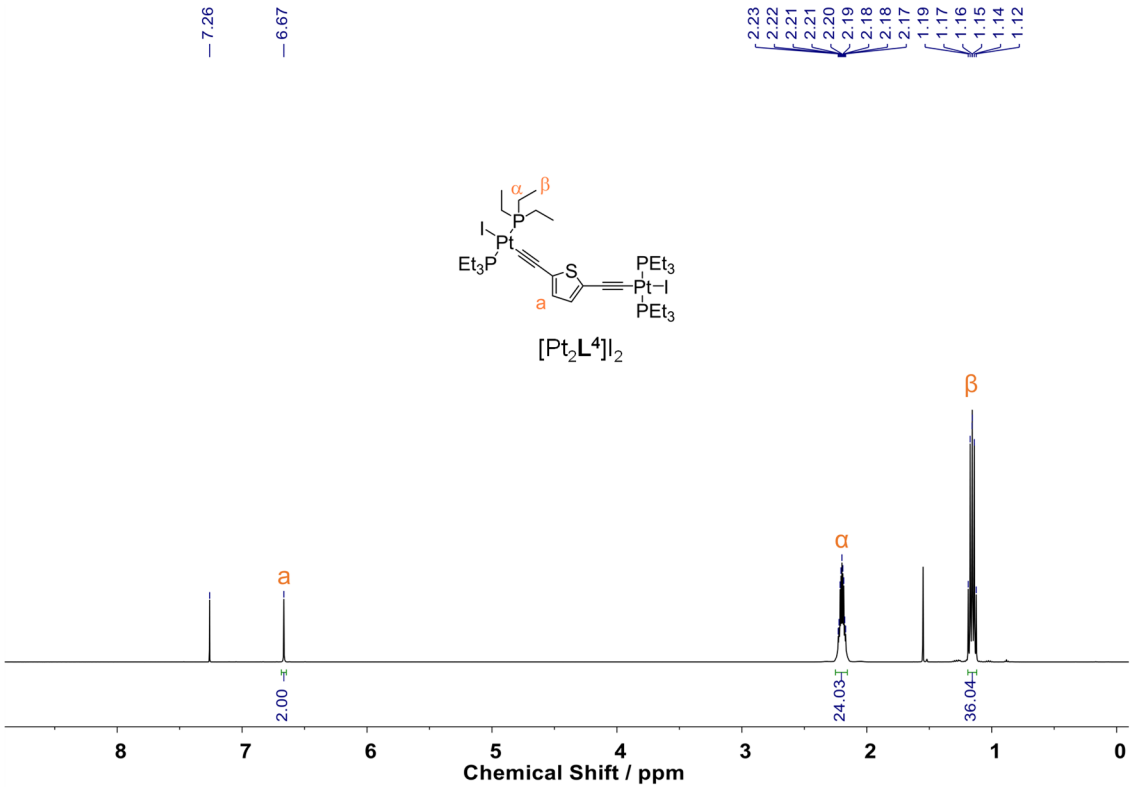

Figure S40. ^{1}H NMR spectrum (500 MHz, $CDCl_3$) of $[Pt_2\mathbf{L^4}]I_2$.

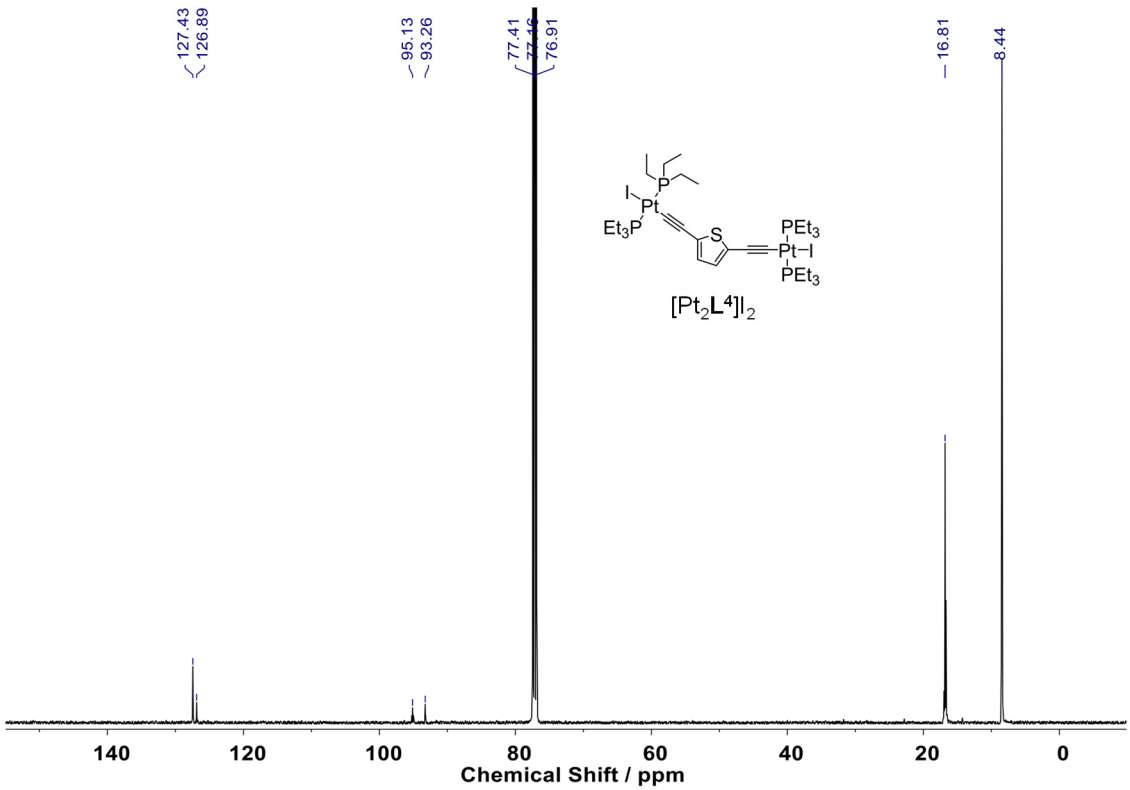

Figure S41. ^{13}C NMR spectrum (125 MHz, $CDCl_3$) of $[Pt_2\mathbf{L^4}]I_2$.

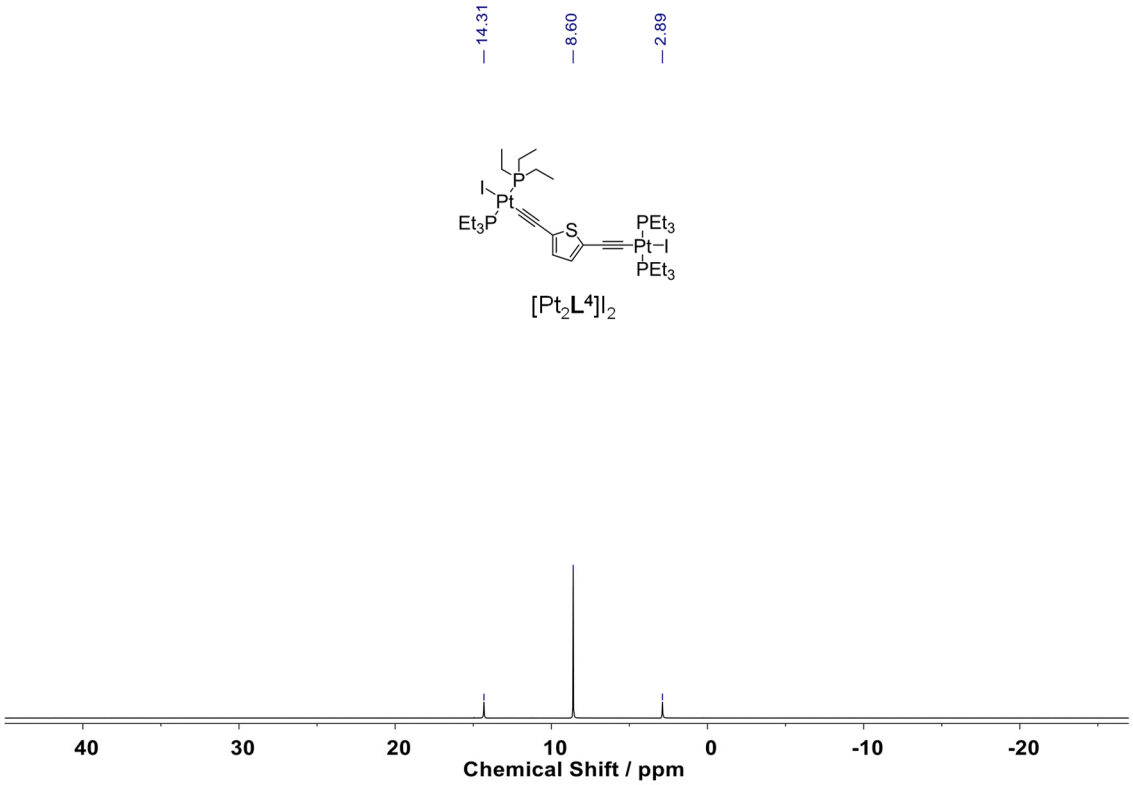

Figure S42. ^{31}P NMR spectrum (202 MHz, $CDCl_3$) of $[Pt_2\mathbf{L^4}]I_2$.

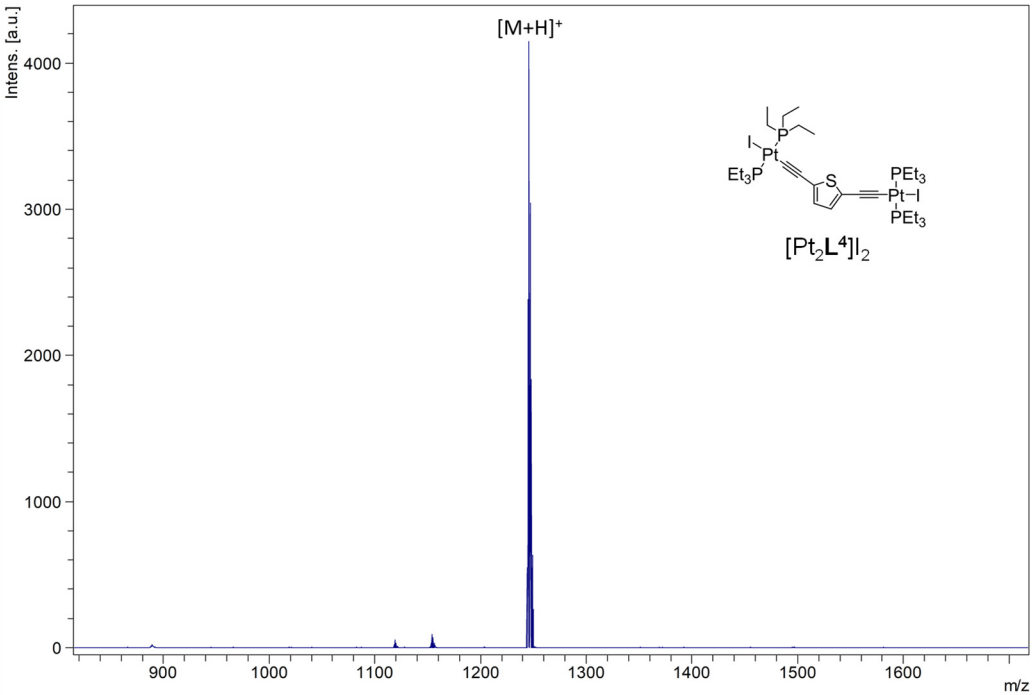

Figure S43. High-resolution MALDI-TOF-MS spectrum of $[Pt_2\mathbf{L^4}]I_2$.

Self-Assembly of Complexes

General Procedure for [$Cd_8L^1_2L^2_4$]: To a $CHCl_3$ solution (5 mL) of ligands, a MeOH solution (5 mL) of $Cd(NO_3)_2{\cdot}4H_2O$ was added. Subsequently, MeCN (5 mL) was added in order to improve the solubility of the resulting mixture. The reaction mixture was stirred at 60 ºC for 12 h to give a homogeneous solution. A 20-fold excess of NH_4PF_6 in MeOH was added to exchange the counterion. After being stirred at 25 °C for 30 mins, the solution was evaporated to dryness under reduced pressure. A white suspension was obtained after the addition of water, which was filtered, washed with H_2O and MeOH, and then dried *in vacuo*. The resultant solid was then dissolved in CD_3CN (6 mg mL^{-1}) and heated at 80 ºC for 8 h. ^{1}H NMR and ESI-MS were employed to monitor the complexation reaction.

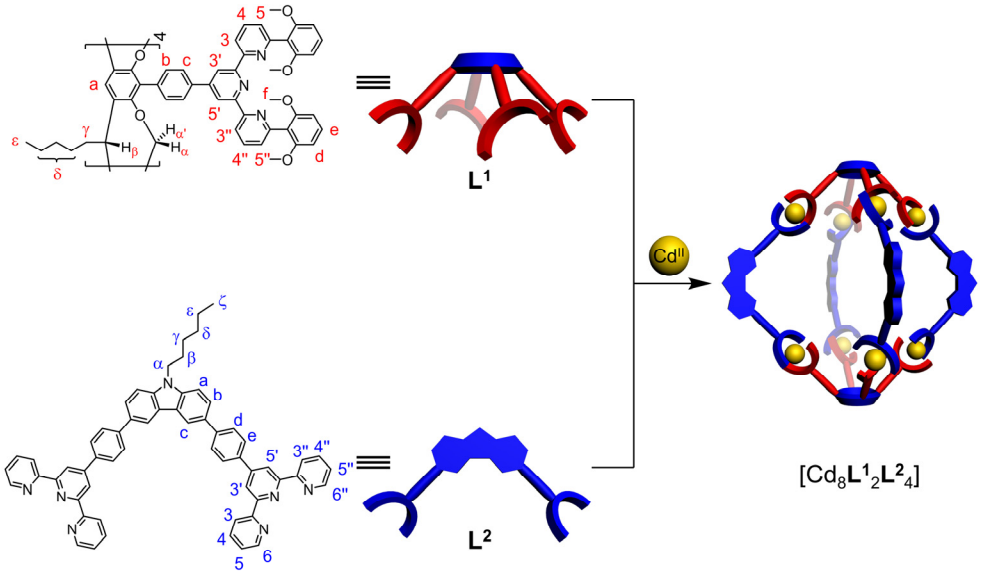

Scheme S5. Self-assembly of dimeric sphere [$Cd_8L^1_2L^2_4$].

[$Cd_8L^1_2L^2_4$]: By the general procedure, after 8 h of heating at 80 ºC, [$Cd_8L^1_2L^2_4$] was obtained in quantitative yield from **L¹** (6.0 μmol, 18.8 mg), **L²** (12.0 μmol, 10.4 mg), $Cd(NO_3)_2{\cdot}4H_2O$ (24.0 μmol, 7.4 mg) and NH_4PF_6 (960.0 μmol, 156 mg). ^{1}H NMR (400 MHz, CD_3CN): δ (ppm) 9.09 (s, 16H), 8.81 (s, 8H), 8.77 (d, J = 8.2 Hz, 16H), 8.53 (d, J = 8.2 Hz, 16H), 8.44 (s, 16H), 8.35 (d, J = 8.2 Hz, 16H), 8.26-8.20 (m, 32H), 8.18-8.07 (m, 32H), 8.07-7.96 (m, 24H), 7.89 (s, 8H), 7.78 (d, J = 8.7 Hz, 8H), 7.58 (d, J = 8.1 Hz, 16H), 7.46 (br, 16H), 7.16 (d, J = 7.0 Hz, 16H), 6.78 (t, J = 8.4 Hz, 16H), 5.86 (d, J = 8.6 Hz, 32H), 5.48 (d, J = 6.8 Hz, 8H), 5.03 (t, J = 7.8 Hz, 8H), 4.63 (d, J = 6.6 Hz, 8H), 4.53 (br, 8H), 2.83 (s, 96H), 2.69 (br,16H), 2.02-1.93 (m, 8H), 1.62-1.55 (m, 48H), 1.46-1.27 (m, 24H), 1.09 (t, J = 7.0 Hz, 24H), 0.90 (t, J = 7.1 Hz, 12H). ^{113}Cd NMR (111 MHz, CD_3CN): δ (ppm) 242.64.

ESI-MS (*m/z*):

Charge state	Composition	Theoretical *m/z*	Experimental *m/z*
5+	$[M - 5PF_6]^{5+}$	2446.0096	2446.0552
6+	$[M - 6PF_6]^{6+}$	2014.0162	2014.0487
7+	$[M - 7PF_6]^{7+}$	1705.7312	1705.7497
8+	$[M - 8PF_6]^{8+}$	1474.2717	1474.2790
9+	$[M - 9PF_6]^{9+}$	1294.3608	1294.3633
10+	$[M - 10PF_6]^{10+}$	1150.4254	1150.4232
11+	$[M - 11PF_6]^{11+}$	1032.6589	1032.6554
12+	$[M - 12PF_6]^{12+}$	934.5265	934.5188
13+	$[M - 13PF_6]^{13+}$	851.4906	851.4779

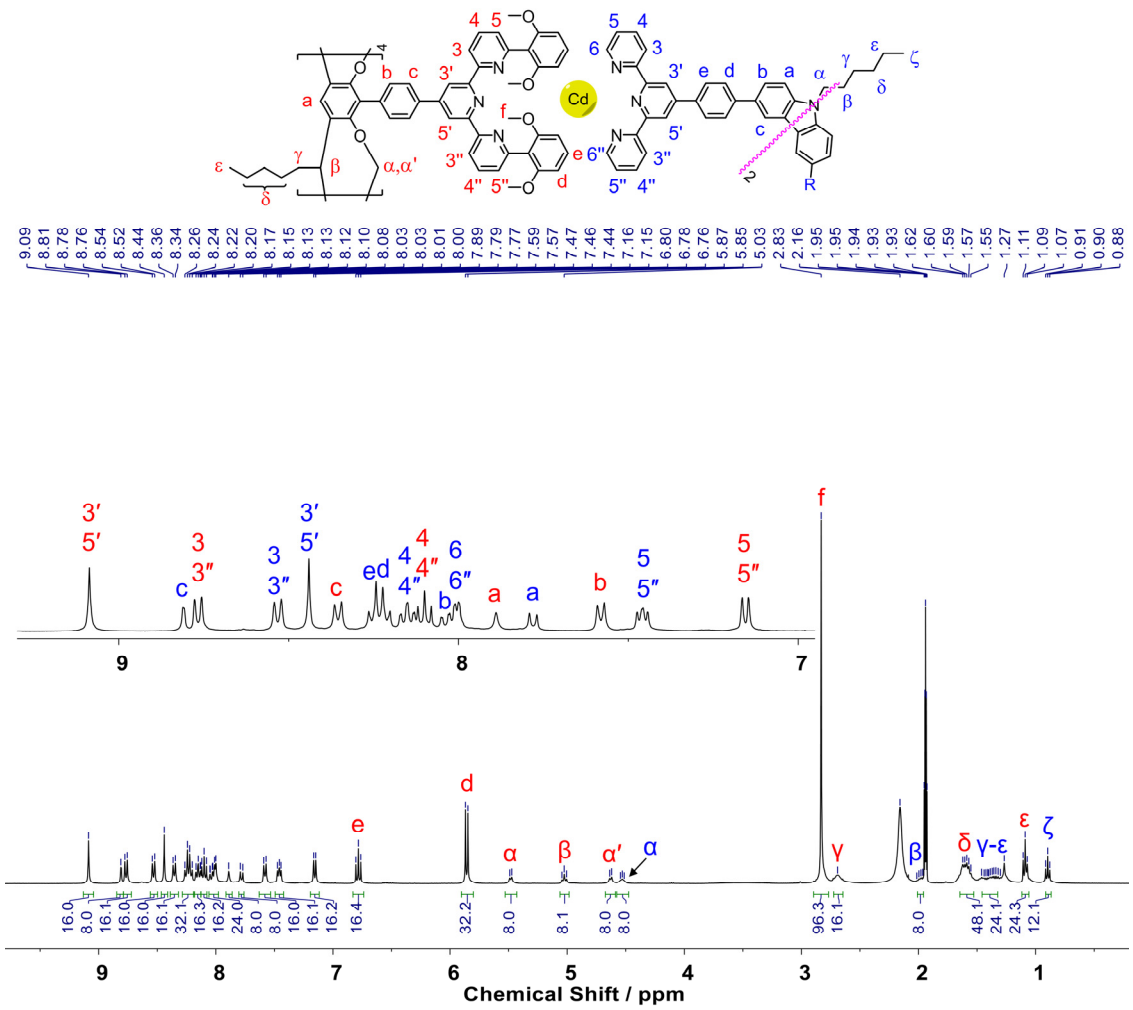

Figure S44. ^{1}H NMR spectrum (400 MHz, CD_3CN) of $[Cd_8\mathbf{L^1}_2\mathbf{L^2}_4]$.

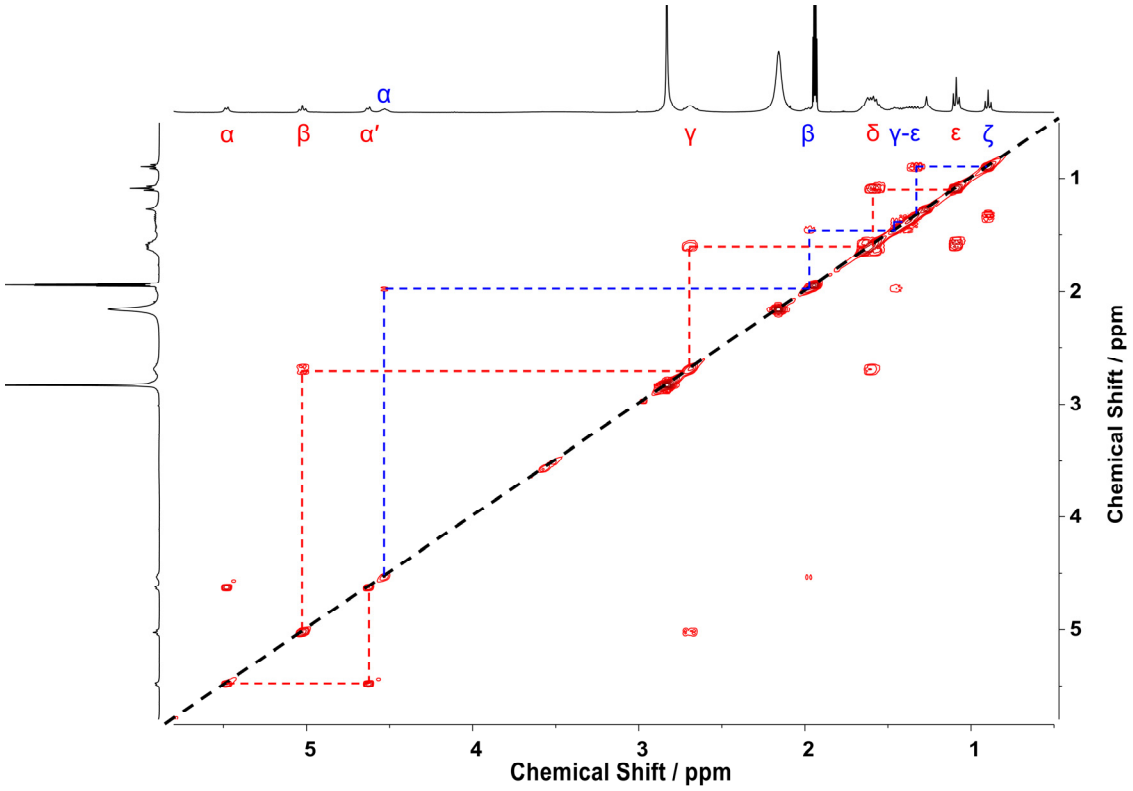

Figure S45. Partial COSY spectrum (400 MHz, CD_3CN) of $[Cd_8\mathbf{L^1}_2\mathbf{L^2}_4]$.

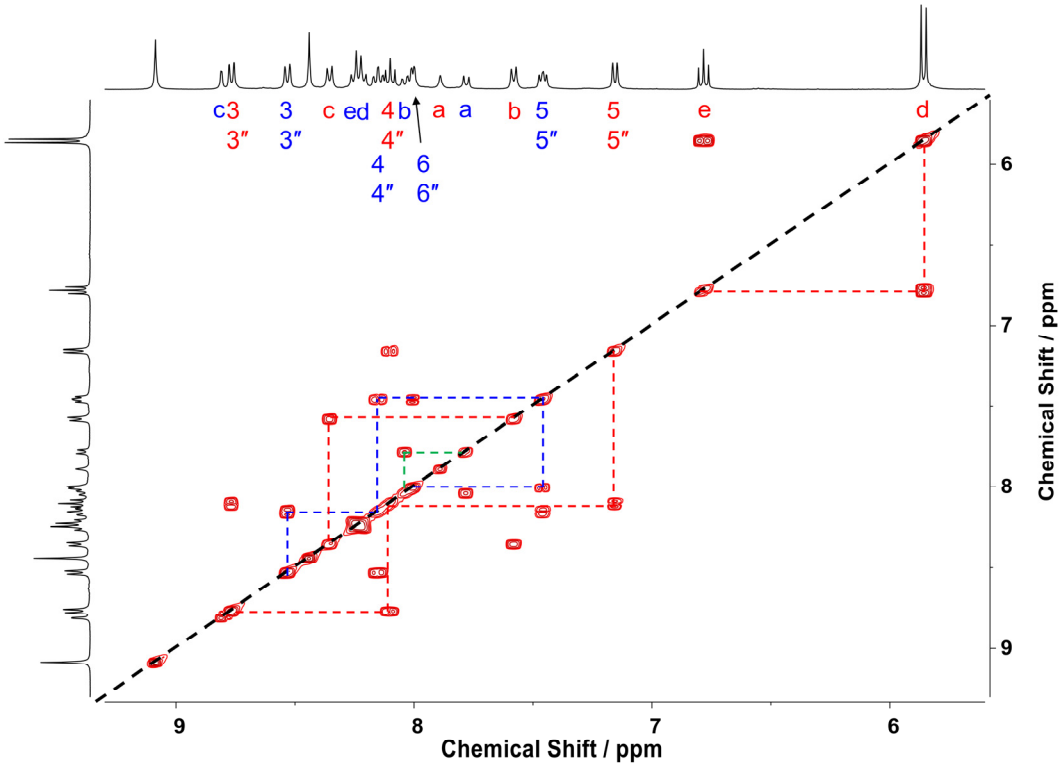

Figure S46. Partial COSY spectrum (400 MHz, CD_3CN) of $[Cd_8\mathbf{L^1}_2\mathbf{L^2}_4]$.

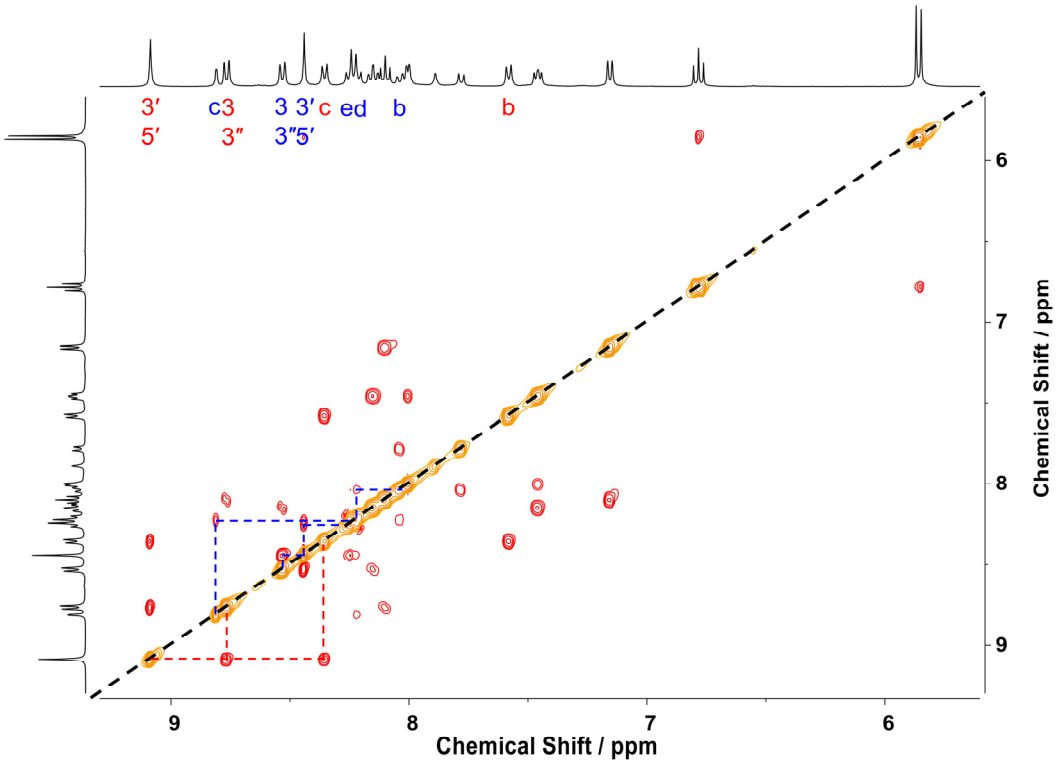

Figure S47. Partial ROESY spectrum (400 MHz, CD_3CN) of $[Cd_8\mathbf{L^1}_2\mathbf{L^2}_4]$.

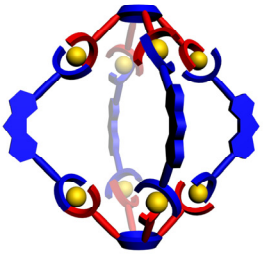

$[Cd_8\mathbf{L^1}_2\mathbf{L^2}_4]$

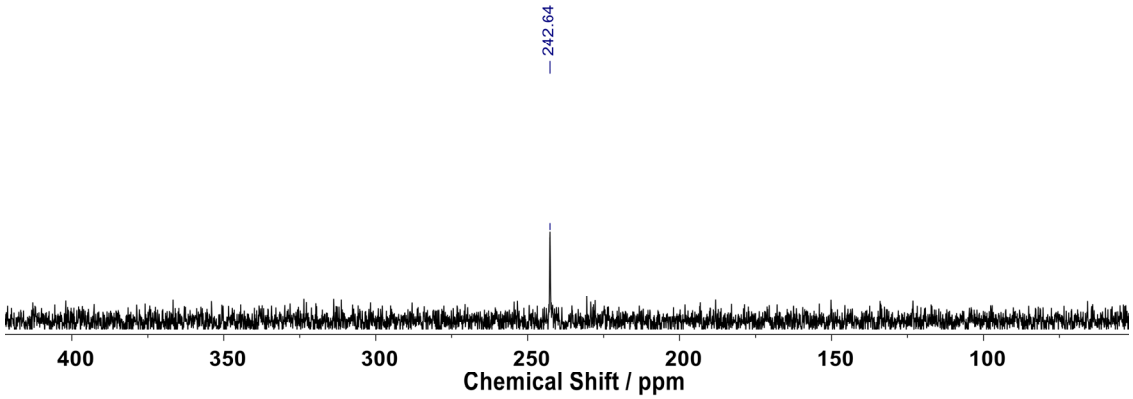

Figure S48. ^{113}Cd NMR spectrum (111 MHz, CD_3CN) of $[Cd_8\mathbf{L^1}_2\mathbf{L^2}_4]$.

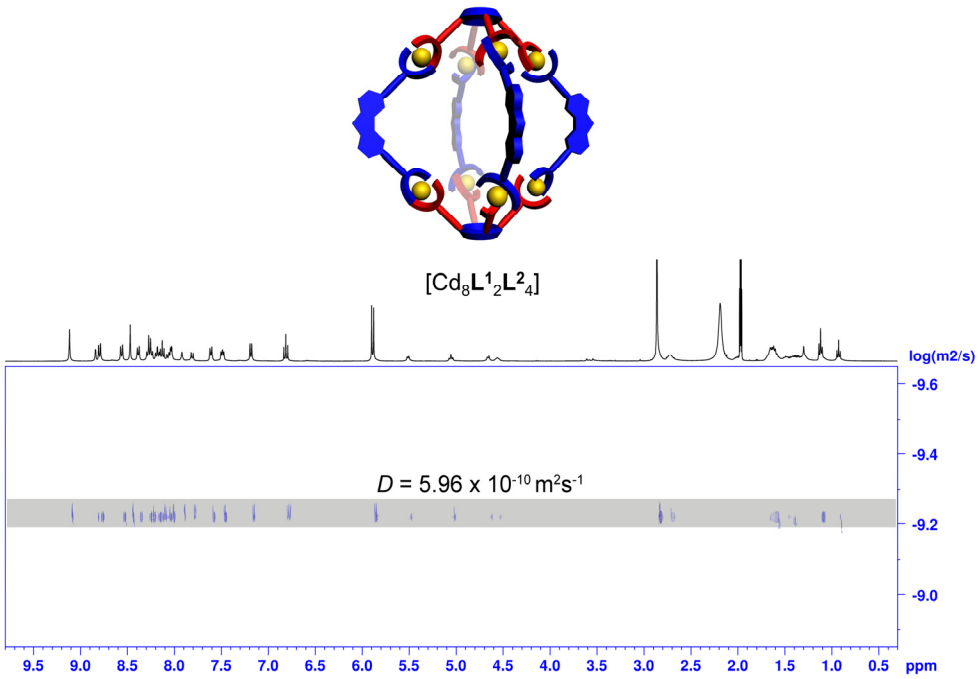

Figure S49. DOSY spectrum (500 MHz, CD_3CN) of $[Cd_8\mathbf{L^1}_2\mathbf{L^2}_4]$.

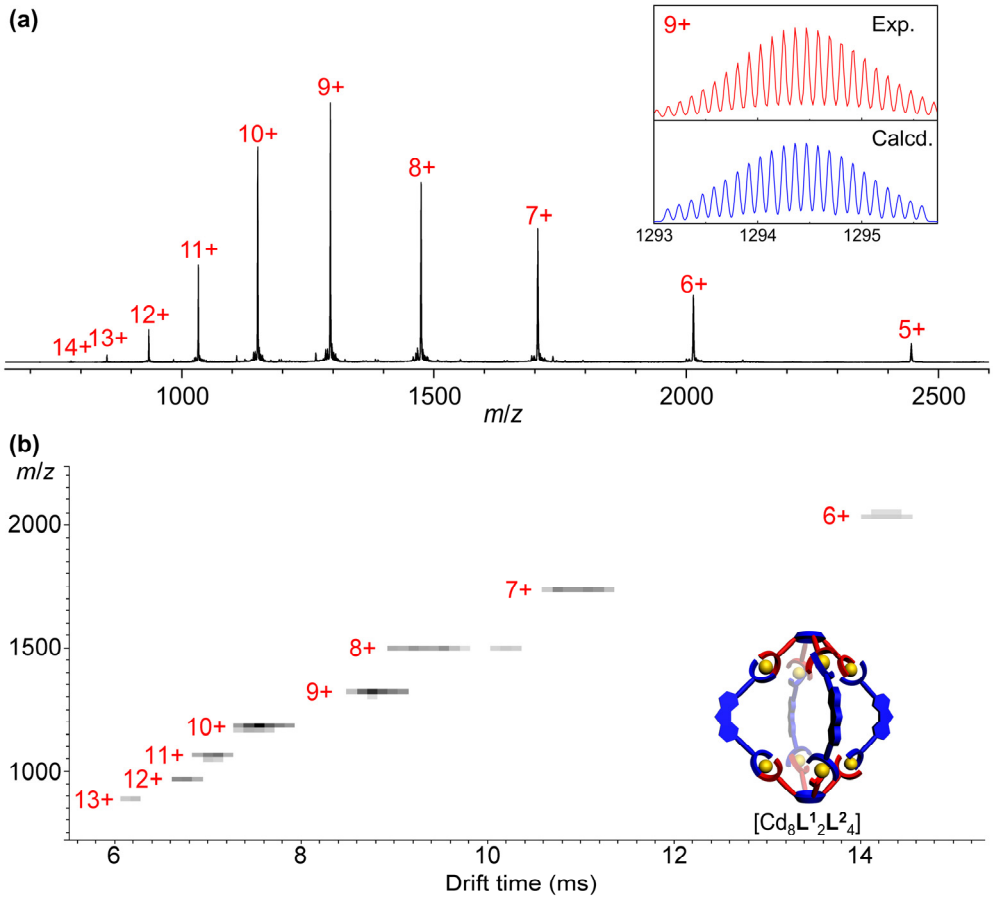

Figure S50. (a) ESI-MS spectrum and (b) TWIM-MS Plot of $[Cd_8\mathbf{L^1}_2\mathbf{L^2}_4]$.

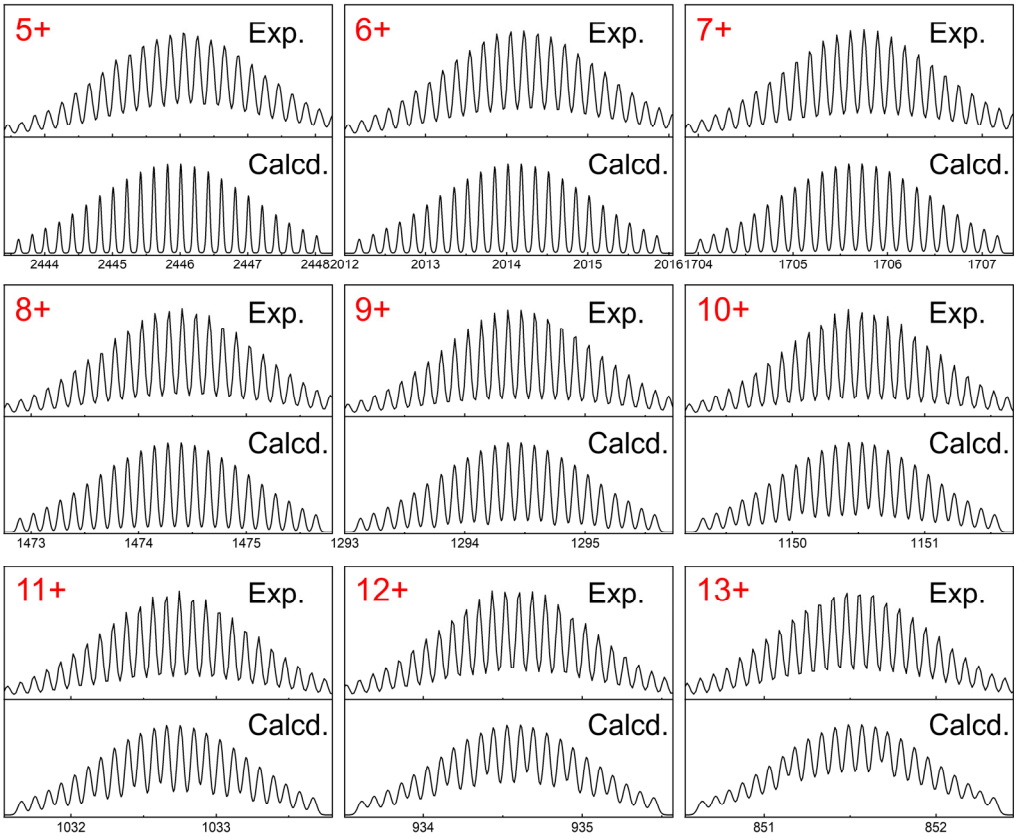

Figure S51. Experimental and theoretical isotope patterns of [Cd_8**L**$^1{}_2$**L**$^2{}_4$].

Table S1. Drift times and collision cross sections (CCSs) for [Cd_8**L**$^1{}_2$**L**$^2{}_4$].

Charge state	*m/z*	Drift time (ms)	Experimental CCS (Å^2)
6+	2014.0	14.11	1300.2
7+	1705.8	10.8	1269.9
8+	1474.3	9.04	1285.7
8+	1474.3	10.03	1380.8
9+	1294.4	8.60	1397.7
10+	1150.4	7.39	1396.1
11+	1032.7	6.95	1470. 1
12+	934.5	6.62	1548.6
13+	851.5	6.06	1572.6
		Average CCS	1394.0 ± 144.6
			Theoretical CCS (Å^2)
		PA CCS	1411.6 ± 35.6
		TM CCS	1622.1 ± 186.7

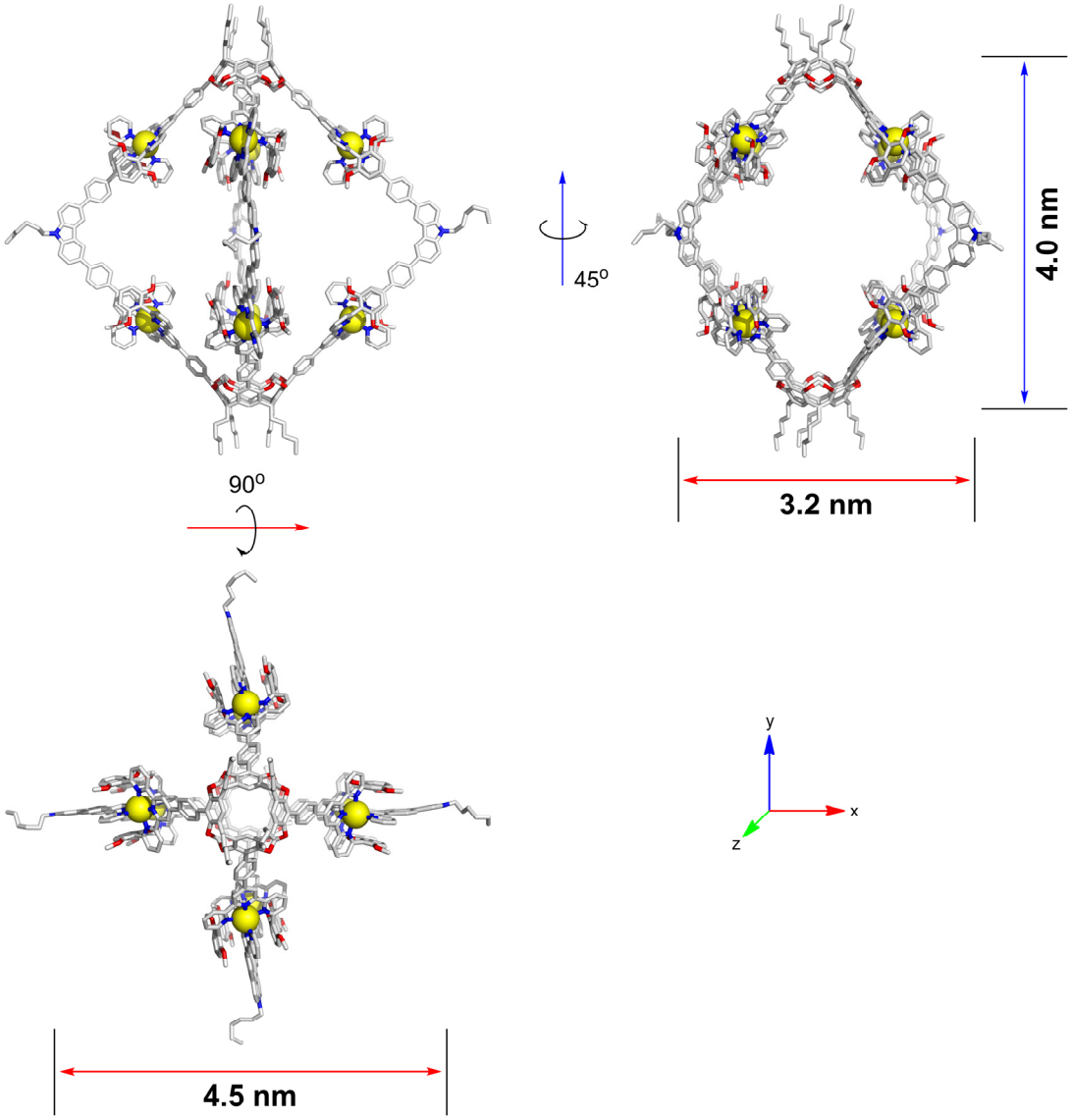

Figure S52. Geometry-optimized structures of $[Cd_8\mathbf{L^1}_2\mathbf{L^2}_4]$.

General Procedure for [$Cd_8L^1_2L^3_4$]: To a $CHCl_3$ solution (6 mL) of ligands, a MeOH solution (6 mL) of $Cd(OTf)_2$ was added. The reaction mixture was stirred at 60 ºC for 12 h to give a homogeneous solution. A yellow solid was obtained in quantitative yield after the solvent mixture was evaporated to dryness under reduced pressure. The resultant solid was then dissolved in CD_3CN (6 mg mL^{-1}) and the solution was stirred at 80 ºC for 8 h. ^1H NMR and ESI-MS were employed to monitor the complexation reaction.

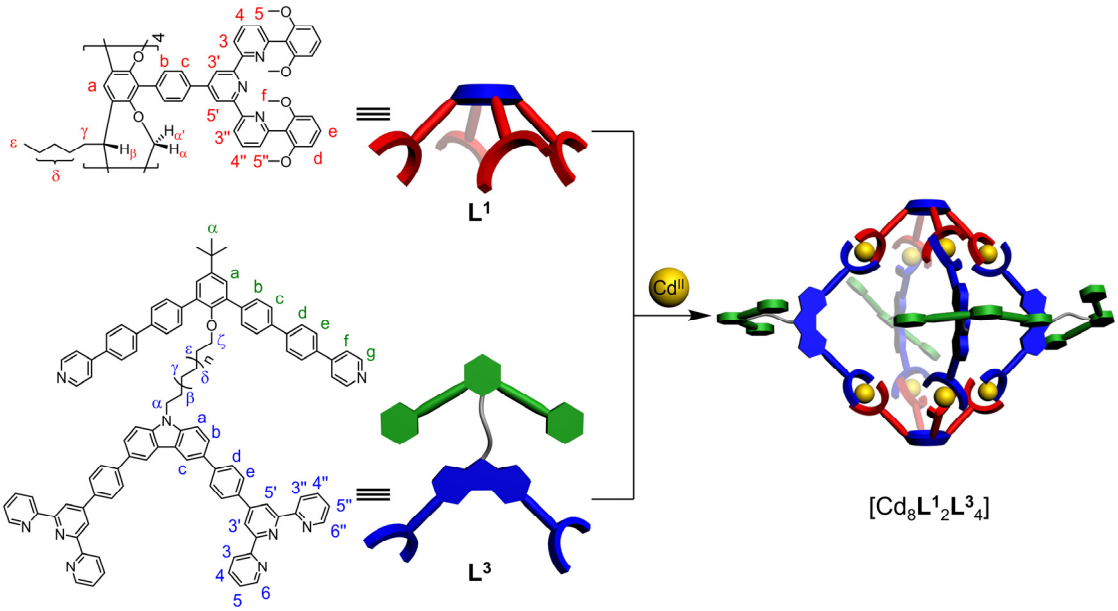

Scheme S6. Self-assembly of complex [$Cd_8L^1_2L^3_4$].

Complex [$Cd_8L^1_2L^{3a}_4$]: By the general procedure, after 8 h of heating at 80 ºC, [$Cd_8\mathbf{L^1}_2\mathbf{L^{3a}}_4$] was obtained in quantitative yield from **L¹** (5.0 μmol, 15.6 mg), **L³ᵃ** (10.0 μmol, 14.4 mg), and $Cd(OTf)_2$ (21.0 μmol, 8.6 mg). ^{1}H NMR (500 MHz, CD_3CN): δ (ppm) 9.13 (s, 16H), 8.82 (d, J = 8.6 Hz, 16H), 8.79 (d, J = 1.9 Hz, 8H), 8.64 (d, J = 6.2 Hz, 16H), 8.56 (d, J = 8.2 Hz, 16H), 8.43-8.37 (m, 32H), 8.18-8.07 (m, 64H), 7.99 (dd, J = 5.1, 1.8 Hz, 16H), 7.93 (dd, J = 8.5, 1.8 Hz, 8H), 7.87 (br, 8H), 7.82 (d, J = 8.5 Hz, 16H), 7.72 (d, J = 8.4 Hz, 16H), 7.69-7.59 (m, 56H), 7.57 (d, J = 7.8 Hz, 16H), 7.45 (m, 24H), 7.14 (d, J = 7.0 Hz, 16H), 6.75 (t, J = 8.4 Hz, 16H), 5.85 (d, J = 8.6 Hz, 32H), 5.47 (d, J = 6.1 Hz, 8H), 5.02 (t, J = 7.7 Hz, 8H), 4.61 (d, J = 7.1 Hz, 8H), 4.29 (br, 8H), 3.30 (br, 8H), 2.82 (s, 96H), 2.68 (br, 16H), 1.65-1.55 (m, 56H), 1.45-1.41 (m, 8H), 1.39 (s, 36H), and 1.08 (t, J = 7.1 Hz, 24H). ^{113}Cd NMR (111 MHz, CD_3CN): δ (ppm) 242.33.

ESI-MS (*m/z*):

Charge state	Composition	Theoretical *m/z*	Experimental *m/z*
6+	$[M - 6OTf]^{6+}$	2406.6553	2406.6643
7+	$[M - 7OTf]^{7+}$	2041.5652	2041.5795
8+	$[M - 8OTf]^{8+}$	1767.7515	1767.7583
9+	$[M - 9OTf]^{9+}$	1554.7836	1554.7777
10+	$[M - 10OTf]^{10+}$	1384.4155	1384.4086
11+	$[M - 11OTf]^{11+}$	1245.0142	1245.0068
12+	$[M - 12OTf]^{12+}$	1128.8503	1128.8306
13+	$[M - 13OTf]^{13+}$	1030.5585	1030.5366
14+	$[M - 14OTf]^{14+}$	946.3797	946.3555
15+	$[M - 15OTf]^{15+}$	873.2930	873.2669

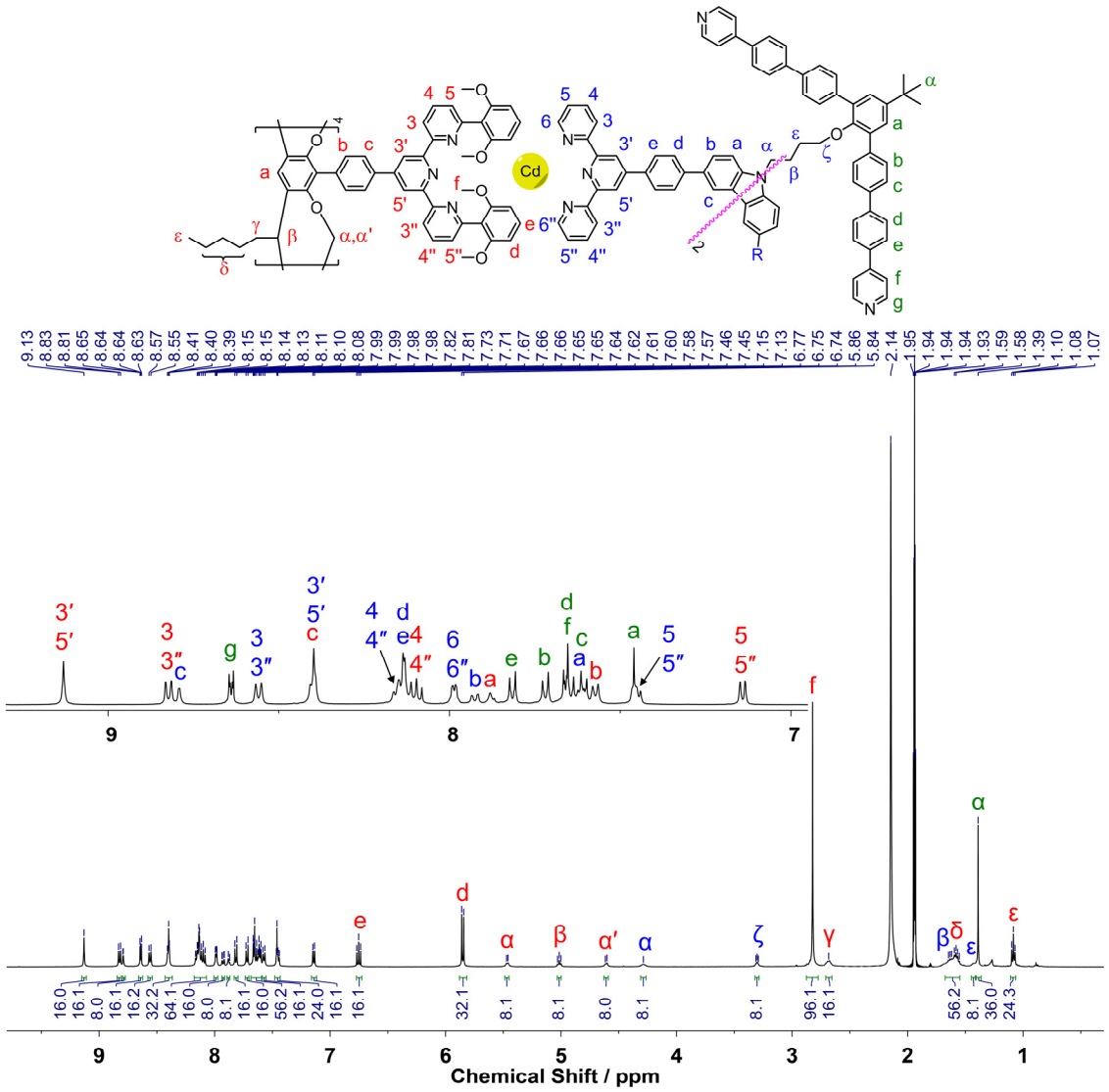

Figure S53. ^{1}H NMR spectrum (500 MHz, CD_3CN) of [Cd_8**L**$^{1}_2$**L**$^{3a}_4$].

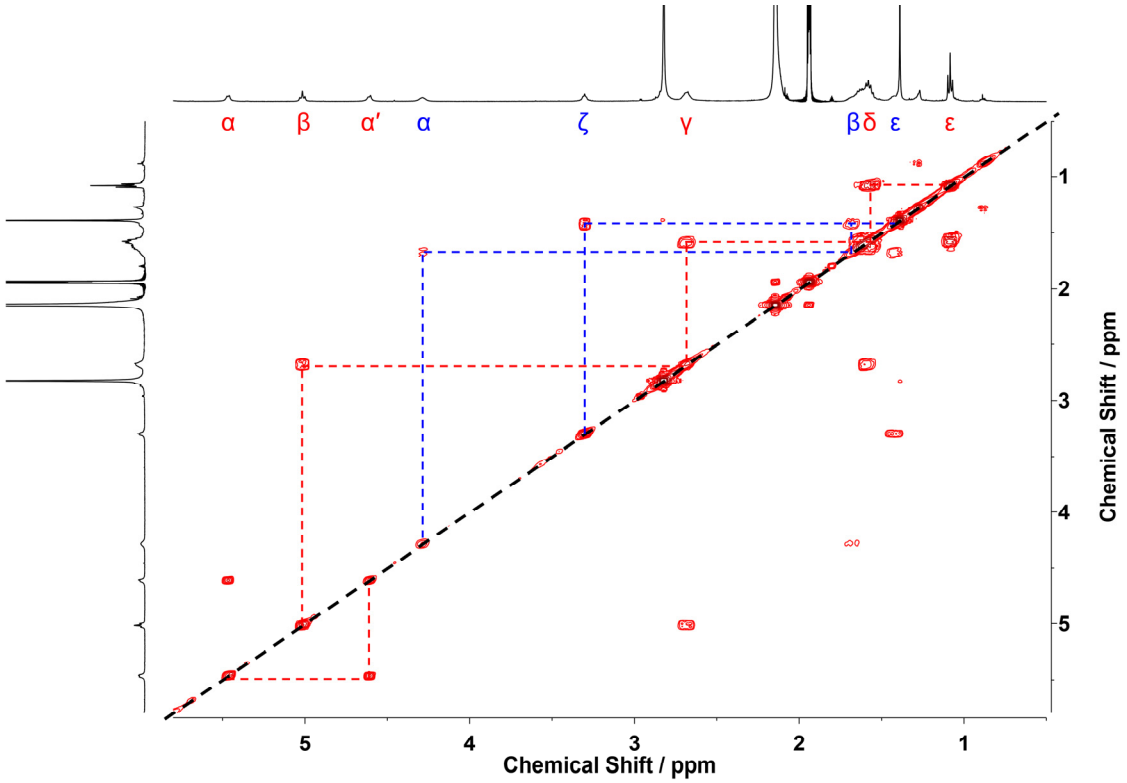

Figure S54. Partial COSY spectrum (500 MHz, CD_3CN) of [Cd_8**L**$^1{}_2$**L**$^{3a}{}_4$].

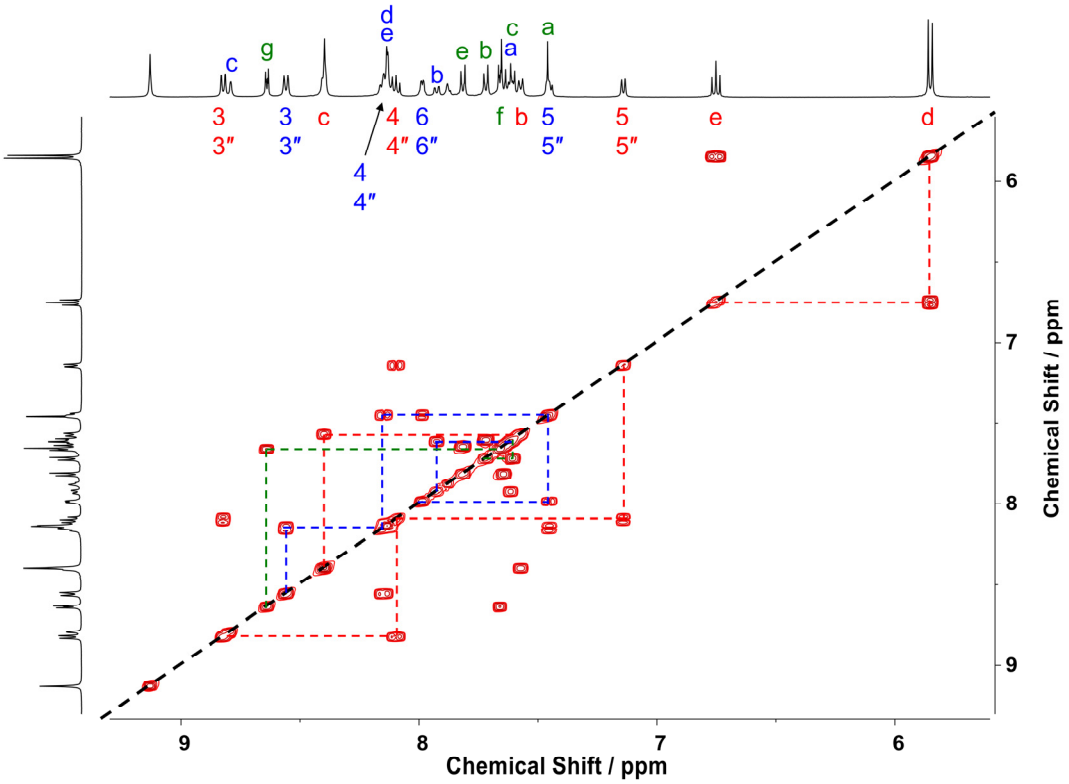

Figure S55. Partial COSY spectrum (500 MHz, CD_3CN) of [Cd_8**L**$^1{}_2$**L**$^{3a}{}_4$].

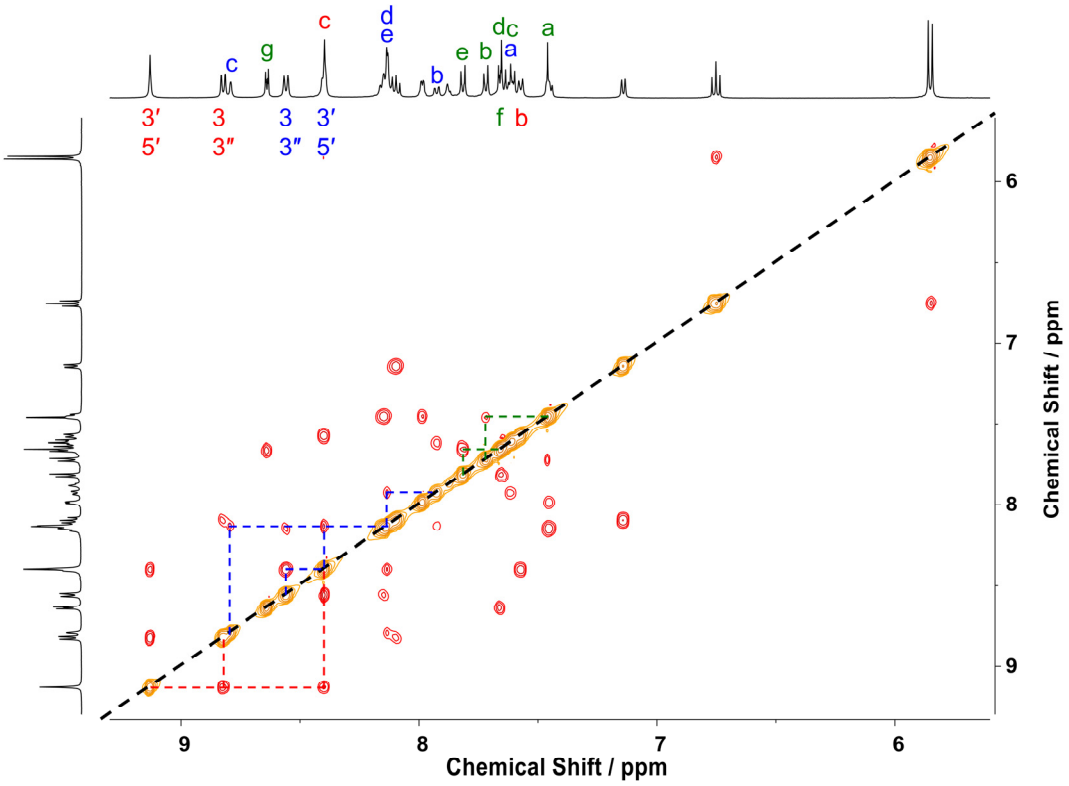

Figure S56. Partial ROESY spectrum (500 MHz, CD_3CN) of $[Cd_8\mathbf{L^1}_2\mathbf{L^{3a}}_4]$.

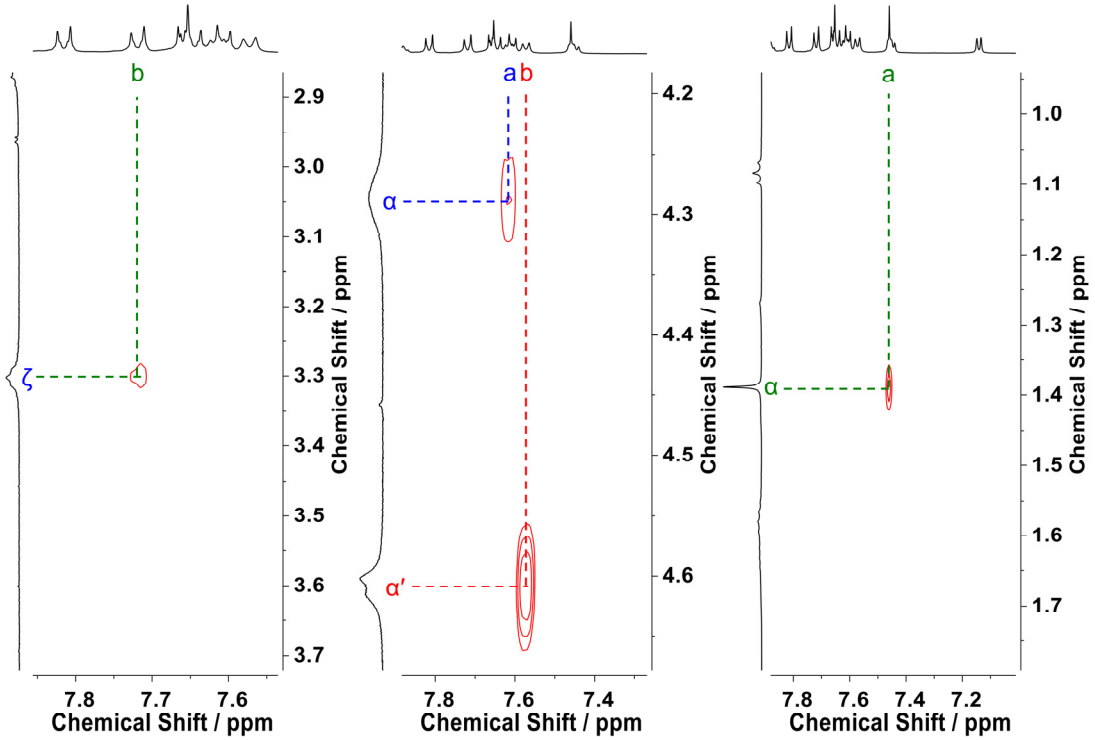

Figure S57. Partial ROESY spectrum (500 MHz, CD_3CN) of $[Cd_8\mathbf{L^1}_2\mathbf{L^{3a}}_4]$.

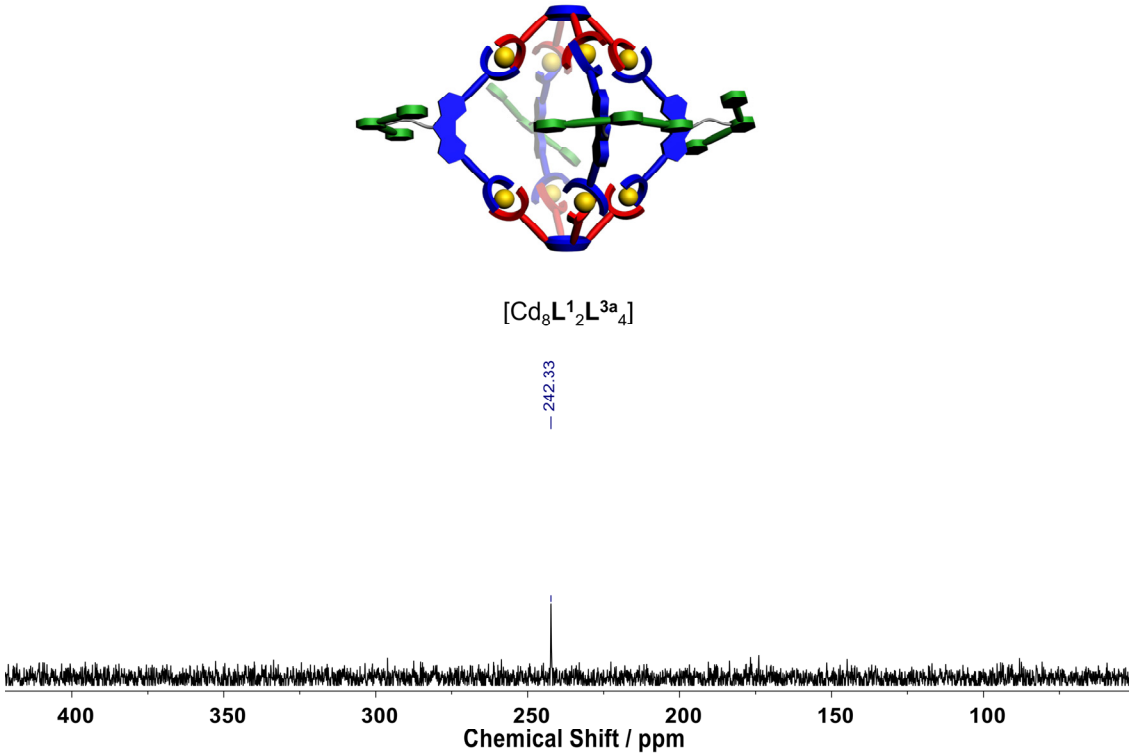

Figure S58. ^{113}Cd NMR spectrum (111 MHz, CD_3CN) of [Cd_8**L**$^1{}_2$**L**$^{3a}{}_4$].

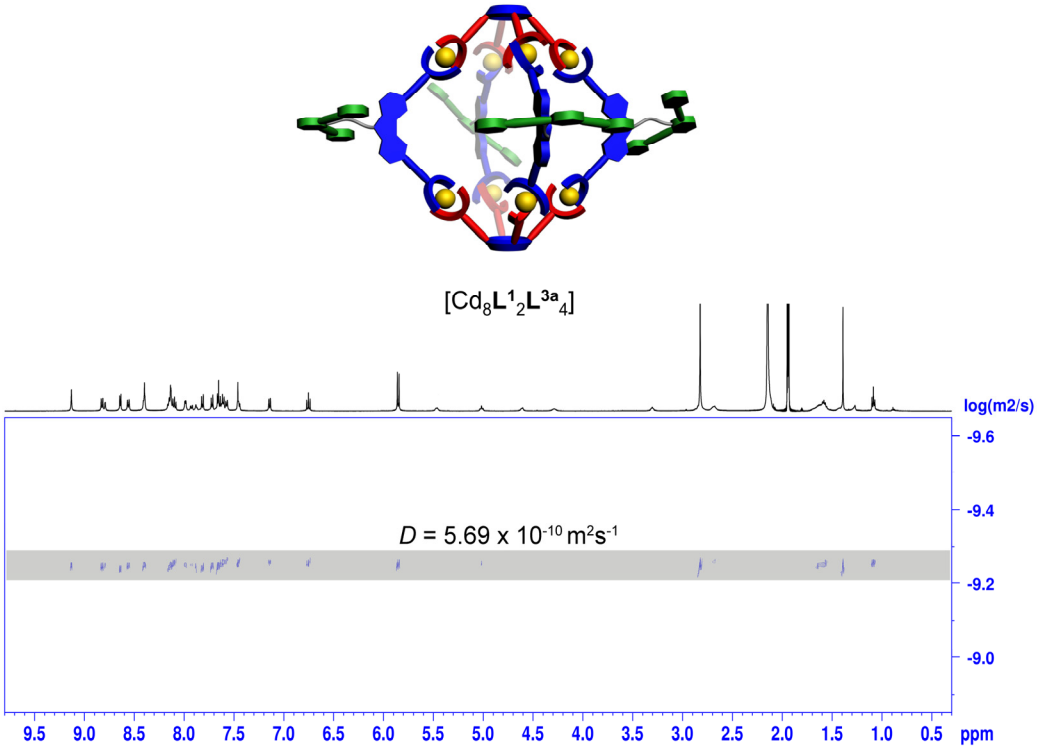

Figure S59. DOSY spectrum (500 MHz, CD_3CN) of [Cd_8**L**$^1{}_2$**L**$^{3a}{}_4$].

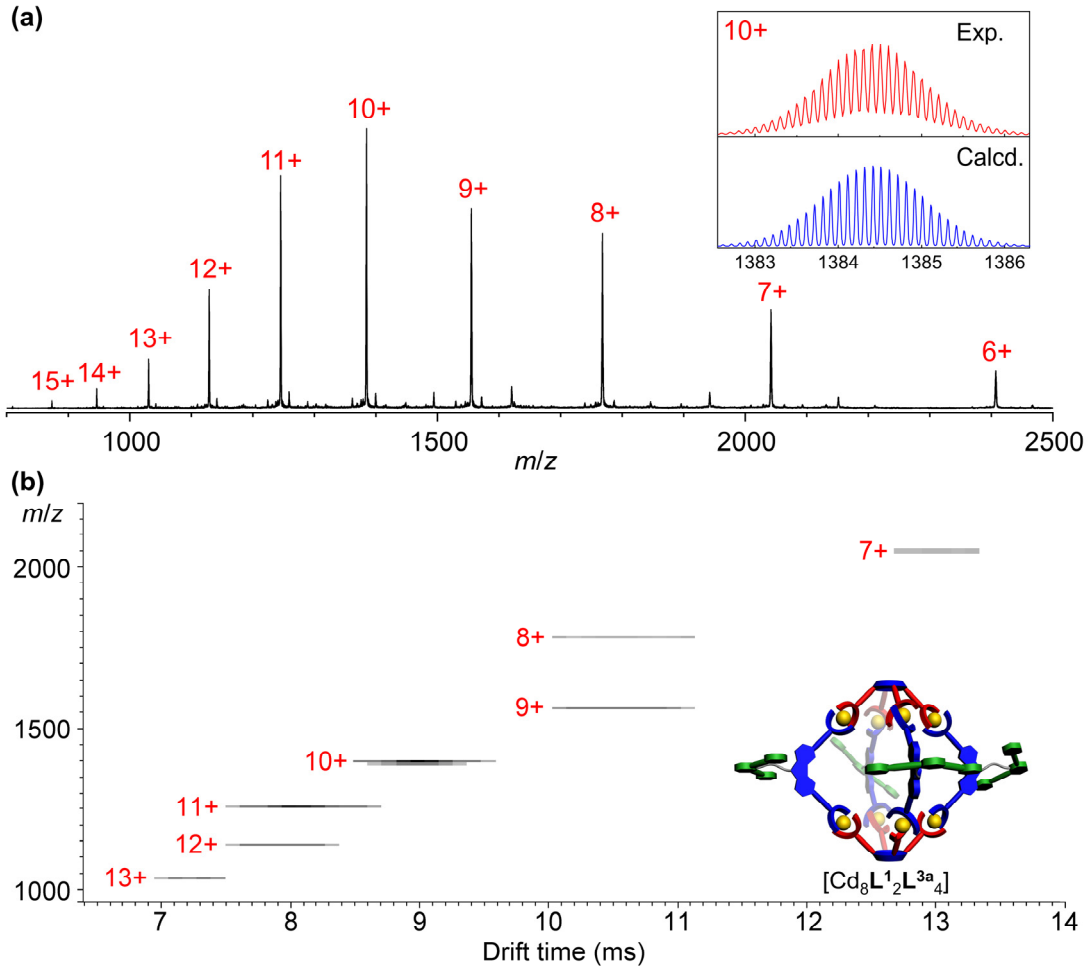

Figure S60. (a) ESI-MS spectrum and (b) TWIM-MS plot of $[Cd_8\mathbf{L^1}_2\mathbf{L^{3a}}_4]$.

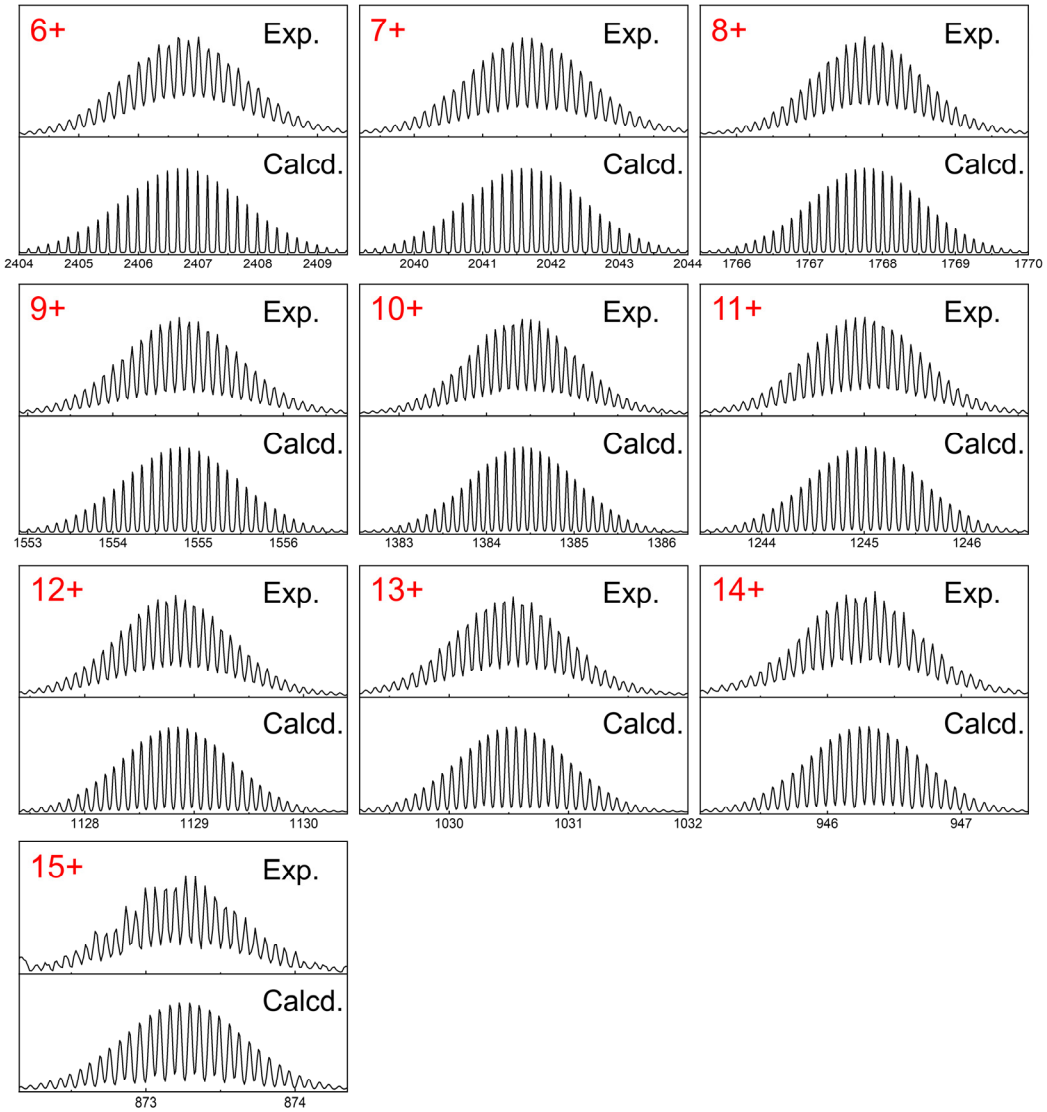

Figure S61. Experimental and theoretical isotope patterns of [Cd_8**L**$^1{}_2$**L**$^{3a}{}_4$].

Table S2. Drift times and collision cross sections (CCSs) for $[Cd_8\mathbf{L^1}_2\mathbf{L^{3a}}_4]$.

Charge state	*m/z*	Drift time (ms)	Experimental CCS (Å^2)
7	2041.6	12.9	1429.4
8	1767.8	10.47	1420.8
9	1554.8	10.36	1587.4
10	1384.4	8.82	1579.9
11	1245.0	7.83	1599.4
12	1128.8	7.83	1745.3
13	1030.5	7.17	1776.4
		Average CCS	1591.3 ± 137.5
			Theoretical CCS (Å^2)
		PA CCS	1614.8 ± 75.3
		TM CCS	1911.1 ± 143.8

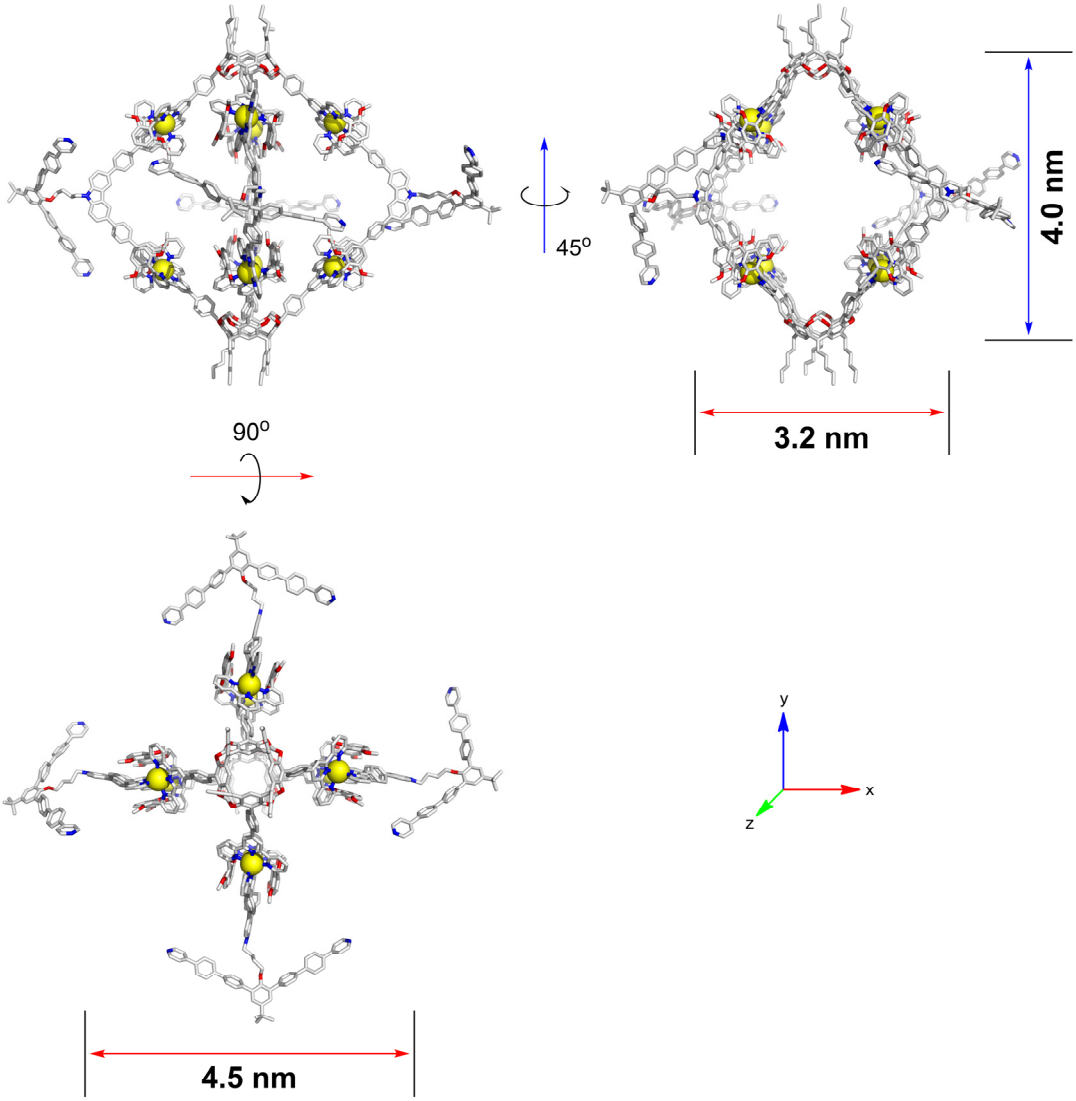

Figure S62. Geometry-optimized structures of [Cd_8**L**$^1{}_2$**L**$^{3a}{}_4$].

Complex [$Cd_8L^1_2L^{3b}_4$]: By the general procedure, after 8 h of heating at 80 ºC, [$Cd_8\mathbf{L^1}_2\mathbf{L^{3b}}_4$] was obtained in quantitative yield from $\mathbf{L^1}$ (5.0 μmol, 15.6 mg), $\mathbf{L^{3b}}$ (10.0 μmol, 14.7 mg), and $Cd(OTf)_2$ (21.0 μmol, 8.6 mg). ^{1}H NMR (500 MHz, CD_3CN): δ (ppm) 9.13 (s, 16H), 8.82 (dd, J = 8.2, 1.0 Hz, 16H), 8.78 (d, J = 1.9 Hz, 8H), 8.59 (d, J = 6.2 Hz, 16H), 8.56 (d, J = 8.2 Hz, 16H), 8.43 (s, 16H), 8.40 (d, J = 7.8 Hz, 16H), 8.19 (d, J = 8.1 Hz, 16H), 8.16-8.07 (m, 48H), 8.01-7.96 (m, 24H), 7.88 (br, 8H), 7.73-7.62 (m, 72H), 7.58 (m, 32H), 7.48-7.43 (m, 24H), 7.14 (d, J = 7.6 Hz, 16H), 6.77 (t, J = 8.4 Hz, 16H), 5.85 (d, J = 8.6 Hz, 32H), 5.46 (d, J = 5.8 Hz, 8H), 5.02 (t, J = 7.6 Hz, 8H), 4.61 (d, J = 5.8 Hz, 8H), 4.32 (br, 8H), 3.26 (t, J = 5.8 Hz, 8H), 2.82 (s, 96H), 2.69 (br, 16H), 1.60 (m, 56H), 1.39 (s, 36H), 1.25-1.11 (m, 24H), and 1.08 (t, J = 7.1 Hz, 24H). ^{113}Cd NMR (111 MHz, CD_3CN): δ (ppm) 242.98.
ESI-MS (*m/z*):

Charge state	Composition	Theoretical *m/z*	Experimental *m/z*
5+	$[M - 5OTf]^{5+}$	2940.7986	2940.7566
6+	$[M - 6OTf]^{6+}$	2425.5068	2425.4814
7+	$[M - 7OTf]^{7+}$	2057.7317	2057.7087
8+	$[M - 8OTf]^{8+}$	1781.8922	1781.8691
9+	$[M - 9OTf]^{9+}$	1567.4685	1567.4458
10+	$[M - 10OTf]^{10+}$	1395.6265	1395.6162
11+	$[M - 11OTf]^{11+}$	1255.2074	1255.2061
12+	$[M - 12OTf]^{12+}$	1138.1941	1138.1925
13+	$[M - 13OTf]^{13+}$	1039.1835	1039.1755
14+	$[M - 14OTf]^{14+}$	954.2480	954.2458
15+	$[M - 15OTf]^{15+}$	880.6978	880.6941
16+	$[M - 16OTf]^{16+}$	816.4076	816.4156

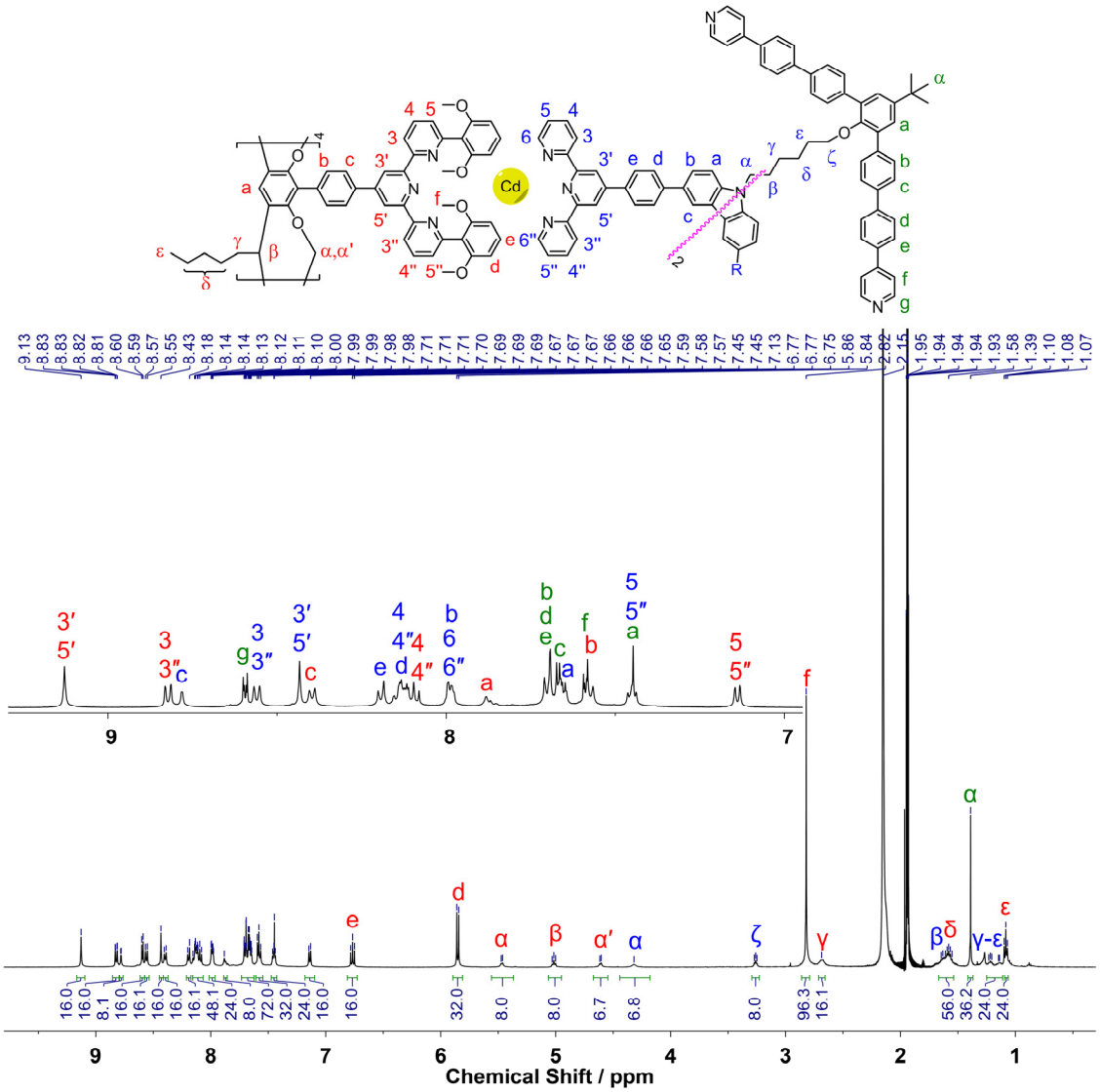

Figure S63. ^{1}H NMR spectrum (500 MHz, CD_3CN) of $[Cd_8\mathbf{L^1}_2\mathbf{L^{3b}}_4]$.

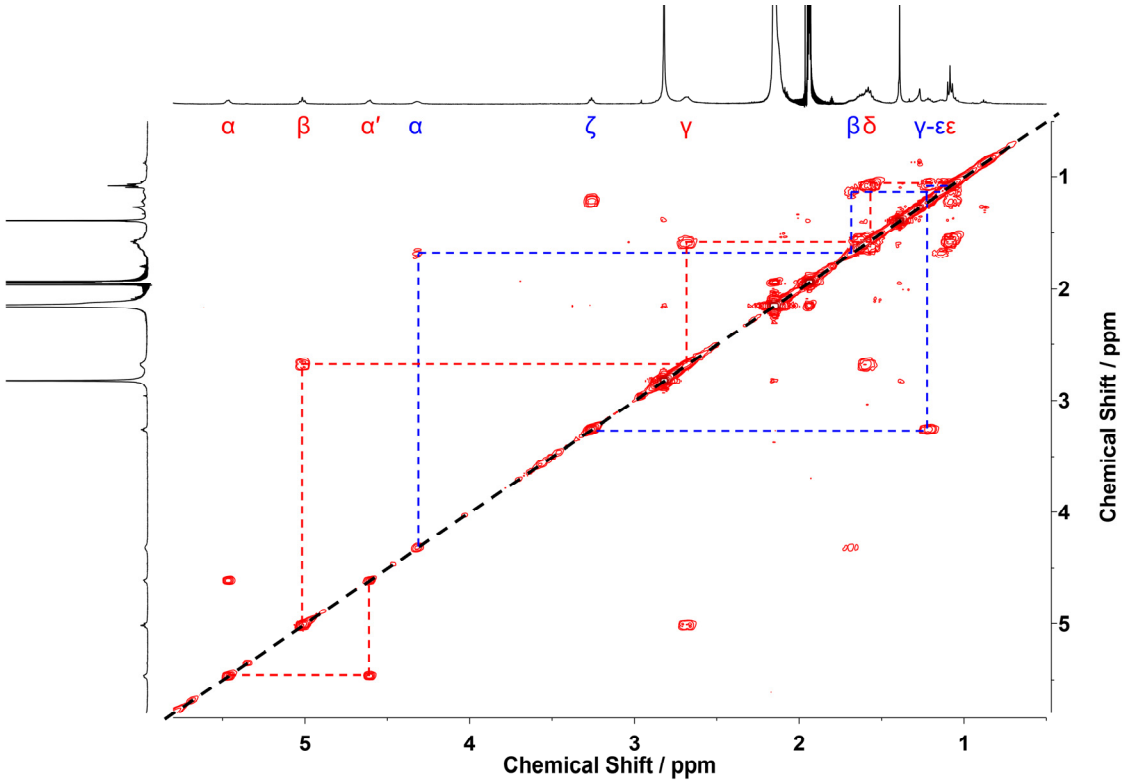

Figure S64. Partial COSY spectrum (500 MHz, CD_3CN) of [Cd_8**L**$^1{}_2$**L**$^{3b}{}_4$].

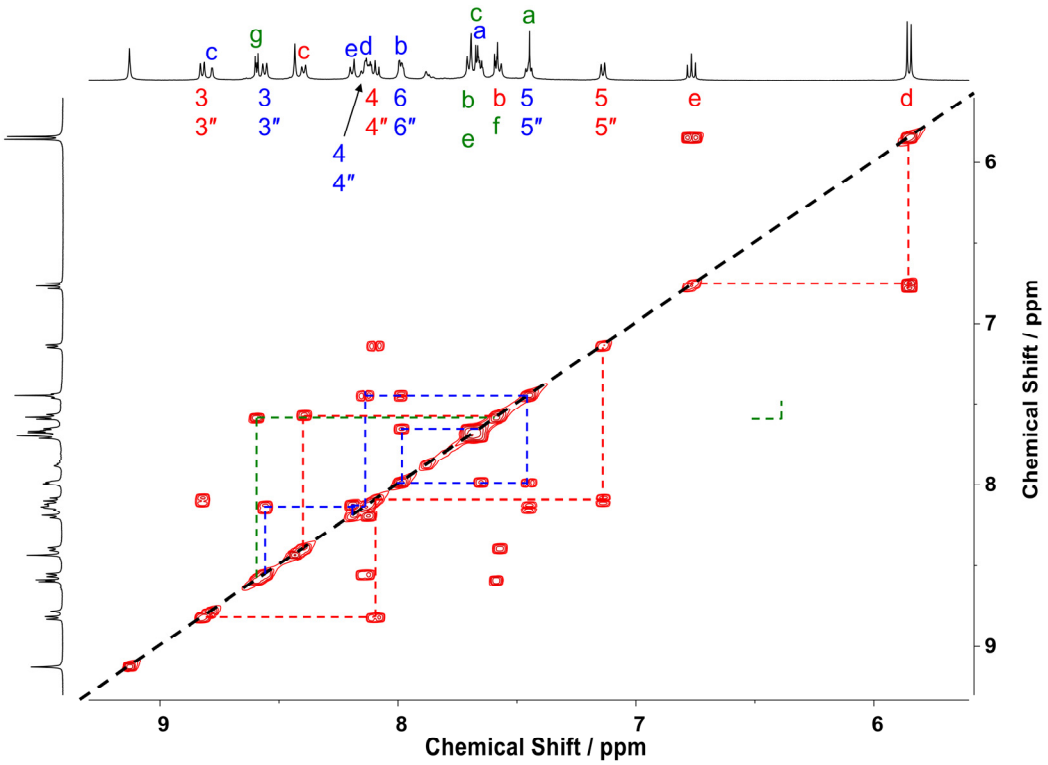

Figure S65. Partial COSY spectrum (500 MHz, CD_3CN) of [Cd_8**L**$^1{}_2$**L**$^{3b}{}_4$].

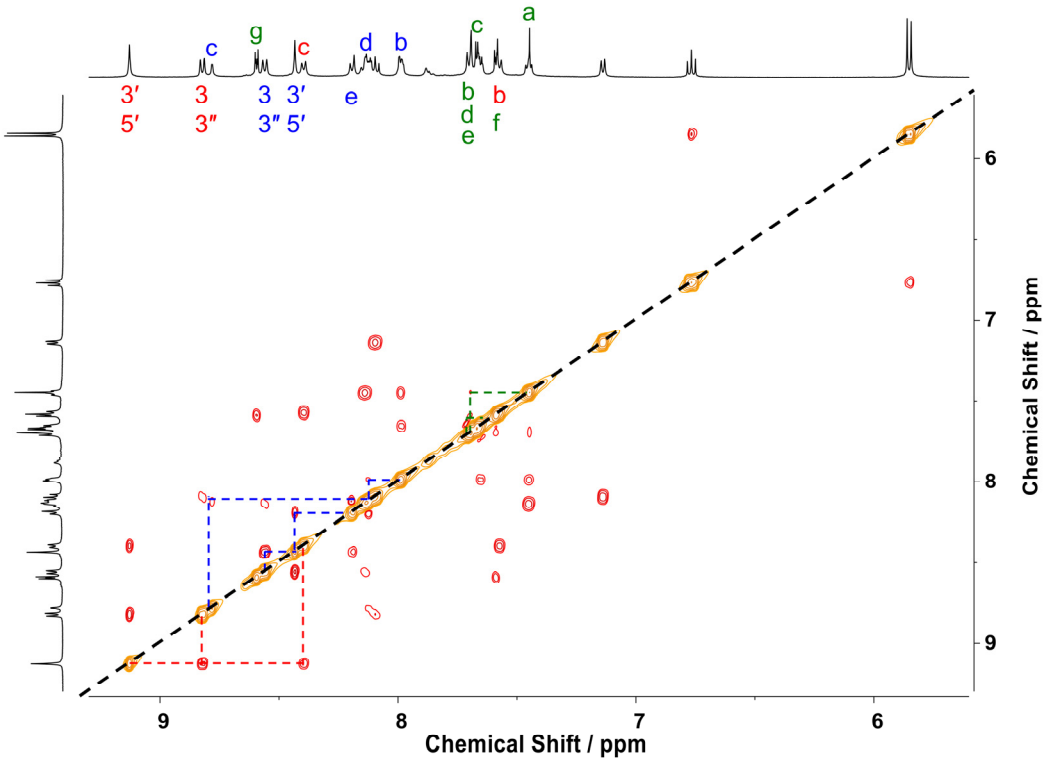

Figure S66. Partial ROESY spectrum (500 MHz, CD_3CN) of $[Cd_8\mathbf{L^1}_2\mathbf{L^{3b}}_4]$.

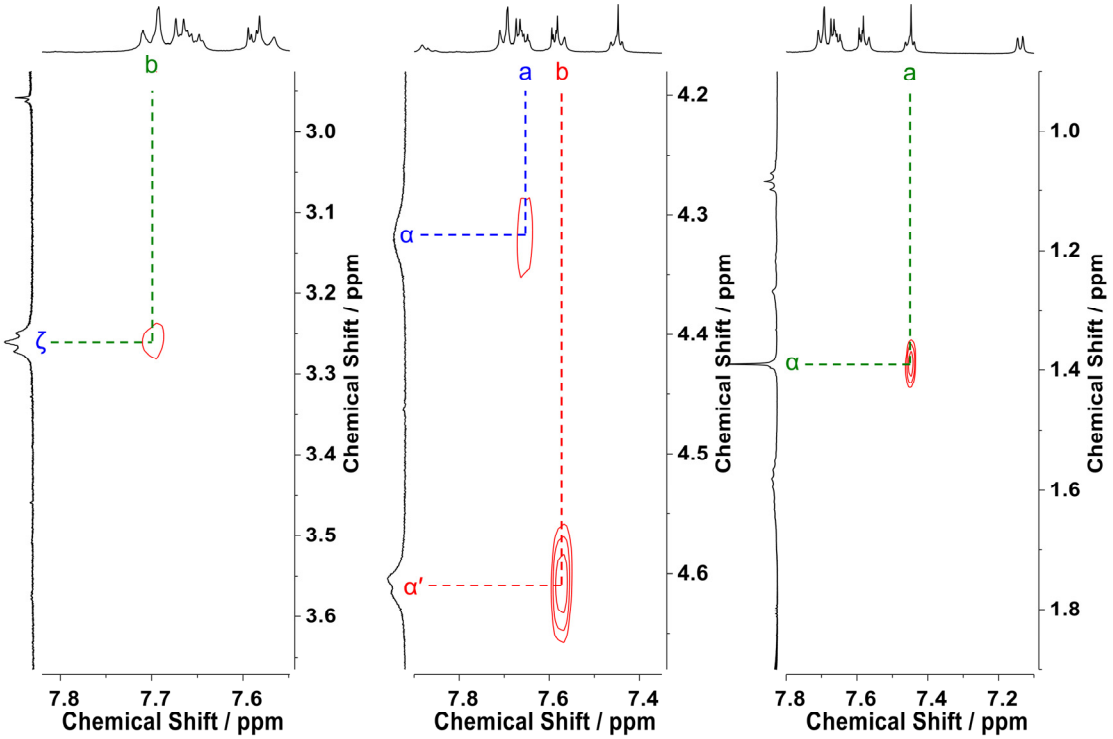

Figure S67. Partial ROESY spectrum (500 MHz, CD_3CN) of $[Cd_8\mathbf{L^1}_2\mathbf{L^{3b}}_4]$.

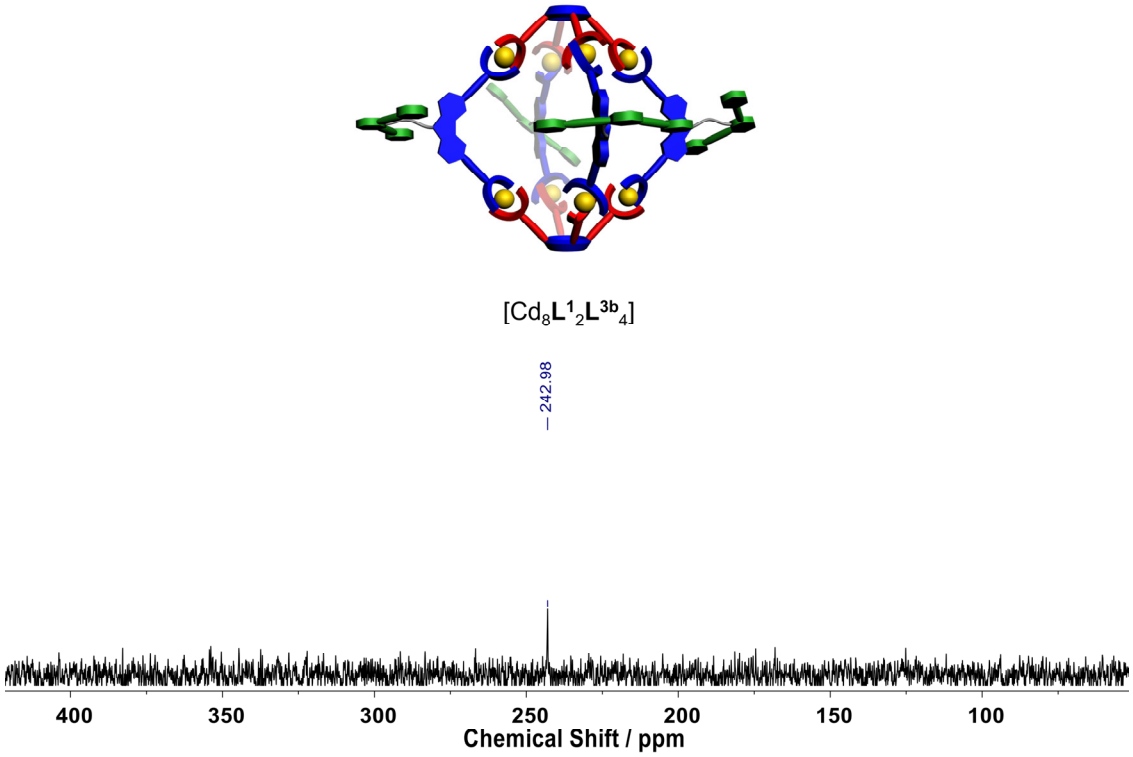

Figure S68. ^{113}Cd NMR spectrum (111 MHz, CD_3CN) of [Cd_8**L**$^1{}_2$**L**$^{3b}{}_4$].

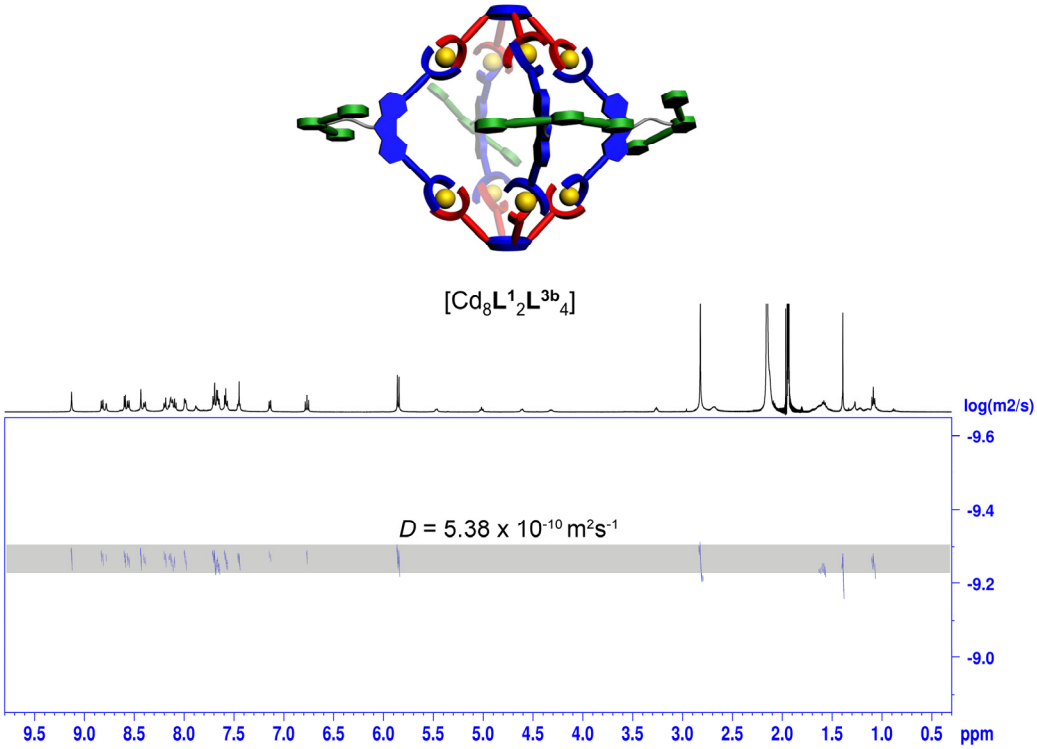

Figure S69. DOSY spectrum (500 MHz, CD_3CN) of [Cd_8**L**$^1{}_2$**L**$^{3b}{}_4$].

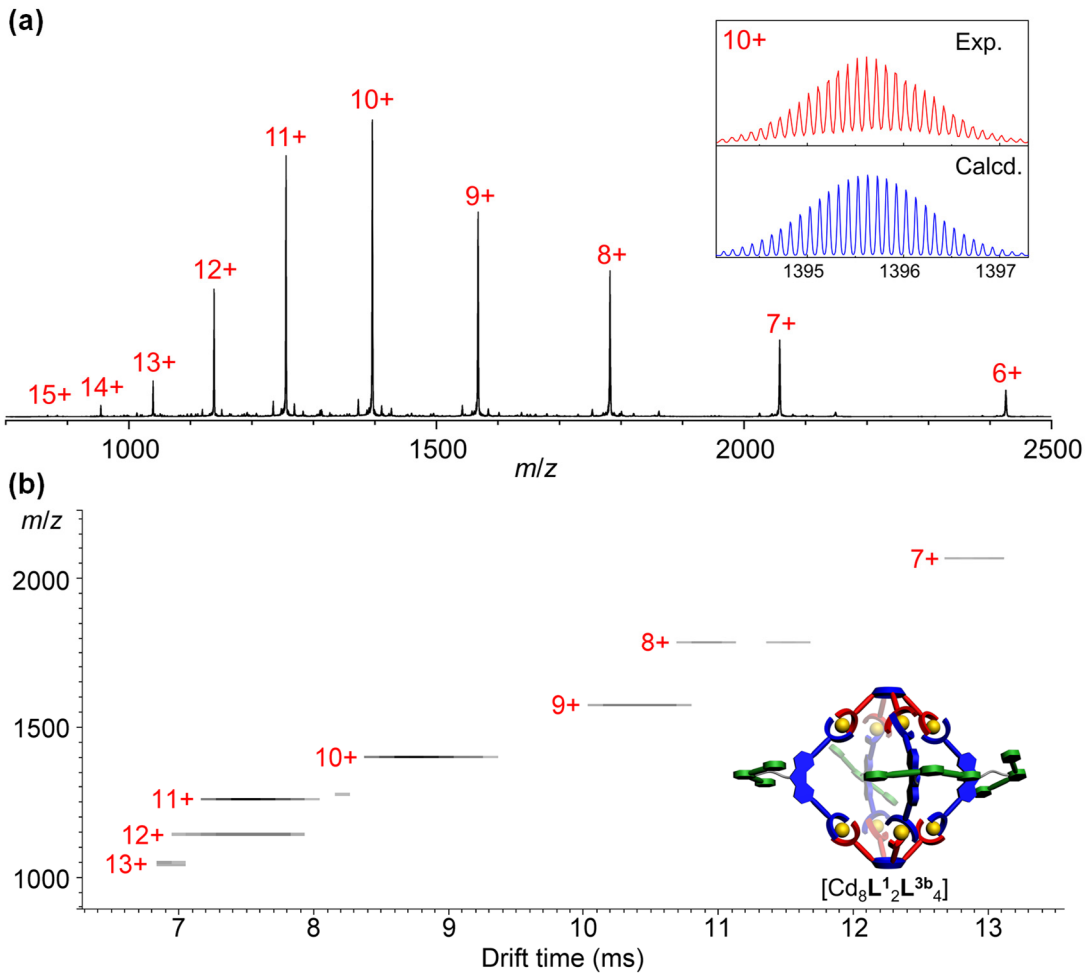

Figure S70. (a) ESI-MS spectrum and (b) TWIM-MS plot of $[Cd_8\mathbf{L^1}_2\mathbf{L^{3b}}_4]$.

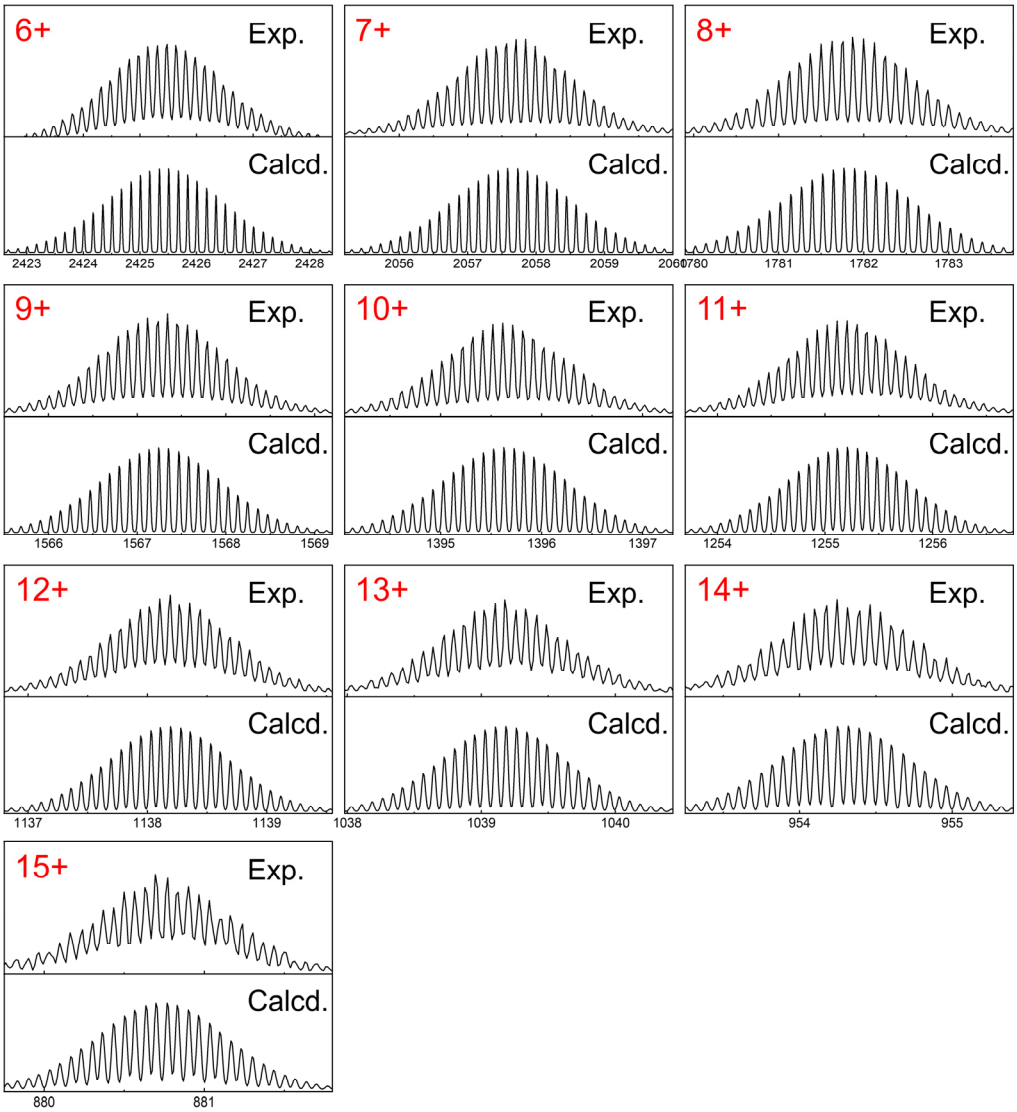

Figure S71. Experimental and theoretical isotope patterns of [Cd_8**L**$^{1}{}_2$**L**$^{3b}{}_4$].

Table S3. Drift times and collision cross sections (CCSs) for $[Cd_8\mathbf{L^1}_2\mathbf{L^{3b}}_4]$.

Charge state	*m/z*	Drift time (ms)	Experimental CCS (Å^2)
7	2057.7	12.68	1413.1
8	1781.9	10.80	1450.9
8	1781.9	11.38	1502.9
9	1567.4	10.14	1564.4
10	1395.6	8.60	1552.4
11	1255.2	7.39	1535.0
12	1138.2	7.39	1675.1
13	1039.2	6.73	1697.0
		Average CCS	1548.9 ± 98.9
			Theoretical CCS (Å^2)
		PA CCS	1595.3 ± 92.8
		TM CCS	1903.4 ± 124.3

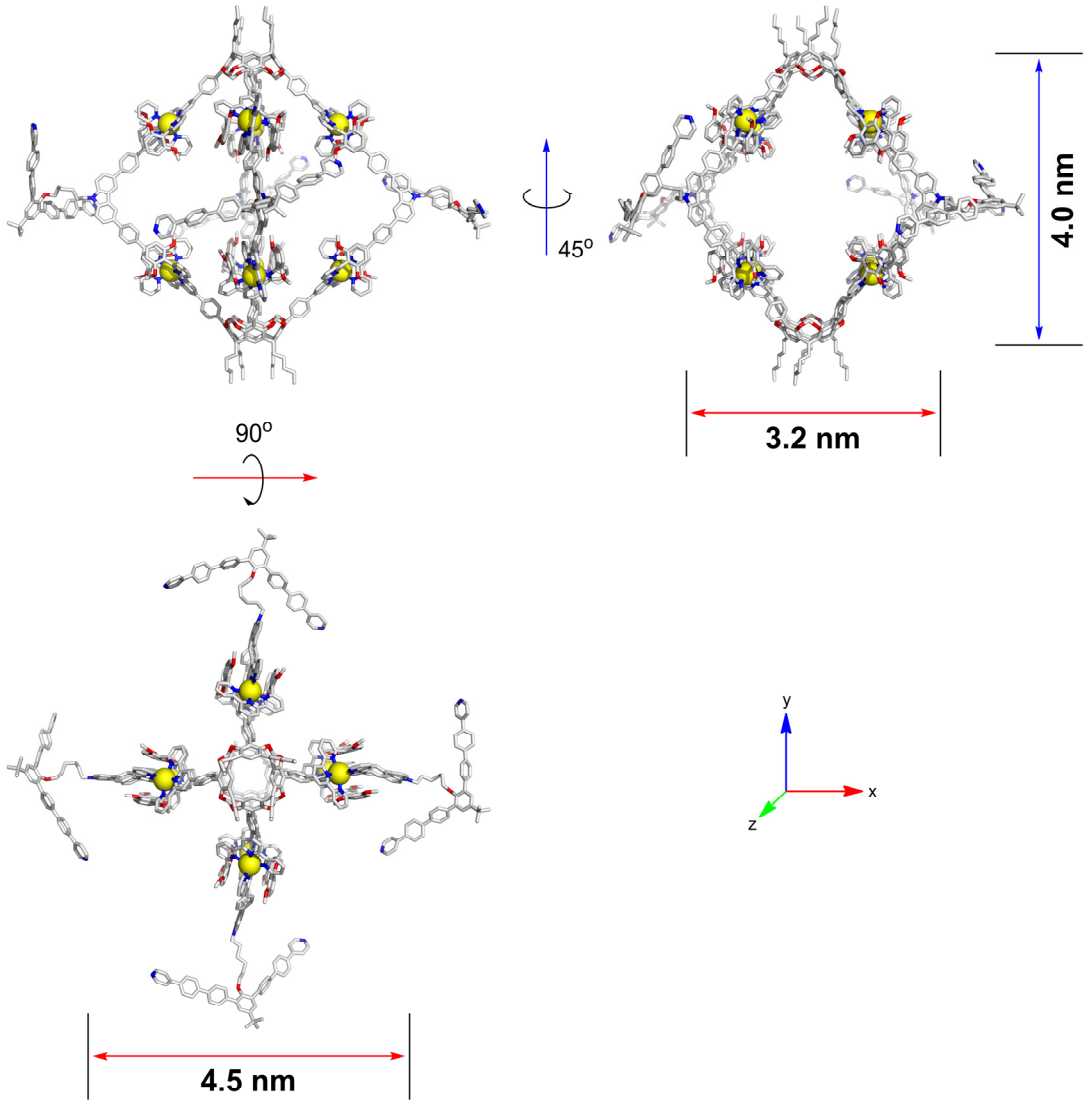

Figure S72. Geometry-optimized structures of $[Cd_8\mathbf{L^1}_2\mathbf{L^{3b}}_4]$.

General Procedure for Heterobimetallic Nano-Saturn Complexes: To a CD_3NO_2 solution of $[Cd_8\mathbf{L^1}_2\mathbf{L^3}_4]$ (~0.4 mM), metalloligand $[Pt_2\mathbf{L^4}](OTf)_2$ was added. The reaction mixture was stirred at 25 °C for 8 h to give a homogeneous solution. ^{1}H NMR and ESI-MS were employed to monitor the complexation reaction.

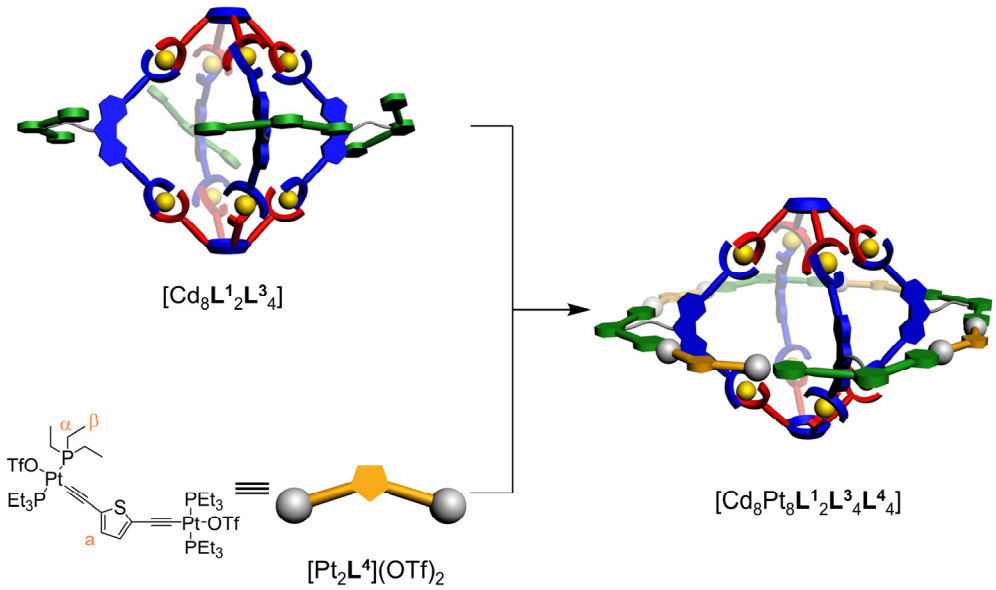

Scheme S7. Self-assembly of heterobimetallic nano-Saturn $[Cd_8Pt_8\mathbf{L^1}_2\mathbf{L^3}_4\mathbf{L^4}_4]$.

Heterobimetallic Nano-Saturn [$Cd_8Pt_8L^1_2L^{3a}_4L^4_4$]: By the general procedure, after being stirred at 25 °C for 8 h, the complex [$Cd_8Pt_8L^1_2L^{3a}_4L^4_4$] was obtained in quantitative yield from [$Cd_8L^1_2L^{3a}_4$] (0.8 μmol, 12.1 mg), metalloligand [Pt_2L^4]$(OTf)_2$ (3.2 μmol, 4.1 mg). ^{1}H NMR (500 MHz, CD_3NO_2): δ (ppm) 9.12 (br, 16H), 8.82 (d, J = 7.9 Hz, 16H), 8.69 (m, 24H), 8.63 (d, J = 8.0 Hz, 16H), 8.53 (br, 16H), 8.32 (br, 16H), 8.20 (m, 32H), 8.16-8.10 (m, 48H), 8.07-7.88 (m, 88H), 7.86 (br, 8H), 7.62 (s, 8H), 7.57 (m, 24H), 7.50 (t, J = 6.0 Hz, 16H), 7.21 (d, J = 7.3 Hz, 16H), 6.85 (t, J = 8.3 Hz, 16H), 6.73 (br, 8H), 5.93 (d, J = 8.3 Hz, 32H), 5.59 (br, 8H), 5.09 (br, 8H), 4.72 (br, 8H), 4.24 (br, 8H), 3.50 (br, 6H), 2.89 (s, 96H), 2.65 (br, 16H), 2.14 (br, 8H), 1.88-1.80 (m, 96H), 1.64-1.50 (m, 48H), 1.46 (s, 36H), 1.41 (br, 8H), 1.15-1.12 (m, 144H), and 1.04 (t, J = 7.2 Hz, 24H). ^{113}Cd NMR (111 MHz, CD_3NO_2): δ (ppm) 241.62. ^{31}P NMR (202 MHz, CD_3NO_2): δ (ppm) 15.77 (s, 16P, ^{195}Pt satellites, $^1J_{Pt\text{-}P}$ = 2306.8 Hz).

ESI-MS (*m/z*):

Charge state	Composition	Theoretical *m/z*	Experimental *m/z*
8+	$[M - 8OTf]^{8+}$	2413.0938	2413.1174
9+	$[M - 9OTf]^{9+}$	2128.6440	2128.6536
10+	$[M - 10OTf]^{10+}$	1900.8861	1900.8956
11+	$[M - 11OTf]^{11+}$	1714.6301	1714.6249
12+	$[M - 12OTf]^{12+}$	1559.2451	1559.2478
13+	$[M - 13OTf]^{13+}$	1427.8495	1427.8431
14+	$[M - 14OTf]^{14+}$	1315.2158	1315.2120
15+	$[M - 15OTf]^{15+}$	1217.2760	1217.2734
16+	$[M - 16OTf]^{16+}$	1132.1333	1132.1271
17+	$[M - 17OTf]^{17+}$	1056.7166	1056.7108

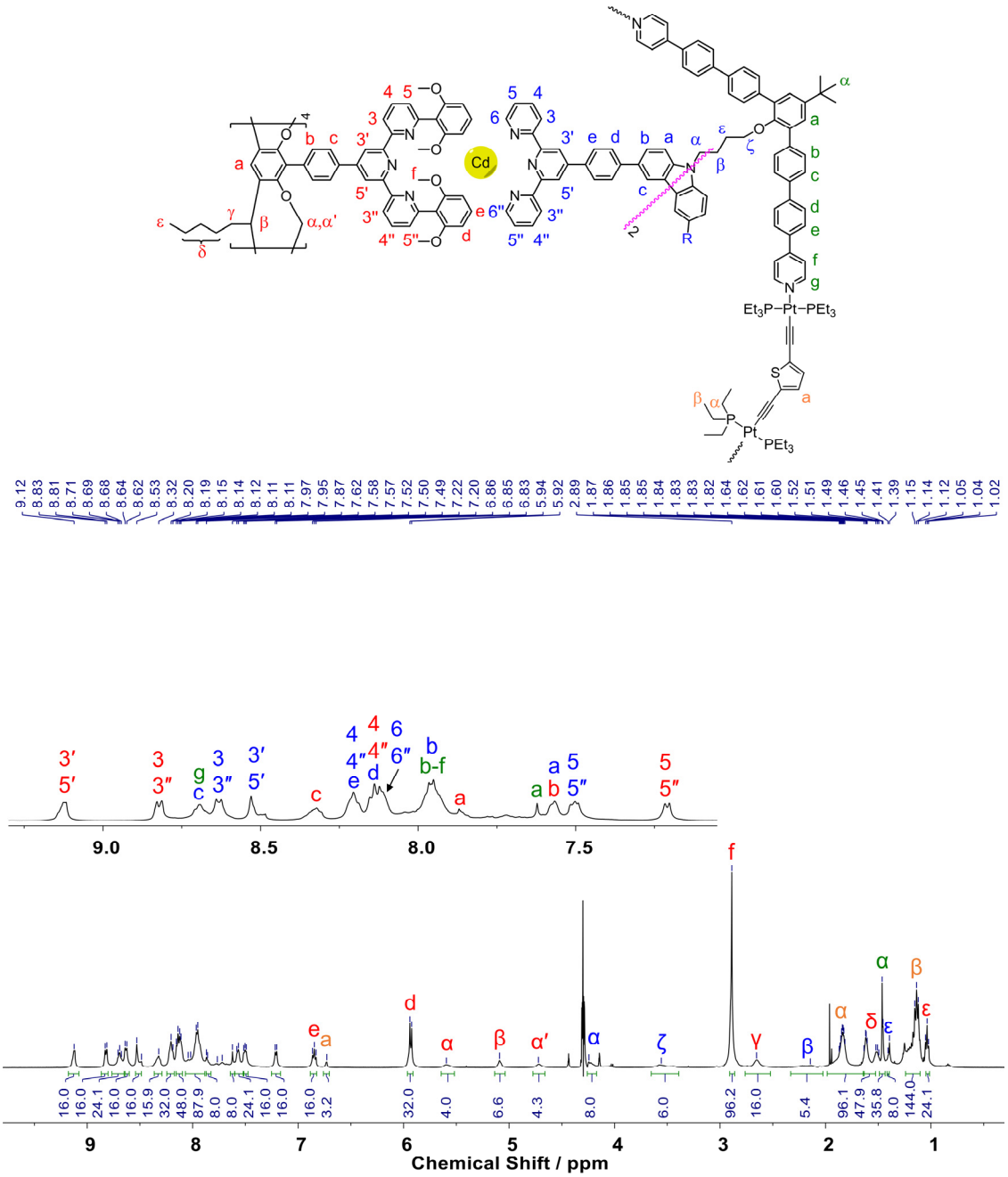

Figure S73. ^{1}H NMR spectrum (500 MHz, CD_3NO_2) of [Cd_8Pt_8**L**$^{1}_{2}$**L**$^{3a}_{4}$**L**$^{4}_{4}$].

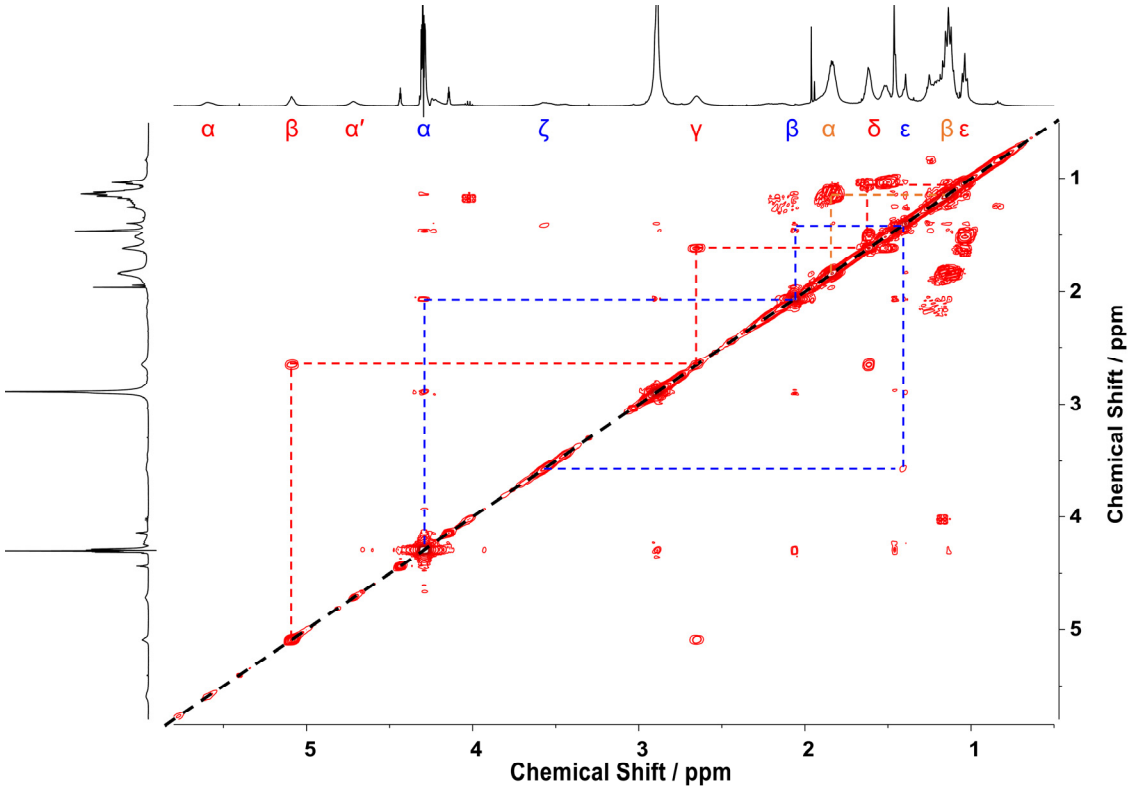

Figure S74. Partial COSY spectrum (500 MHz, CD_3NO_2) of [Cd_8Pt_8**L**$^1{}_2$**L**$^{3a}{}_4$**L**$^4{}_4$].

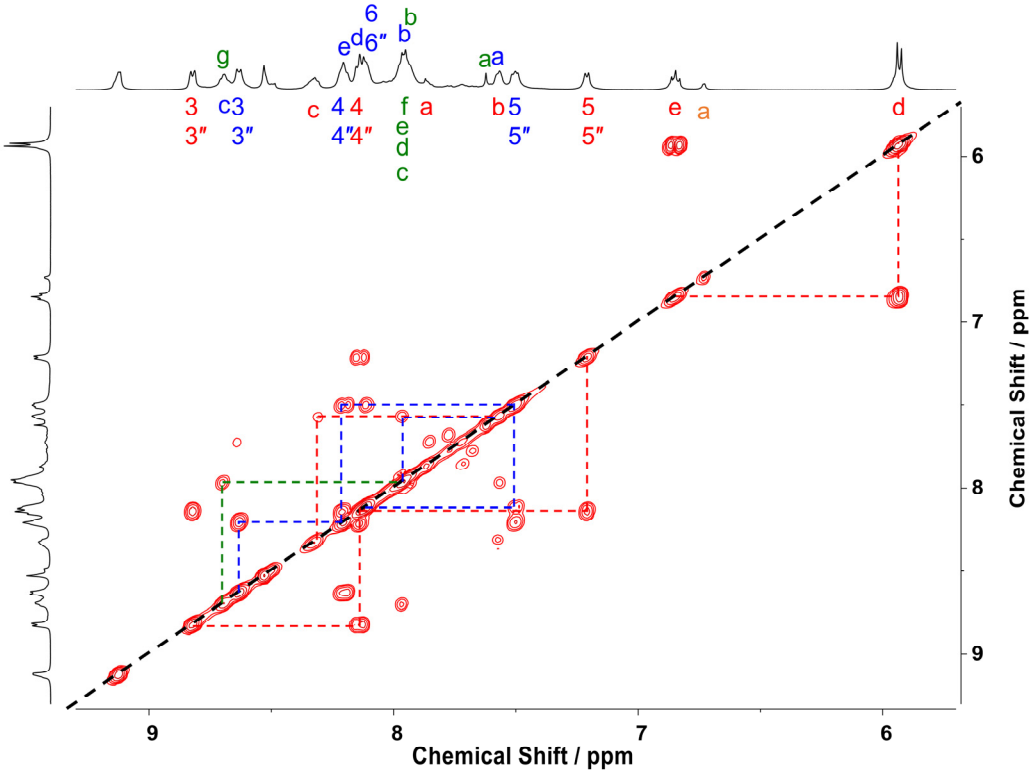

Figure S75. Partial COSY spectrum (500 MHz, CD_3NO_2) of [Cd_8Pt_8**L**$^1{}_2$**L**$^{3a}{}_4$**L**$^4{}_4$].

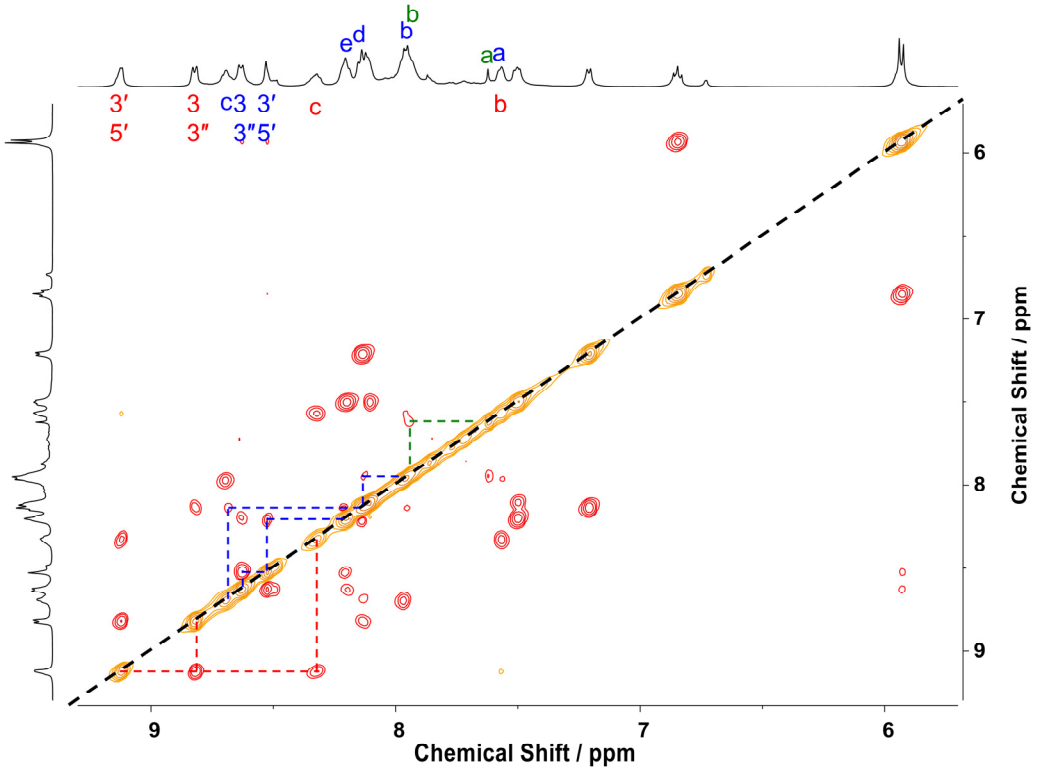

Figure S76. Partial ROESY spectrum (500 MHz, CD_3NO_2) of [Cd_8Pt_8**L**$^1{}_2$**L**$^{3a}{}_4$**L**$^4{}_4$].

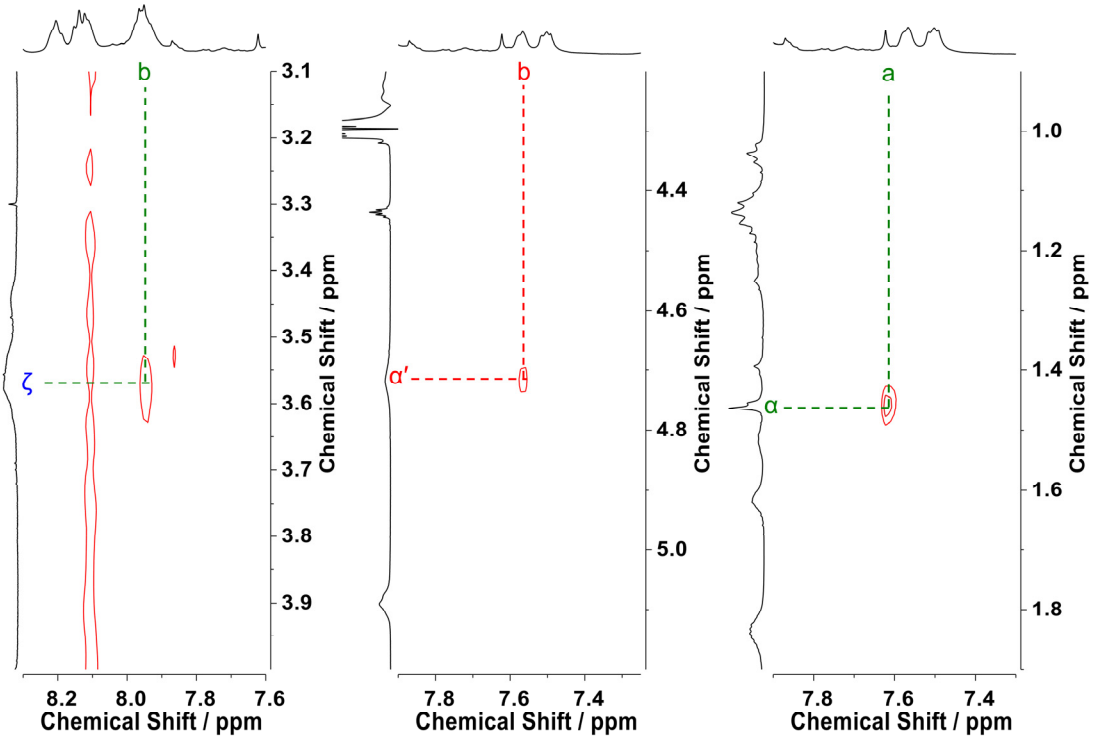

Figure S77. Partial ROESY spectrum (500 MHz, CD_3NO_2) of [Cd_8Pt_8**L**$^1{}_2$**L**$^{3a}{}_4$**L**$^4{}_4$].

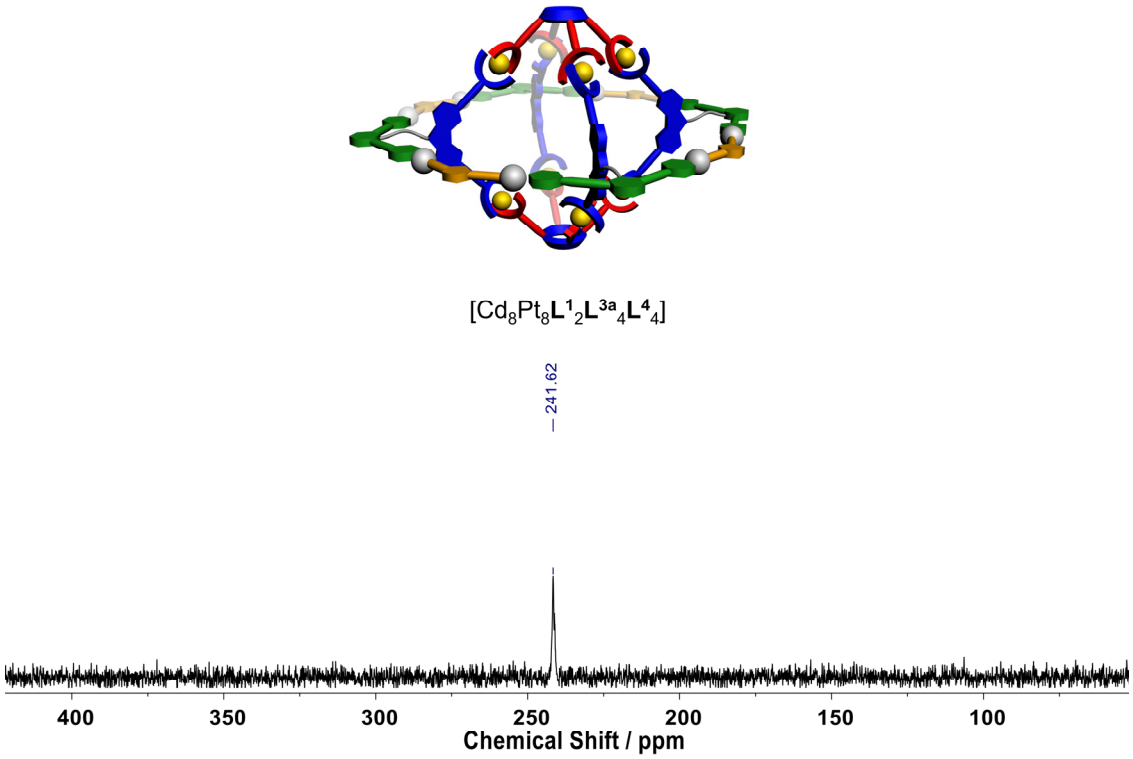

Figure S78. ^{113}Cd NMR spectrum (111 MHz, CD_3NO_2) of $[Cd_8Pt_8\mathbf{L^1}_2\mathbf{L^{3a}}_4\mathbf{L^4}_4]$.

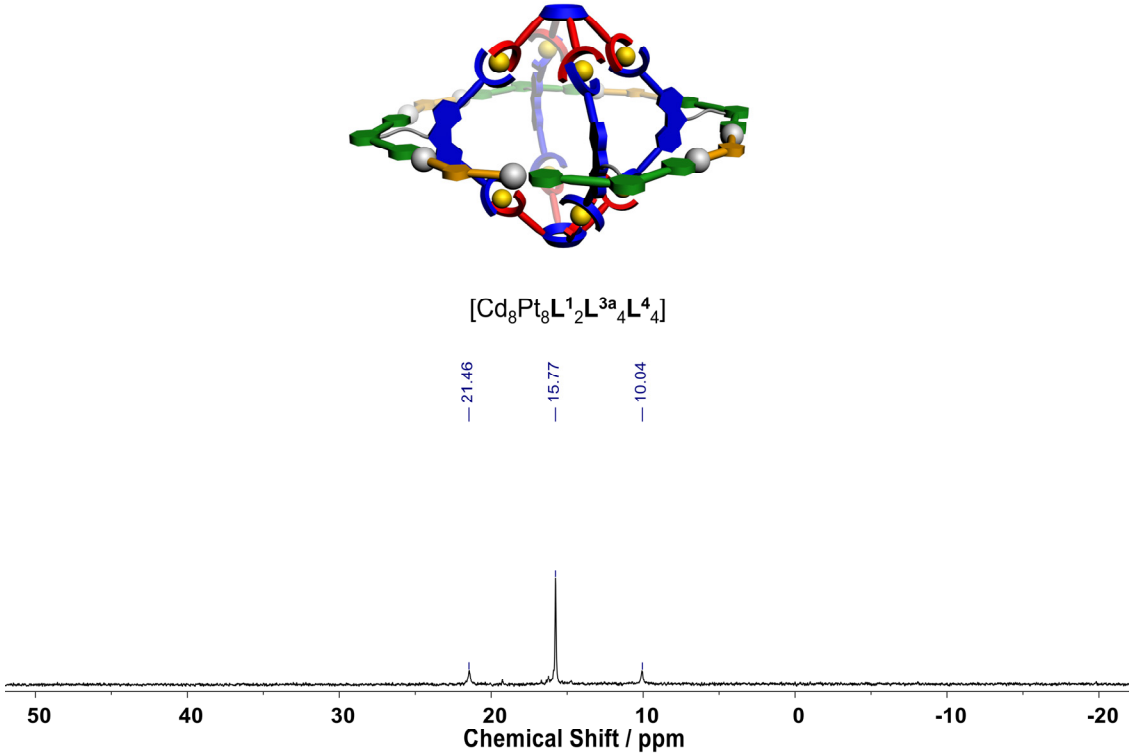

Figure S79. ^{31}P NMR spectrum (202 MHz, CD_3NO_2) of $[Cd_8Pt_8\mathbf{L^1}_2\mathbf{L^{3a}}_4\mathbf{L^4}_4]$.

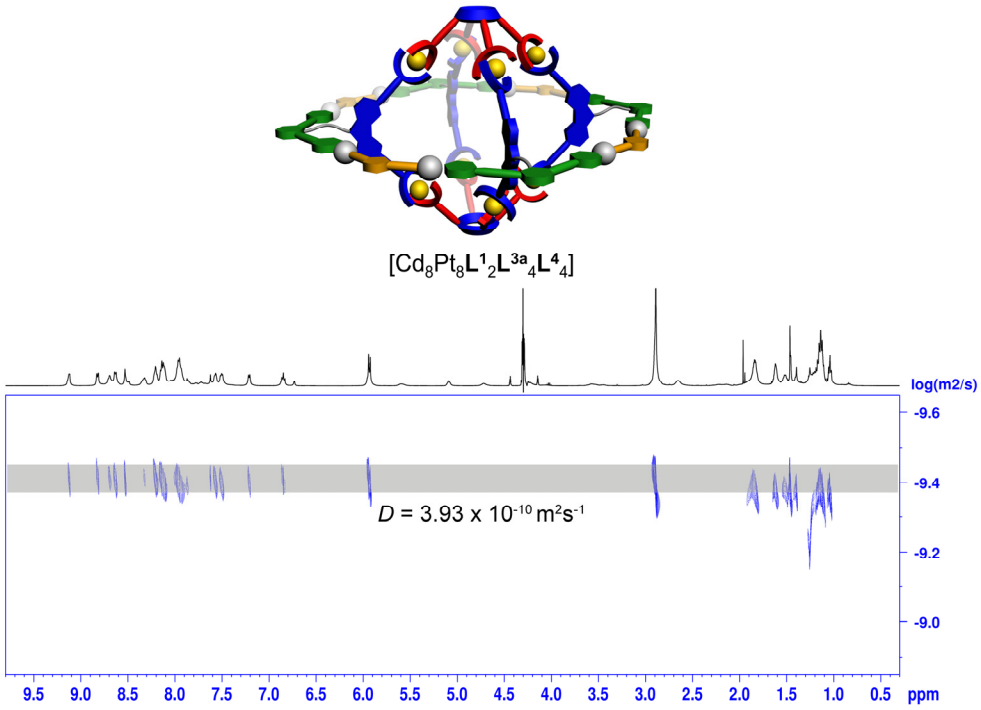

Figure S80. DOSY spectrum (500 MHz, CD_3NO_2) of $[Cd_8Pt_8\mathbf{L^1}_2\mathbf{L^{3a}}_4\mathbf{L^4}_4]$.

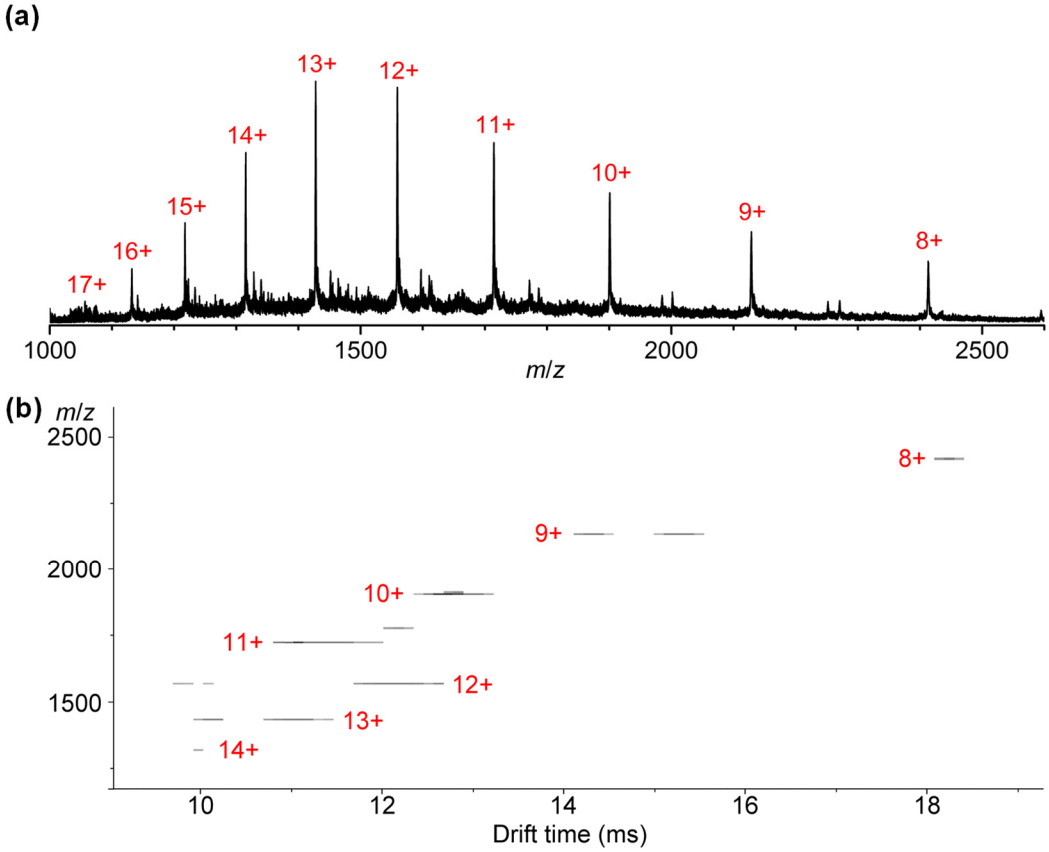

Figure S81. (a) ESI-MS spectrum and (b) TWIM-MS plot of $[Cd_8Pt_8\mathbf{L^1}_2\mathbf{L^{3a}}_4\mathbf{L^4}_4]$.

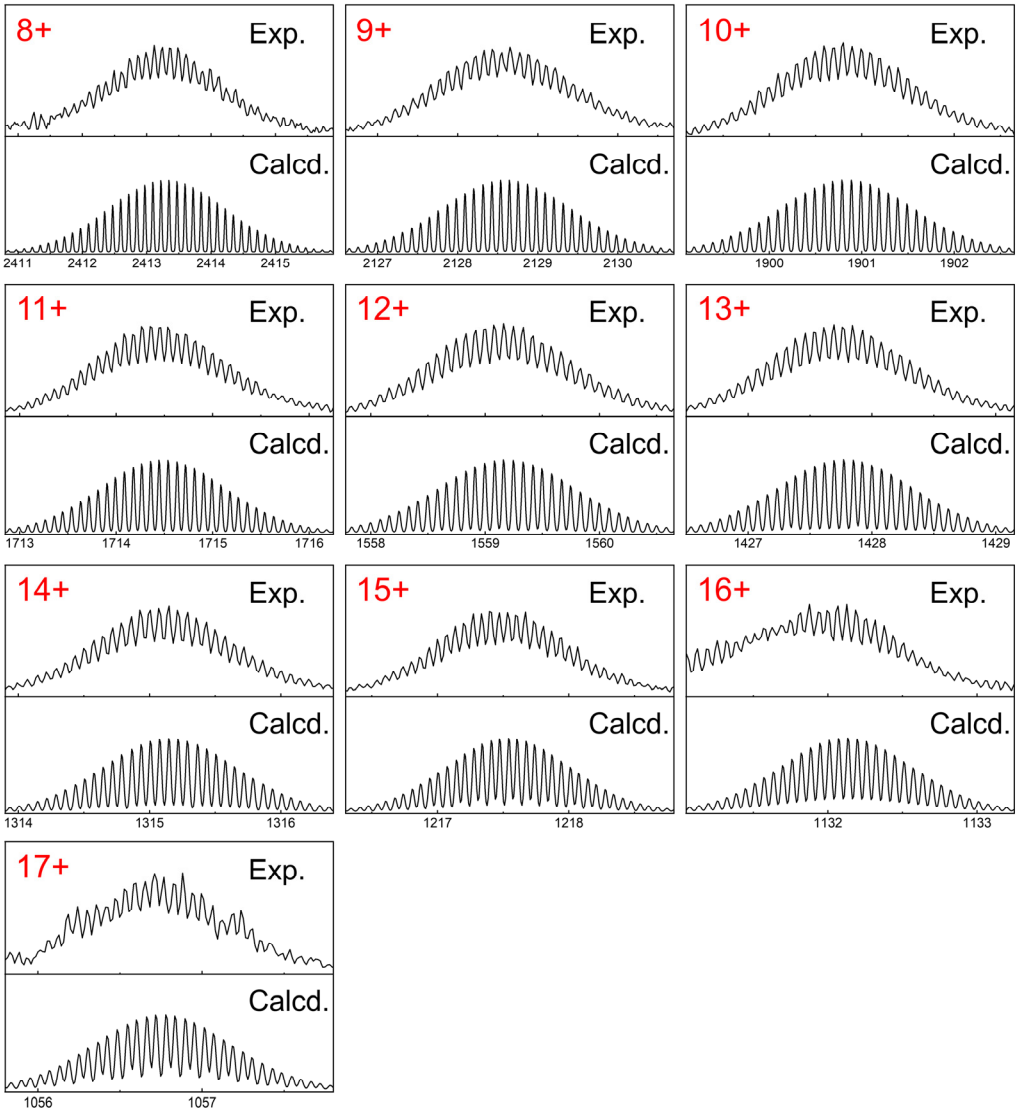

Figure S82. Experimental and theoretical isotope patterns of $[Cd_8Pt_8\mathbf{L^1}_2\mathbf{L^{3a}}_4\mathbf{L^4}_4]$.

Table S4. Drift times and collision cross sections (CCSs) for $[Cd_8Pt_8\mathbf{L^1}_2\mathbf{L^{3a}}_4\mathbf{L^4}_4]$.

Charge state	*m/z*	Drift time (ms)	Experimental CCS (Å^2)
8	2413.1	18.08	2035.8
9	2128.7	14.11	1949.5
9	2128.7	15.10	2037.9
10	1900.9	12.57	2007.0
11	1714.6	10.80	1994.7
11	1714.6	11.25	2050.3
12	1559.2	9.59	2007.4
12	1559.2	9.92	2054.4
12	1559.2	11.91	2324.3
13	1427.8	9.92	2226.1
13	1427.8	10.92	2376.0
14	1315.2	9.81	2379.7
		Average CCS	2120.3 ± 159.3
			Theoretical CCS (Å^2)
		PA CCS	2271.7 ± 7.3
		TM CCS	2610.4 ± 36.84

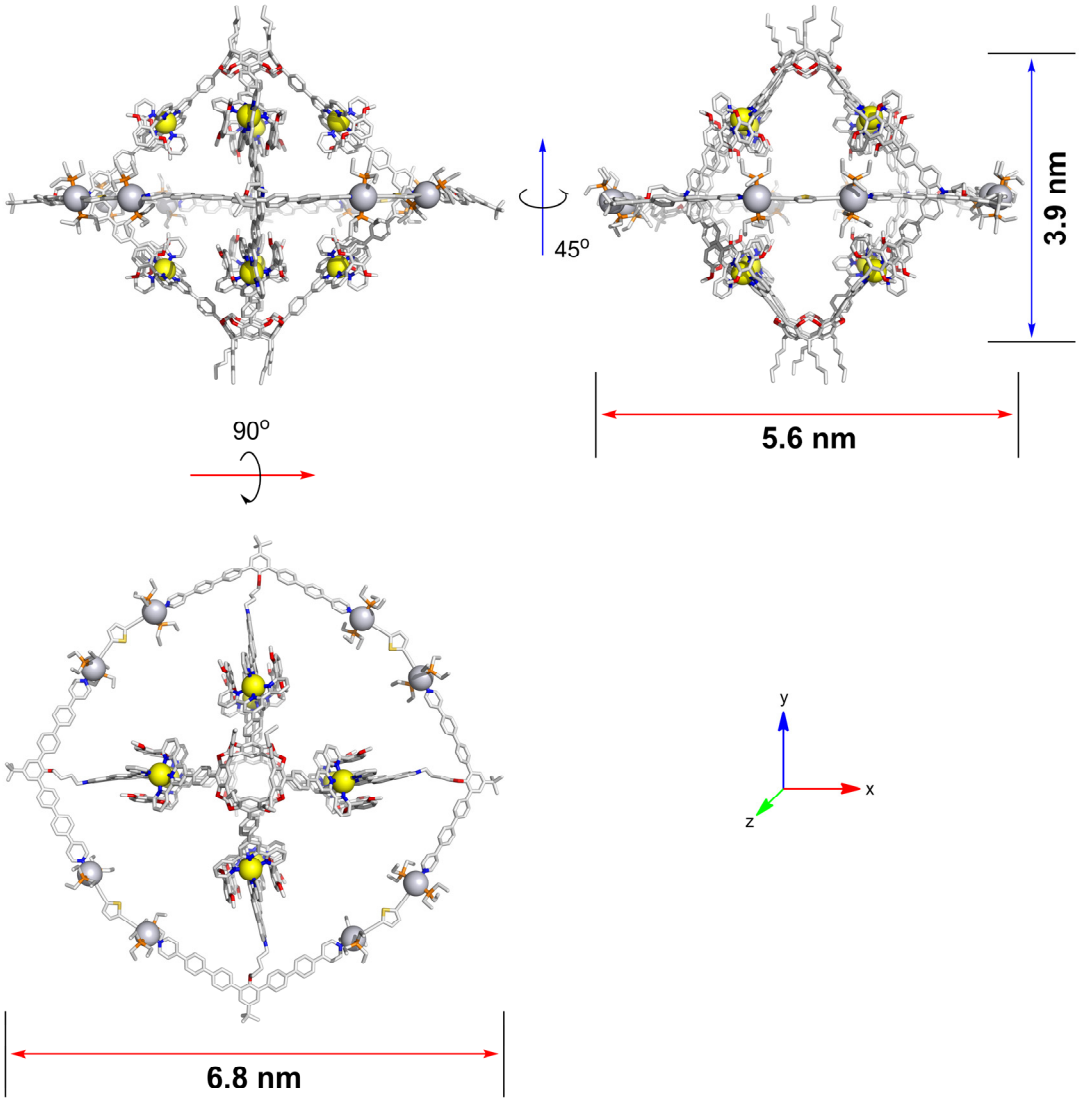

Figure S83. Geometry-optimized structures of $[Cd_8Pt_8\mathbf{L^1}_2\mathbf{L^{3a}}_4\mathbf{L^4}_4]$.

Heterobimetallic Nano-Saturn [$Cd_8Pt_8L^1_2L^{3b}_4L^4_4$]: By the general procedure, after being stirred for 8 h at 25 °C, the complex [$Cd_8Pt_8L^1_2L^{3b}_4L^4_4$] was obtained in quantitative yield from [$Cd_8L^1_2L^{3b}_4$] (770.0 nmol, 11.9 mg), metalloligand [Pt_2L^4]$(OTf)_2$ (3.1 μmol, 4.0 mg). ^{1}H NMR (500 MHz, CD_3NO_2): δ (ppm) 9.14 (s, 16H), 8.83 (d, J = 8.1 Hz, 16H), 8.71 (m, 24H), 8.64 (d, J = 8.2 Hz, 16H), 8.54 (s, 16H), 8.34 (d, J = 7.4 Hz, 16H), 8.27-8.08 (m, 80H), 8.07-7.91 (m, 72H), 7.87 (d, J = 8.3 Hz, 16H), 7.80 (br, 8H), 7.61-7.54 (m, 32H), 7.51 (t, J = 5.9 Hz, 16H), 7.22 (d, J = 7.4 Hz, 16H), 6.86 (t, J = 8.5 Hz, 16H), 6.76 (s, 8H), 5.94 (d, J = 8.6 Hz, 32H), 5.59 (br, 8H), 5.10 (br, 8H), 4.72 (br, 8H), 4.24 (br, 8H), 3.40 (br, 8H), 2.90 (s, 96H), 2.65 (br, 16H), 2.22 (br, 8H), 1.93-1.75 (m, 96H), 1.65-1.59 (m, 32H), 1.54-1.49 (m, 16H), 1.46-1.39 (m, 42H), 1.31-1.23 (m, 16H), 1.17-1.13 (m, 144H), and 1.04 (t, J = 7.2 Hz, 24H). ^{113}Cd NMR (111 MHz, CD_3NO_2): δ (ppm) 241.82. ^{31}P NMR (202 MHz, CD_3NO_2): δ (ppm) 15.75 (s, 16P, ^{195}Pt satellites, $^1J_{Pt\text{-}P}$ = 2294.7 Hz).

ESI-MS (*m/z*):

Charge state	Composition	Theoretical *m/z*	Experimental *m/z*
7+	$[M - 7OTf]^{7+}$	2795.9741	2795.9619
8+	$[M - 8OTf]^{8+}$	2427.7344	2427.7317
9+	$[M - 9OTf]^{9+}$	2141.4385	2141.4282
10+	$[M - 10OTf]^{10+}$	1911.8955	1911.8965
11+	$[M - 11OTf]^{11+}$	1724.3625	1724.3643
12+	$[M - 12OTf]^{12+}$	1568.5029	1568.5005
13+	$[M - 13OTf]^{13+}$	1436.2402	1436.2332
14+	$[M - 14OTf]^{14+}$	1323.1544	1323.1527
15+	$[M - 15OTf]^{15+}$	1225.0167	1225.0198
16+	$[M - 16OTf]^{16+}$	1139.0161	1139.0067

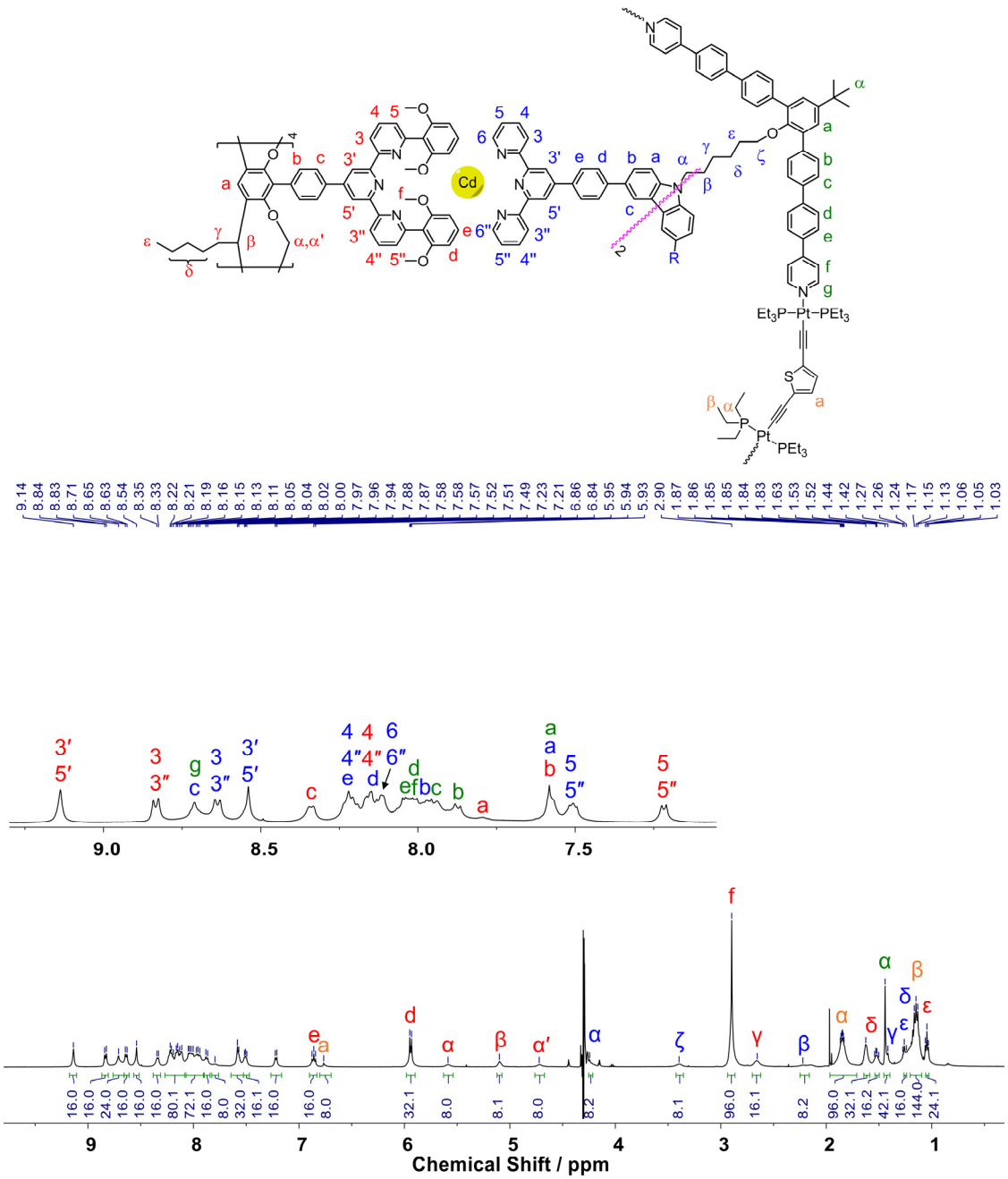

Figure S84. ^{1}H NMR spectrum (500 MHz, CD_3NO_2) of [Cd_8Pt_8**L**$^{1}_{2}$**L**$^{3b}_{4}$**L**$^{4}_{4}$].

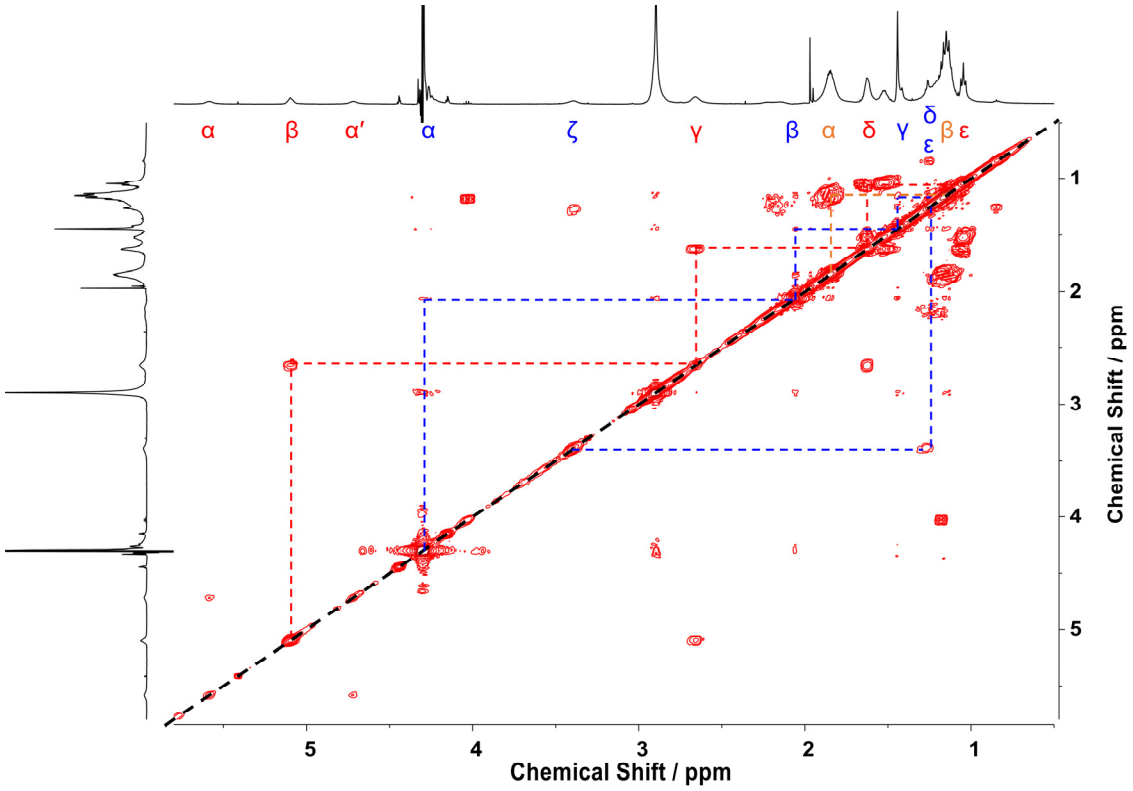

Figure S85. Partial COSY spectrum (500 MHz, CD_3NO_2) of [Cd_8Pt_8**L**$^1{}_2$**L**$^{3b}{}_4$**L**$^4{}_4$].

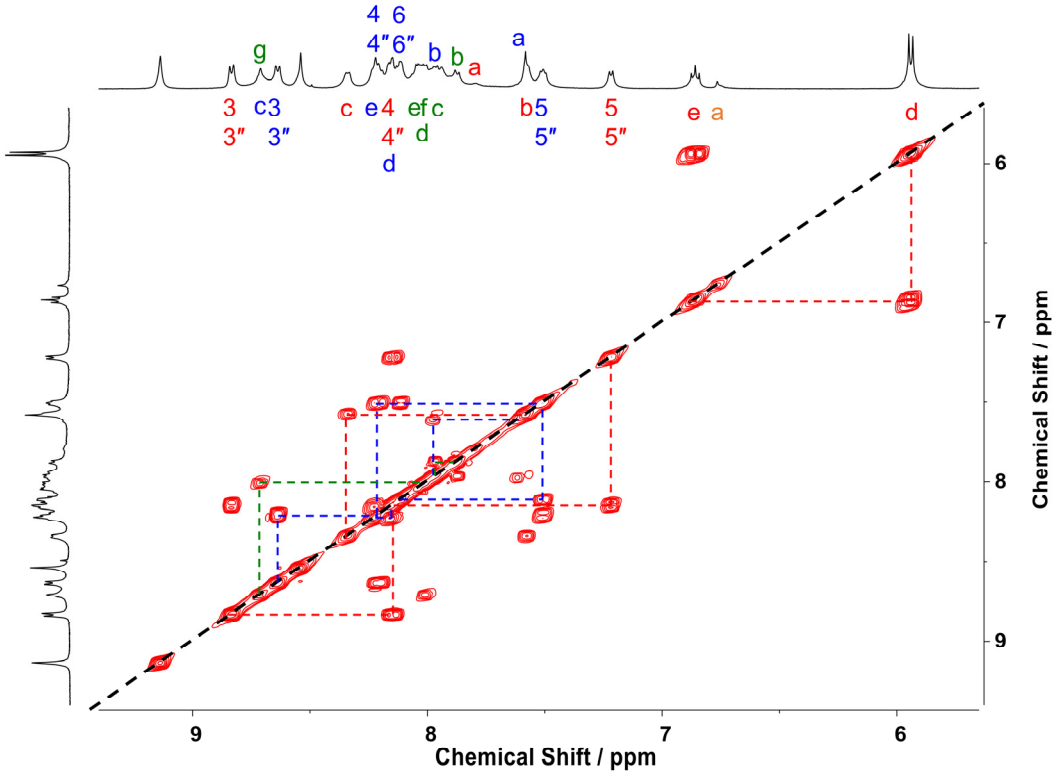

Figure S86. Partial COSY spectrum (500 MHz, CD_3NO_2) of [Cd_8Pt_8**L**$^1{}_2$**L**$^{3b}{}_4$**L**$^4{}_4$].

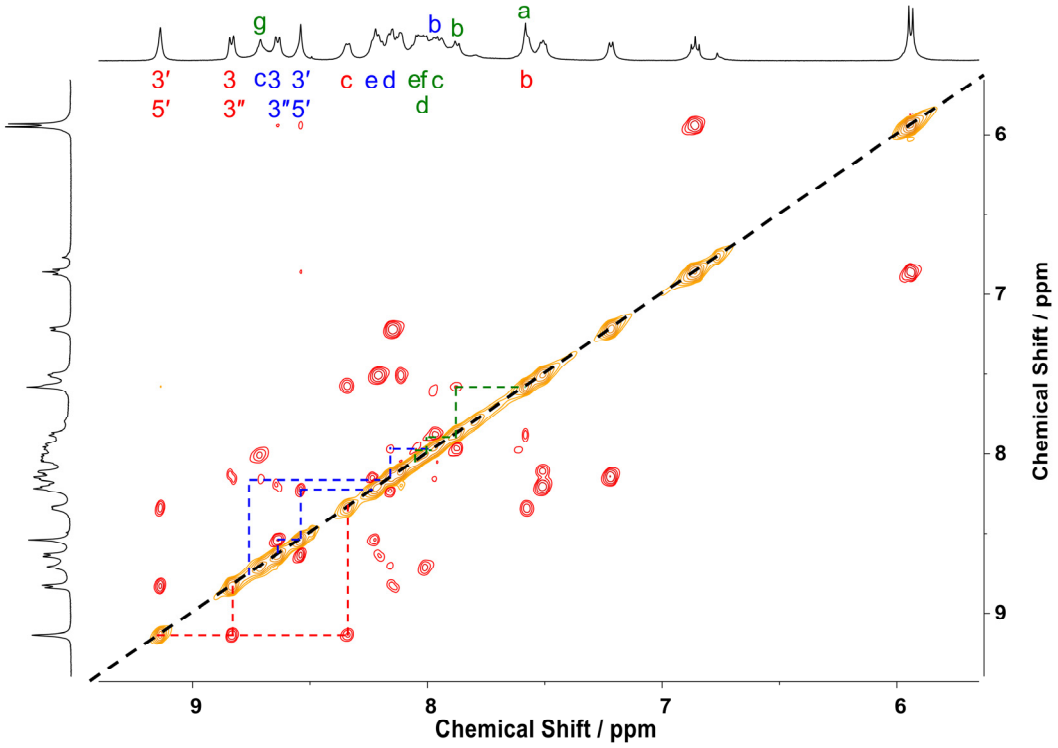

Figure S87. Partial ROESY spectrum (500 MHz, CD_3NO_2) of [Cd_8Pt_8**L**$^1{}_2$**L**$^{3b}{}_4$**L**$^4{}_4$].

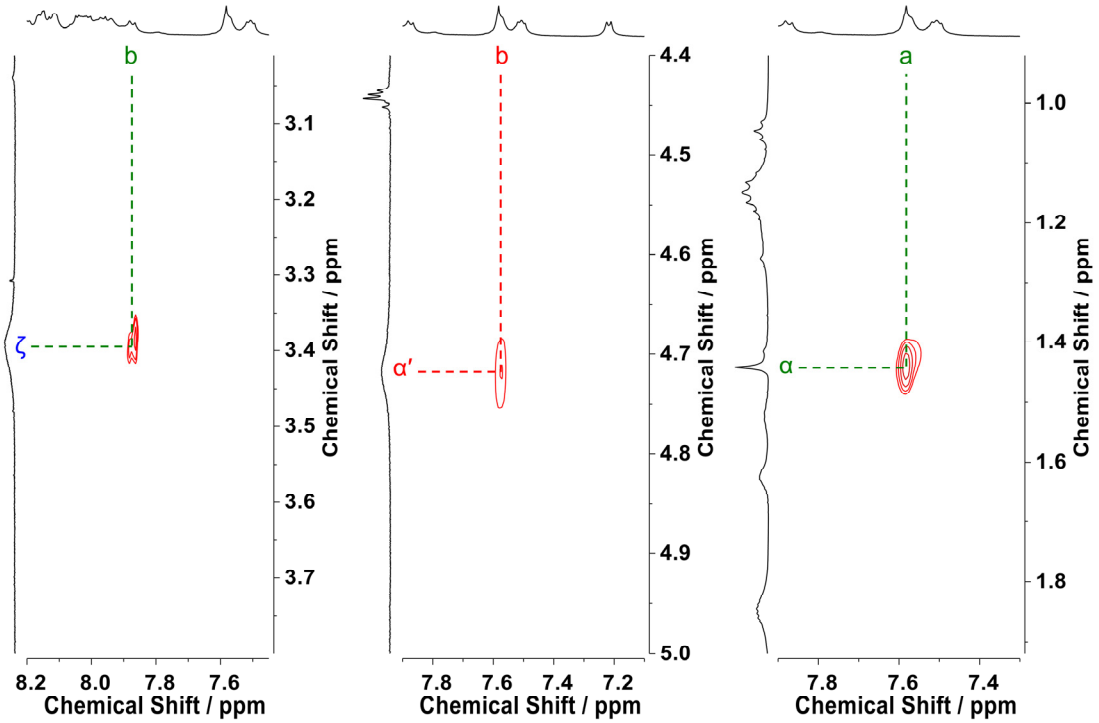

Figure S88. Partial ROESY spectrum (500 MHz, CD_3NO_2) of [Cd_8Pt_8**L**$^1{}_2$**L**$^{3b}{}_4$**L**$^4{}_4$].

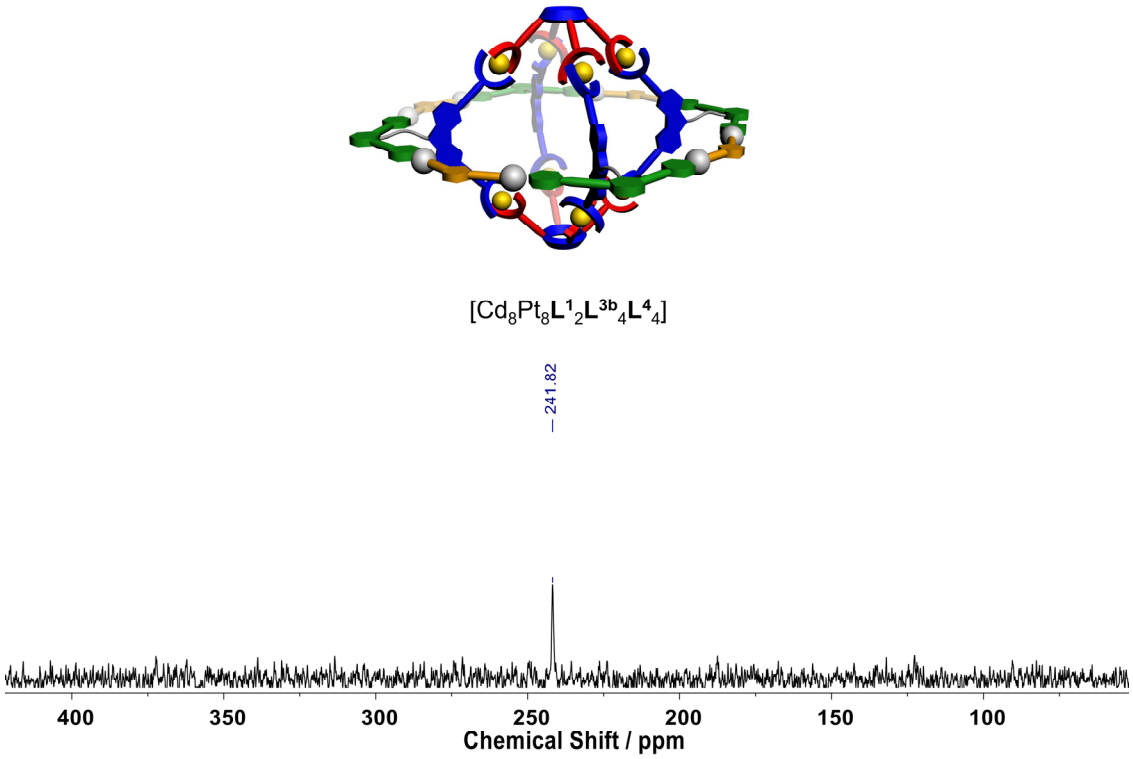

Figure S89. ^{113}Cd NMR spectrum (111 MHz, CD_3NO_2) of [Cd_8Pt_8**L**$^1{}_2$**L**$^{3b}{}_4$**L**$^4{}_4$].

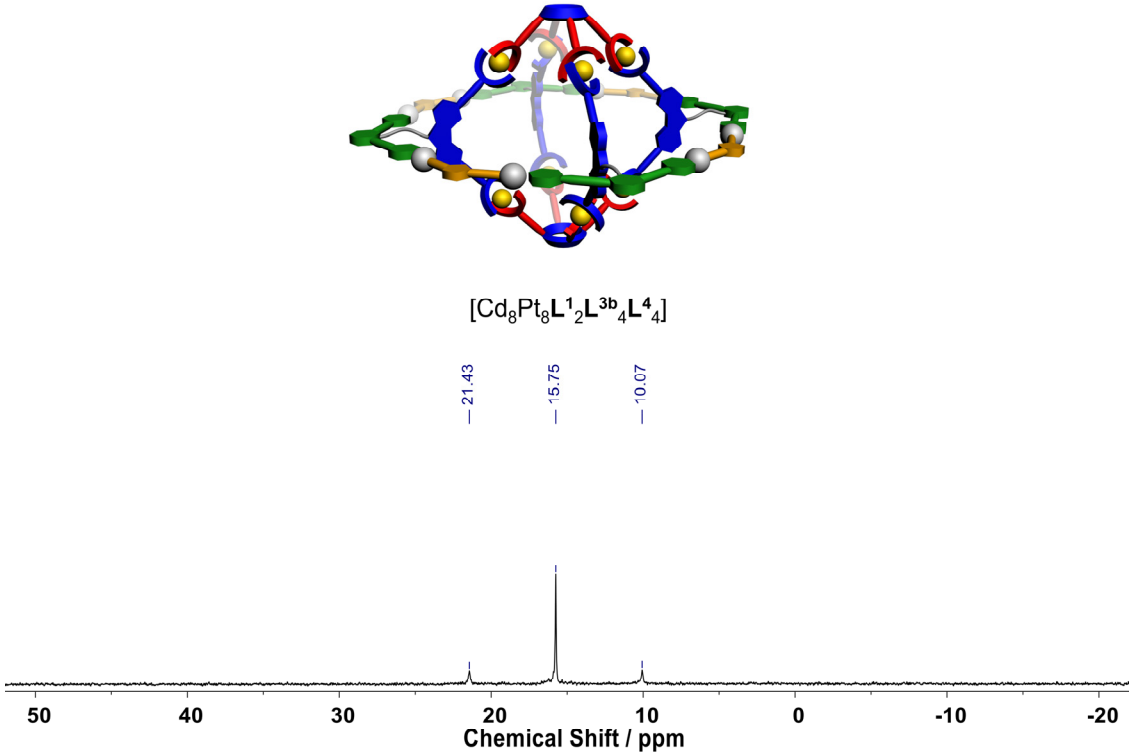

Figure S90. ^{31}P NMR spectrum (202 MHz, CD_3NO_2) of [Cd_8Pt_8**L**$^1{}_2$**L**$^{3b}{}_4$**L**$^4{}_4$].

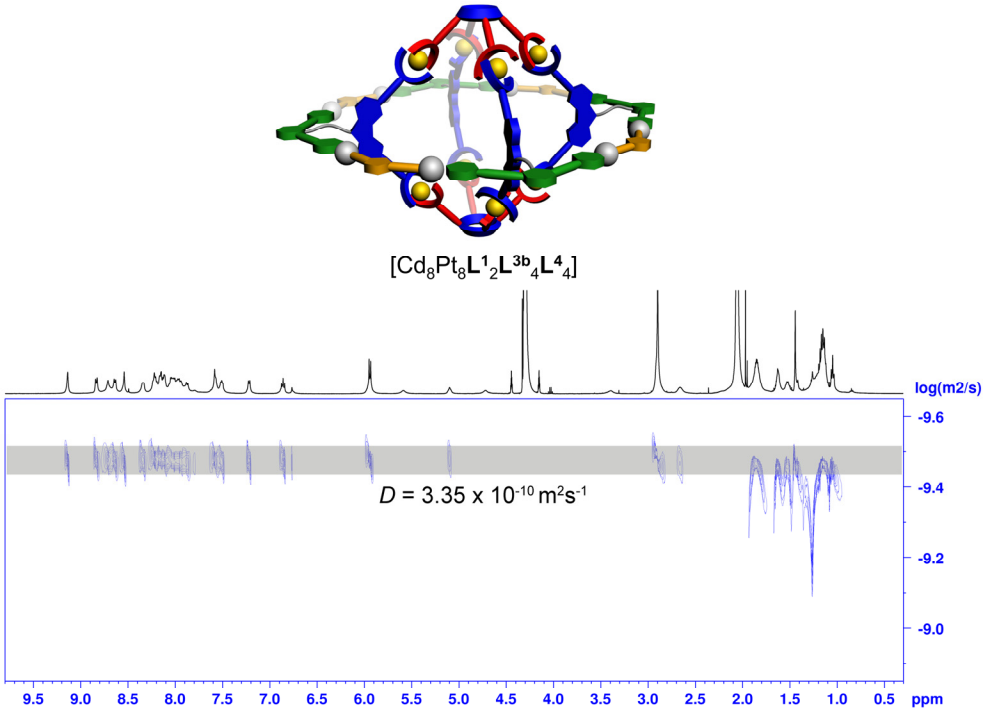

Figure S91. DOSY spectrum (500 MHz, CD_3NO_2) of [Cd_8Pt_8**L**$^1{}_2$**L**$^{3b}{}_4$**L**$^4{}_4$].

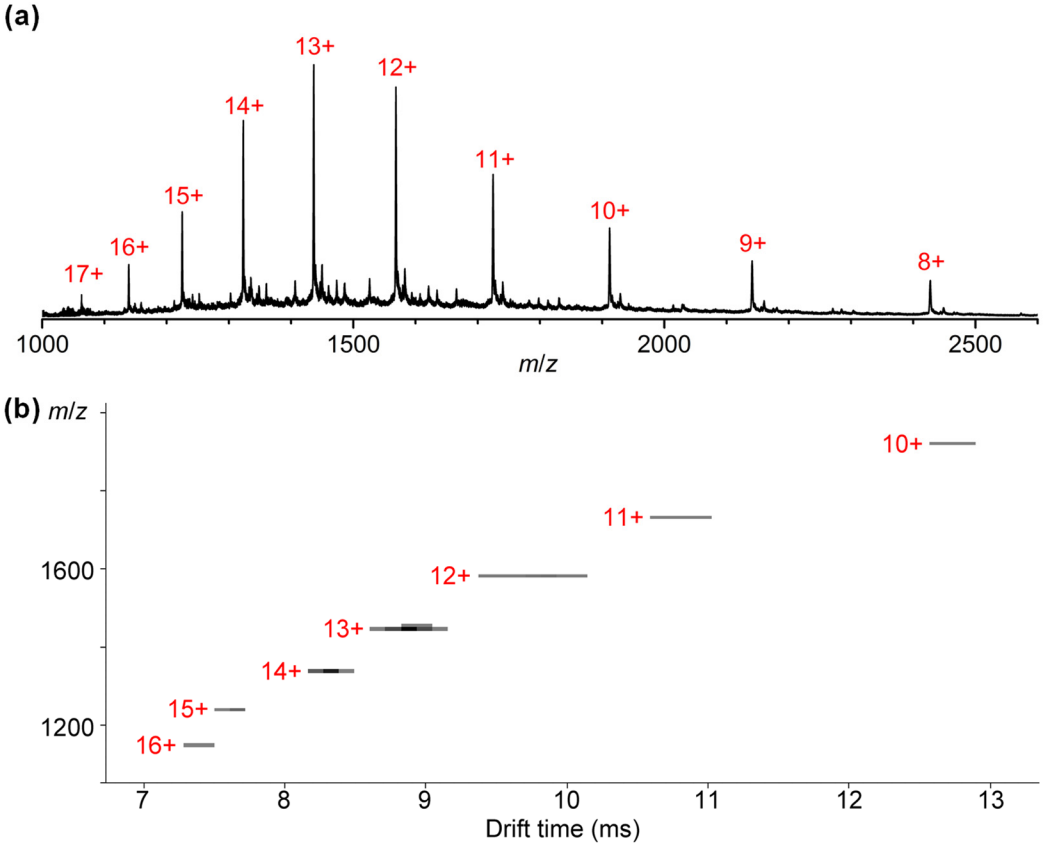

Figure S92. (a) ESI-MS spectrum and (b) TWIM-MS plot of [Cd_8Pt_8**L**$^1{}_2$**L**$^{3b}{}_4$**L**$^4{}_4$].

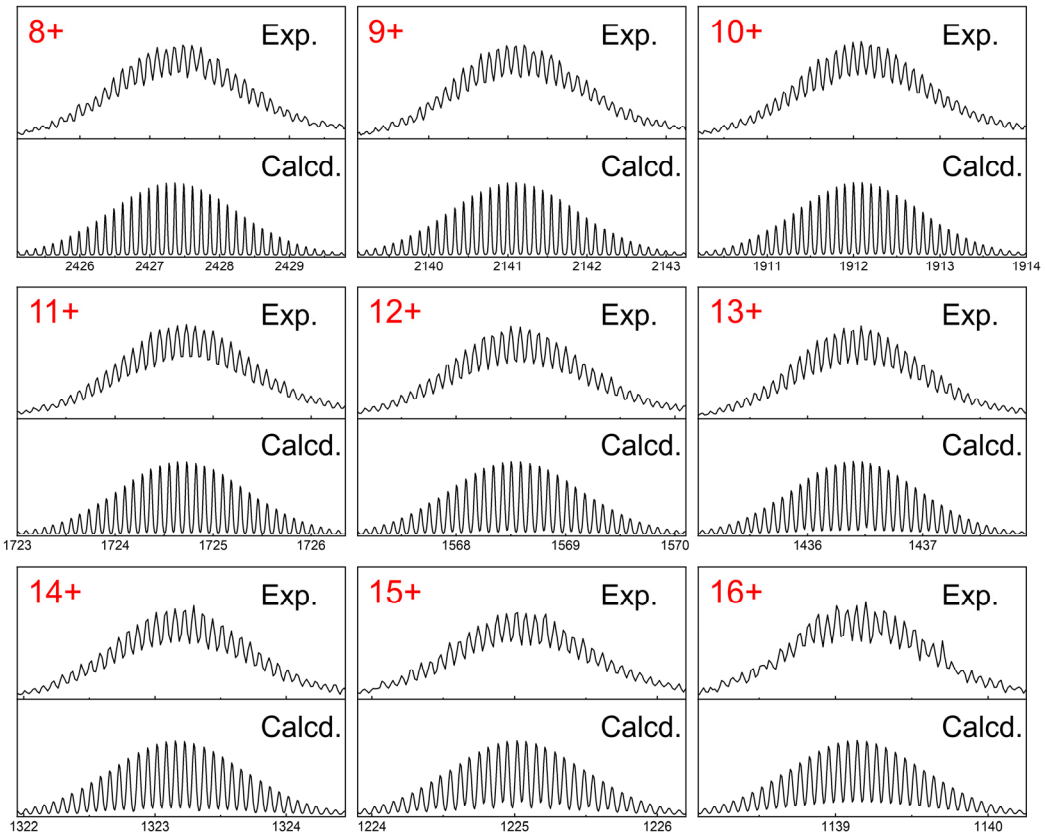

Figure S93. Experimental and theoretical isotope patterns of [$Cd_8Pt_8\mathbf{L^1}_2\mathbf{L^{3b}}_4\mathbf{L^4}_4$].

Table S5. Drift times and collision cross sections (CCSs) for [$Cd_8Pt_8\mathbf{L^1}_2\mathbf{L^{3b}}_4\mathbf{L^4}_4$].

Charge state	*m/z*	Drift time (ms)	Experimental CCS (Å^2)
10	1911.9	12.57	2006.9
11	1724.4	10.69	1980.9
12	1568.5	9.70	2023.1
13	1436.2	8.71	2035.4
14	1323.2	8.16	2094.8
15	1225.0	7.50	2115.0
16	1139.0	7.17	2185.1
		Average CCS	2063.0 ± 71.7
			Theoretical CCS (Å^2)
		PA CCS	2281.0 ± 9.4
		TM CCS	2624.5 ± 46.3

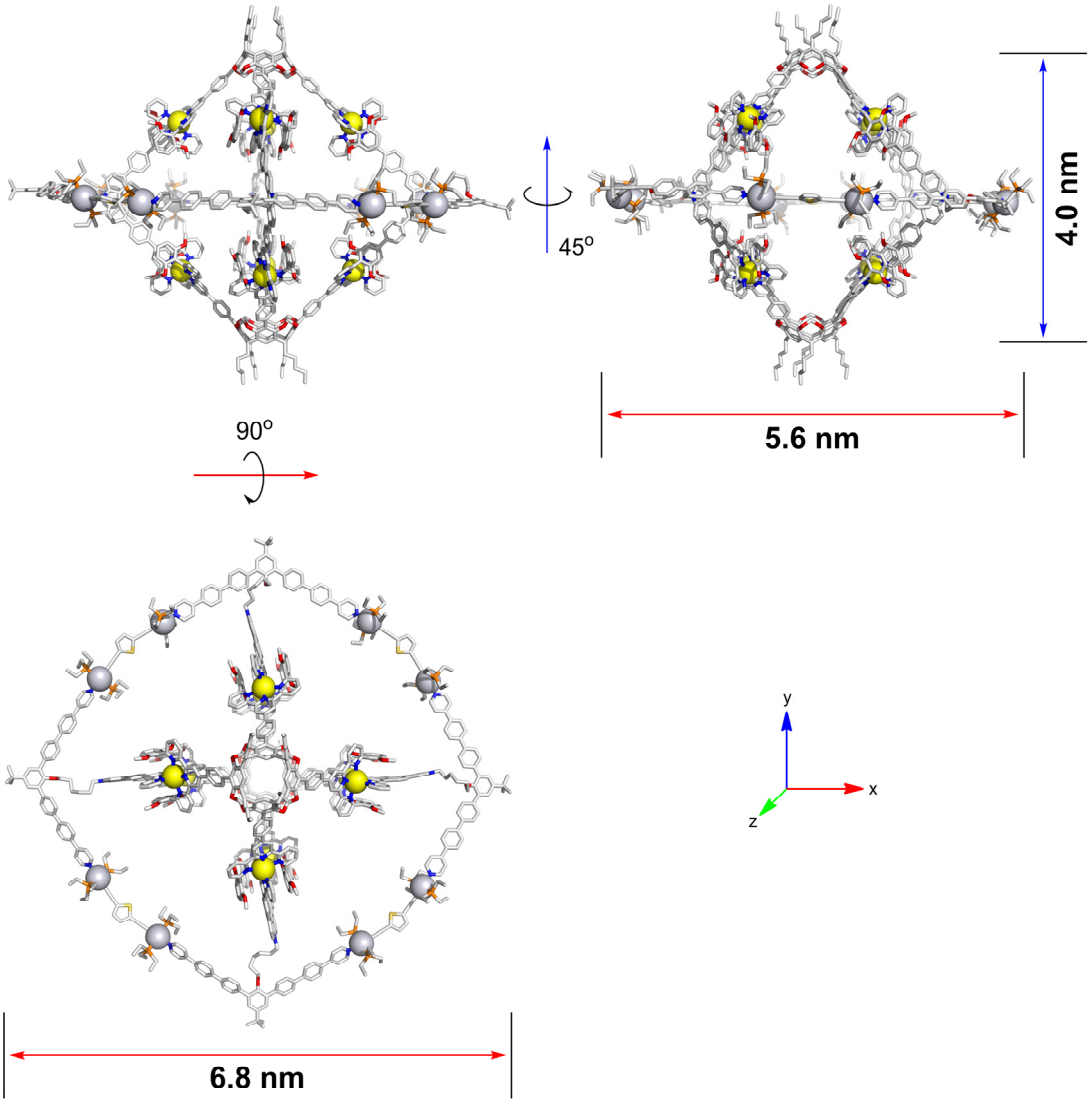

Figure S94. Geometry-optimized structures of $[Cd_8Pt_8\mathbf{L^1}_2\mathbf{L^{3b}}_4\mathbf{L^4}_4]$.

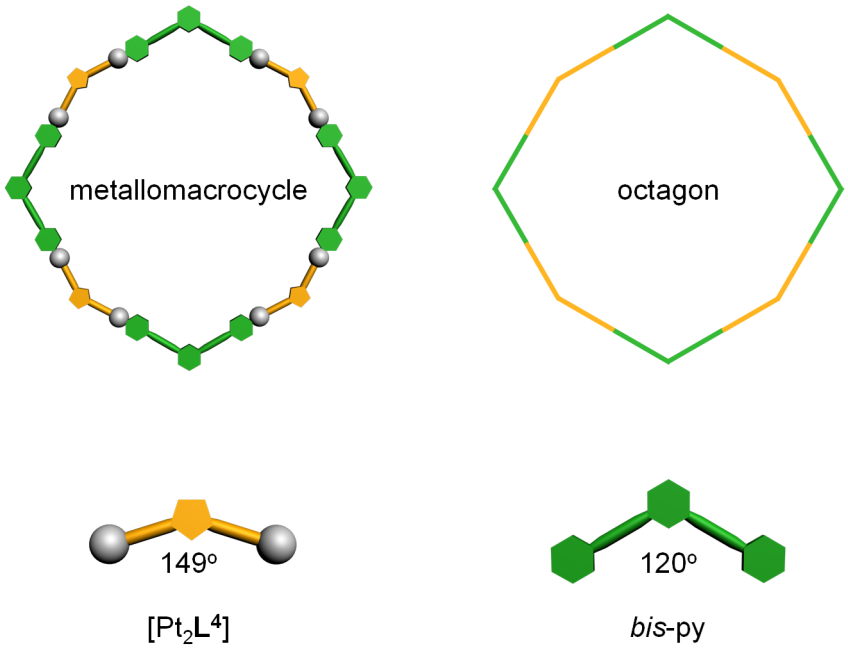

Figure S95. Cartoon representation of the octagonal metallomacrocycle derived from [Pt_2**L**^{4}] and *bis*-py ligands. The formula for calculating the sum of interior angles of a polygon is S = (N – 2) × 180°, where N is the number of vertices of a polygon. The interior angle sum of an octagon is 1080°. The ring of nano-Saturn complexes is a metallomacrocycle formed from four 149°-bent [Pt_2**L**^{4}] motifs and four 120°-bent *bis*-py moieties, which is very close to an ideal octagon.

Cavity Volume Calculation

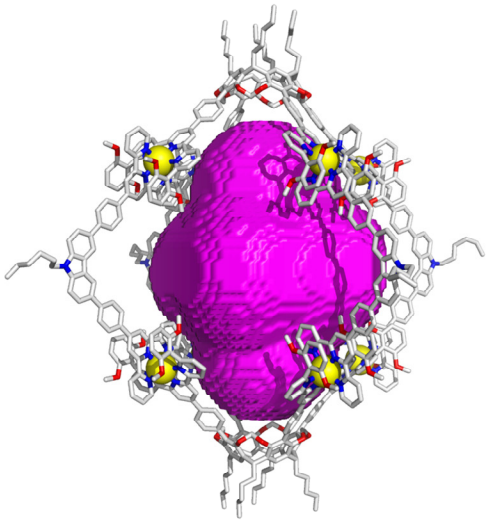

Volume Information	
Voxel size:	0.5 Å
Volume:	6368 Å^3
Surface area:	1753 Å^2
Sphericity, Ψ:	0.95
Effective radius:	10.90 Å
Center of Mass:	(-0.5, -0.7, -0.5) Å

Figure S96. Cavity volume (purple surface) in the geometry-optimized model of $[Cd_8\mathbf{L}^1{}_2\mathbf{L}^2{}_4]$ is estimated to be 6,368 Å^3 by the 3V web server.[13] The calix[4]resorcinarene-based nano-Saturn complexes with such a large cavity would have potential applications in construction of 2D or 3D porous materials through selective coordination chemistry.

References

1. Y. T. Chan, X. Li, J. Yu, G. A. Carri, C. N. Moorefield, G. R. Newkome and C. Wesdemiotis, *J. Am. Chem. Soc.*, 2011, **133**, 11967–11976.
2. M. F. Mesleh, J. M. Hunter, A. A. Shvartsburg, G. C. Schatz and M. F. Jarrold, *J. Phys. Chem.*, 1996, **100**, 16082–16086.
3. K. Thalassinos, M. Grabenauer, S. E. Slade, G. R. Hilton, M. T. Bowers and J. H. Scrivens, *Anal. Chem.*, 2009, **81**, 248–254.
4. C. B. Aakeroy, N. Schultheiss and J. Desper, *Org. Lett.*, 2006, **8**, 2607-2610.
5. S. Y. Wang, J. Y. Huang, Y. P. Liang, Y. J. He, Y. S. Chen, Y. Y. Zhan, S. Hiraoka, Y. H. Liu, S. M. Peng and Y. T. Chan, *Chem. Eur. J.*, 2018, **24**, 9274-9284.
6. P. Wen, Z. Gao, R. Zhang, A. Li, F. Zhang, J. Li, J. Xie, Y. Wu, M. Wu and K. Guo, *J. Mater. Chem. C*, 2017, **5**, 6136-6143.
7. Z. Zhang, H. Wang, X. Wang, Y. Li, B. Song, O. Bolarinwa, R. A. Reese, T. Zhang, X. Q. Wang, J. Cai, B. Xu, M. Wang, C. Liu, H. B. Yang and X. Li, *J. Am. Chem. Soc.*, 2017, **139**, 8174-8185.
8. H. Tan, H. Liu, X. Chen, H. Chen and S. Qiu, *Org. Biomol. Chem.*, 2015, **13**, 9977-9983.
9. C. S. Jiang, R. Zhou, J. X. Gong, L. L. Chen, T. Kurtan, X. Shen and Y. W. Guo, *Bioorg. Med. Chem. Lett.*, 2011, **21**, 1171-1175.
10. G. Zhan, M.-A. Dubois, Y. Makoudi, S. Lamare, J. Jeannoutot, X. Bouju, A. Rochefort, F. Palmino and F. Chérioux, *J. Phys. Chem. C*, 2017, **121**, 8427-8434.
11. L. He, S. C. Wang, L. T. Lin, J. Y. Cai, L. Li, T. H. Tu and Y. T. Chan, *J. Am. Chem. Soc.*, 2020, **142**, 7134-7144.
12. S. S. Roy, S. R. Chowdhury, S. Mishra and S. K. Patra, *Chem. Asian J.*, 2020, **15**, 3304-3313.
13. N. R. Voss and M. Gerstein, *Nucleic Acids Res.*, 2010, **38**, W555-W562.